LAPPEENRANTA-LAHTI UNIVERSITY OF TECHNOLOGY LUT
School of Energy Systems
Energy Technology
Master's Thesis

Santeri Mäntynen

EXPERIMENTAL STUDY ON THE DRYING KINETICS OF THICK POROUS BIOBASED FIBROUS MATERIALS

Examiners: Professor, D.Sc. Esa Vakkilainen & Postdoctoral Researcher Ekaterina Sermyagina
Instructors: Senior Scientists Janne Keränen & Elina Pääkkönen

ABSTRACT

Lappeenranta-Lahti University of Technology
School of Energy Systems
Energy Technology

Santeri Mäntynen

Experimental study on the drying kinetics of thick porous biobased fibrous materials

Master's Thesis 2021

Examiners: Professor, D.Sc. Esa Vakkilainen & Postdoctoral Researcher Ekaterina Sermyagina
Instructors: Senior Scientists Janne Keränen & Elina Pääkkönen

116 pages, 52 figures, 9 tables and 1 appendix

Keywords: Drying, microwave, air impingement, foam forming, fiber, evaporation, drying rate

In this thesis, drying of thick porous biobased fibrous materials is studied. Laboratory scale drying experiments are performed in VTT Jyväskylä, Central Finland. Drying is investigated by drying foam-formed fibrous materials made from wood pulp(s), water and surfactant (SDS). The objectives are to find efficient drying method(s) that suit for thick porous biobased materials, could use renewable energy sources and investigation of quality of the fiber structures during drying.

The research consists of literature and experimental parts. Literature part focuses on foam forming and used raw materials, primary energy trends and its effect on selected drying methods in the future and fundamentals of drying through heat transfer methods, phases of drying and examples of selected drying methods. Experimental part focuses on air impingement and microwave drying performed on a laboratory scale.

The most promising results from investigated drying methods gave the microwave drying. Over 4-times higher momentarily drying rates and 18-times higher average drying rates were reached with microwave drying compared to impingement drying. The quality control of the samples tended to be quite difficult with both drying methods, but even more difficult with microwave drying. Surface tended to expand and collapse due to fast temperature and pressure increase caused by microwaves and structures of some samples were destroyed. Increased sample consistency was found to increase the sample resistance.

TIIVISTELMÄ

Lappeenrannan-Lahden teknillinen yliopisto
School of Energy Systems
Energiatekniikka

Santeri Mäntynen

Paksujen huokoisten biopohjaisten materiaalien kuivaus

Diplomityö 2021

Tarkastaja: Professori Esa Vakkilainen & tutkijatohtori Ekaterina Sermyagina
Ohjaaja: Erikoistutkijat Janne Keränen & Elina Pääkkönen

116 sivua, 52 kuvaa, 9 taulukkoa ja 1 liite

Hakusanat: Kuivaus, mikroaalto, päällepuhallus, vaahtorainaus, kuitu, haihduttaminen, haihdutusnopeus

Työssä analysoidaan paksujen huokoisten biopohjaisten kuitumateriaalien kuivausta. Kuivauskokeita tehdään laboratorioympäristössä VTT:n Jyväskylän toimipisteellä, Keski-suomessa. Kuivausta tutkitaan kuivaamalla vaahtorainattuja kuitumateriaaleja. Kuitumateriaalien raaka-aineina toimivat puupohjainen sellu, vesi ja surfaktantti (SDS). Tavoitteina on löytää tehokkaita kuivatusmenetelmiä, jotka soveltuvat paksujen huokoisten biopohjaisten materiaalien kuivaukseen sekä pystyvät hyödyntämään uusiutuvia energianlähteitä kuivatuksessa ja tutkia kuiturakenteiden laatuparametrejä kuivatuksen aikana.

Tutkimus koostuu kirjallisuuskatsauksesta sekä kokeellisesta osasta. Kirjallisuuskatsauksessa käsitellään vaahtorainausta sekä siihen käytettäviä raaka-aineita, primäärienergian kehittymistä sekä sen vaikutusta valittuihin kuivatusmenetelmiin tulevaisuudessa ja kuivauksen perusteita läpikäymällä lämmönsiirron, kuivausprosessin ja valittujen kuivatusmenetelmien teoriaa. Kokeellisen osan pääpaino on laboratorioympäristössä tehtävät päällepuhallus- ja mikroaaltokuivauskokeet.

Lupaavimpia tuloksia tarkastelluista kuivatusmenetelmistä antoi mikroaaltokuivaus. Mikroaaltokuivauksella saavutettiin yli neljä kertaa suurempia hetkellisiä kuivatusnopeuksia ja 18-kertaa suurempia keskimääräisiä kuivatusnopeuksia verrattuna päällepuhalluskuivaukseen. Molemmat kuivatusmenetelmät, mutta varsinkin mikroaaltokuivaus, tuottivat ongelmia rakenteiden laadun hallinnassa. Näytteen pinnan nähtiin turpoavan ja romahtavan mikroaaltojen aiheuttaman nopean sisäisen lämmön- ja paineennousun takia. Joidenkin näytteiden rakenteet hajosivat tästä syystä täysin. Sakeuden noston huomattiin lisäävän näytteen kestävyyttä.

PREFACE

This thesis was made for VTT as a part of the project named Piloting Alternatives for Plastic (PAfP). The project is designed to take laboratory developed biobased fiber materials towards the commercial use to replace plastic. Thank you, VTT, for the opportunity.

I would like to thank my instructors Janne Keränen and Elina Pääkkönen for the subject and from great tutoring and assisting throughout the process. I would also like to thank the laboratory personnel and Oleg Timofeev for introducing me to laboratory work.

From the university, I would like to thank my examiners Esa Vakkilainen and Ekaterina Sermyagina for the guiding and fast responding when needed. The comments and suggestions were always understandable and clear.

Thanks to the whole team and my superior Jarmo Kouko for helping me to learn the ropes. I feel like it was always easy to find the needed help. I also learned a lot from working as a part of a project team.

I enjoyed my studentship in LUT for all my six years. I feel like I have learned a lot during these years due to high quality education and the possibility to exploit learned knowledge in the working life. I am also glad for making a lot of new friends during my time in LUT.

Finally, I would like to thank my family, friends, and the better half from the ongoing support and encouragement.

Jyväskylä, November 2021

Santeri Mäntynen

TABLE OF CONTENTS

SYMBOLS

Roman

A	area, proportion of fiber length to radius	m^2, -
BW	basis weight	kg/m^2
c	speed of light, unit value	m/s, €/t
C	cost	€, k€
c_p	specific heat capacity	J/kgK, kJ/kgK
DR	drying rate	$kg/m^2/h$
$d.s.c.$	dry solids content	%
E	energy consumption, energy demand	kWh, kWh/kg, kWh/t
f	frequency	1/s
F	force	N
h	enthalpy, heat	kJ/kg
H	height, thickness	m, mm
m	mass	g, kg, t
$\dot{m}$	mass flow	kg/s, t/h
n	number of personnel	-
p	pressure	bar, Pa
P	power	W
$\dot{P}$	power density	W/m^3
q	heat flow, heat flux	W/m^2, W
Q	heat energy	kJ
s	hourly salary	€/h
t	time	h, s
T	temperature	ºC, K
ΔT	temperature change	K
v	speed, velocity	m/min, mm/min, m/s
V	volume	m^3
w	width	m
X	moisture ratio	kg/kg
ΔX	change in moisture ratio	kg/kg

Greek

α	heat transfer coefficient	W/m^2K
ε'	dielectric constant of the material	-
Φ	liquid fraction	%, -
λ	wavelength	m

Subscripts

a	air
abs	absorption
avg	average
c	compressing
cond	conduction
cons	consumption
conv	convection
d	dry
E	energy
el	electricity
ev	evaporation
ex	exhaust
fiber	fiber
h	annual
heat	heating
i	current measured point
mat	material
p	propagation
prod	produced
rad	radiator
RM	raw material
s	surface
surf	surfactant
tot	total
v	vapor

w	water
0	previous measured point

Abbreviations

AC	alternate current
ADC	analog-to-digital converter
BSD	bubble size distribution
BSKP	bleached softwood kraft pulp
CMC	britical moisture content
CMP	chemimechanical pulp
COP	coefficient of performance
CSF	Canadian standard freeness
CTMP	Chemithermomechanical pulp
DC	direct current
FB	forming board
HB	headbox
HiVac	high vacuum section
HW	hardwood
IR	infrared
SDS	sodium dodecyl sulphate
SW	softwood
TMP	thermomechanical pulp
TSU	top suction unit
VFB	vacuum foil box

1 INTRODUCTION

1.1 Background

Primary energy use is changing as the increased amount of electricity is being produced from renewable energy sources. New energy sources are coming to support old ones in electricity production, also in the form of waste heat recovery. Of the industrial processes, drying is process that requires a lot of energy, which enables the need of exploitation of renewable energy sources also in the drying of large variety of products in order to increase the use of renewable energy in industry. In practice drying methods in the industry for this purpose could be dryers that use renewable electricity directly as a power source and dryers that use electricity indirectly. Solar or wind power could be examples of renewable primary energy sources for dryers that use electricity directly and high temperature heat pumps for dryers that use electricity indirectly.

The existing energy-consuming industrial processes that produce EPS-packaging, filtration or insulation products currently use mainly non-renewable materials. Sought for renewable alternatives for these is on-going. These materials are porous, and renewable alternatives are being developed for abovementioned insulation, packaging or filtering. Such materials can be produced from wood fibers and their efficient production demands quality maintaining drying conditions. Main parts of the process are known already, as manufacturing of porous fiber structures has similarities with papermaking process, except that press section is missing to maintain the structure thick and porous. In addition, instead of water, bubbly foam is used as a suspending medium for fiber suspension that enables high air content contained by bubbles. The process, in which bubbly foam is generated is called foam forming. (Smith et al. 1974, 107; Pääkkönen 2020; Ylli 2020.)

1.2 The main objectives of the work

At the beginning of the work, the main objective was to find efficient drying method(s), that could use renewable energy sources, for thick porous biobased fibrous materials. Water removal and energy efficiencies were investigated. An additional objective was to investigate parameters affecting the quality of the structures during drying and the cost of drying.

1.3 Research questions

The main research questions were following.

1. Analysis and investigation of existing drying methods that are expected to be suitable and efficient in drying thick porous biobased fibrous materials. The main considered parameters are heat transfer and water evaporation capacity, possibility to use renewable electricity as energy source and adaptability in the near future.
2. Feasibility of such drying methods for commercial scale operation.
3. Possibilities to control the quality of the product during drying.

The first research task was to explore literature related to the topic in order to reveal the most potential drying methods. After that, the drying experiments were performed on a laboratory scale for the suitable drying methods.

1.4 Outline of the thesis

This thesis includes a literature overview (Chapters 2-5) and an experimental section (Chapters 6-10).

Chapter 2 provides basic information of foam forming. Characteristics of foam are discussed, followed by the principles and advantages of the process. Also, some utilization and product examples are shown.

In Chapter 3, raw materials that are used for foam forming and their properties are discussed. Pulping methods for the renewable pulp types used in the experimental part are briefly explained.

In Chapter 4, primary energy use and its effect on selected methods of microwave and impingement drying methods are discussed. Possible energy sources in the future for these drying methods are examined. The usability of heat pumps and the potential of renewable electricity are discussed.

Different heat transfer methods are presented in Chapter 5, followed by an explanation of the drying process and its phases. Applicability and main limitations for the selected product are presented. The theory of selected drying methods of microwave drying, and impingement

drying is shown briefly. Advantages and utilization examples of these methods are discussed.

Chapter 6 shows the objectives, materials and methods used in the laboratory experiments. Preparation of foam formed samples is followed by the introduction of drying and measuring equipment.

Chapter 7 presents the experimental results. Graphics based on mass change calculations and temperature measurements for both drying methods are presented for selected samples. Microwave power correction calculations were made to gain information from the power that is emitted to water in the sample. Visual quality and tomography imaging analysis were made for selected samples. Compression strength experiments were made for selected samples. At the end of the chapter, average energy consumption calculations during drying for the most used microwave power levels were made and results are shown.

In Chapter 8, possible operational cost calculations for microwave drying process is presented. Drying process is considered to be flexible and movable and process dimensioning is based on the measures of 40 ft container. Flexibility of such system arises from electricity use as an energy source, which is widely available and requires no power plant nearby. Costs considered are energy, raw material, and labor costs.

Chapter 9 includes a discussion on the drying experiment results. And the most important results are summarized in Chapter 10 along with the future suggestions for studies.

1.5 Requirements for new technology

In the production of thick porous fibrous materials from renewable materials, drying plays an important role. If the mechanical press section, which typically removes a major amount of water, is not used, the importance of the dryer section significantly increases. This process requirement arises from of the low density of the end product. The dryer should be energy efficient and at the same time maintain the quality of the product. The dryer section is usually the longest section in paper machines (Knowpap). To keep the costs low, the dryer section should be as efficient as possible, and the drying method should be as energy-efficient as possible. To keep the drying section short and production volumes high, drying should happen fast. To keep the heat and energy losses in the production as low as possible, suitable

drying parameters, depending on the dried product, are important to find and understand. However, energy recovery systems are separate units and their utilization costs in the drying processes increase with the decreased size of the process. The flexibility of the drying can be added if electricity is used as energy. Due to this, energy does not have to be produced at own production site, which saves space and costs at the production end. Thus, production location selection becomes flexible.

Savings in the material costs can be achieved if material quality can be kept at a good level during drying and less or even no reject is produced. Production is automatically increased if drying capacity is improved. Drying machines are limited in the terms of drying capacity, and always require some space.

2 FOAM FORMING

This section discusses the fundamentals of the foam forming process, the foams and their consistency, pilot-scale process applications and product examples. The focus is to get acquainted with the process and the possibilities that are achievable with it.

2.1 Basics of foam forming

The foam forming process was invented first in the 1960s for papermaking. However, foam forming was not used largely in the paper industry at that time and only a few companies used this new technology in their paper mills in the 1970s and 1980s. Nowadays the interest in foam forming has risen again, because of the demand of producing biobased materials to the markets and its potential to produce porous structures for various uses. Also, novel structures with long fibers can be produced. (Hjelt. et al. 2020, 31; Koponen et al. 2018, 482; Kouko et al. 2021, 15.)

Foam forming is a process that makes it possible to produce different kinds of fiber products from a variety of raw materials. The products vary from lightweight packaging materials to construction materials. The advantages of the process compared to water laid forming are its efficiency in energy, raw material and water consumptions. (Hjelt et al. 2020, 1; Koponen et al. 2018, 482.)

2.1.1 About the foams

Foams are multiphase systems, which means that they consist of gas and solid material or liquid. The gas content in foam is usually high, making the structures very light. Foams can be categorized into two main categories: solid foams and liquid foams. Solid foams are used for example in insulation, cushioning and packaging applications. Based on the structure of solid foams, they can be categorized into open cell structures and closed cell foams. In open cell foams, the pores are connected and in closed cell foams, they do not. Formed structures in foam forming are fibrous open cell structures. (Kiiskinen et al. 2019, 499-500.)

Categorizing of liquid foams is based on the liquid fraction Φ, which means the ratio between liquid volume and total volume of foam. Liquid foams are classified as dry foams,

wet foams or bubbly liquids depending on the liquid fraction. In dry foams the liquid fraction is small, and the shape of bubbles is polyhedral while in wet foams where the liquid fraction is larger the shape of bubbles is approximately spherical. In bubbly liquids the shape of bubbles is perfectly spherical and bubbles are relatively free to move. Different foam categories and bubble shapes for different liquid fractions can be seen in Figure 1. There is a critical liquid fraction point at about $\Phi \approx 36$ %, where the bubble shape transforms to spherical (Figure 1). Solid- like foam with connected bubbles is transformed to liquid-like foam with disconnected bubbles in this point and foam is considered as a bubbly liquid. This is also called "jamming transition". Because of jamming, foams have sustained stress and they behave elastically. (Langevin 2017, 48; Kiiskinen et al. 2019, 499-500; Hjelt et al. 2020, 2-3.)

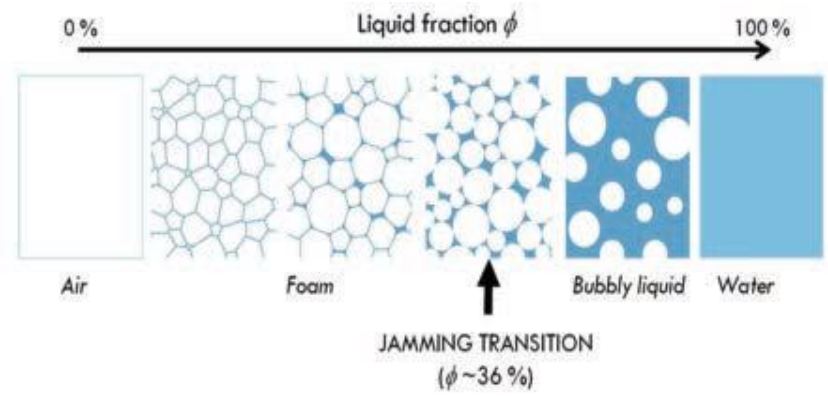

Figure 1: Liquid foam categories for different liquid fractions. (Kiiskinen et al. 2019, 499.)

Foamability and foam stability are the characteristics often used when the foam is characterized. Foamability is usually measured as the rate of volume increase of foam when a specific amount of mixing energy is used. Solution temperature, the composition of the foaming agent and the concentration affect the foamability of a solution. Foam stability is measured by defining the half-life time of the foam or by surveying the transformations in bubble size distribution (BSD). Half-life time means the time that it takes when half of the foam is collapsed. Increasing the foam temperature decreases the half-life time. Three main processes affect foam stability: foam drainage, coarsening and bubble coalescence. Drainage is a process where gravity forces liquid to drain out of foam. Coarsening occurs when large bubbles grow, and small bubbles shrink due to gas diffusion. Coalescence happens when the bubbles connect together because of the rupture in the liquid film between them. (Langevin 2017, 47; Kiiskinen et al. 2019, 500; Hjelt et al. 2020, 3.)

Bubble size distribution (BSD) is also one important measured characteristic of foams. It affects the stability of the foam by creating liquid carrying channels between bubbles when bubble size increases. This enables liquid to transfer more easily and the dewatering phase is enhanced. In a mechanical mixing of the foam, BSD can be narrowed, and average bubble size can be reduced by increasing the mixing speed. (Kiiskinen et al. 2019, 500.)

Liquid foams are thermodynamically unstable, so they will collapse in time. The edges of the film called Plateau borders contain most of the liquid flow. Plateau borders connect three films and nodes connect four Plateau borders. To slow down the collapsing of the foam, stabilizing foaming agents called surfactants must be used. Their role is to decelerate the speed of drainage, coarsening and coalescence. (Langevin 2017, 48.) Foams can be categorized as pseudoplastic fluids. It means that under high shear force conditions, they have low viscosity and under low shear force conditions, high viscosity. (Smith et al. 1974, 107.)

In fiber foams phenomenon called flocculation can happen between fibers. Flocculation happens when high shear forces are directed to fibers and they start to rotate, collide with each other and form bundles called flocs. Fiber distribution becomes unstable as a result of flocculation. When a critical concentration of $6/A^2$, where A is the proportion of fiber length to fiber radius, is exceeded flocculation occurs. For wood pulp fibers, this A value is 60-300. (Punton 1975, 180.)

Dewatering (drainage) of the foam and its resistance against deformation can be improved with increased viscosity. If shear forces directed to foam are low and viscosity of foam is high, fiber movements decrease, and flocculation of fibers is prevented. This allows the web to form and drain faster to a dispersed state. (Radvan and Gatward. 1972, 748; Smith et al. 1974, 107.)

2.1.2 Principle of the process

To generate foam in the foam forming process, fibers, water, and foaming agent (surfactant) have to be mechanically mixed to reach proper air content. This air content is usually 55-75 % (Smith et al. 1974, 107). Air content must be as high as possible to produce as porous structures as possible, but foam still should be liquid-like to enable its processibility (Koponen et al. 2020, 9639). As a result of mixing, small air bubbles involving aqueous foam as a transporting medium of the fibers are formed (Pöhler et al. 2017, 368). The diameter of

formed bubbles is usually between 20-200 µm (Smith et al. 1974, 107; Punton 1975, 185). Forming takes place in a mixing tank or can be done with inline generation. Mixing in a tank is the more common and popular way of forming foam. (Hjelt et al. 2020, 11; Kouko et al. 2021, 15-16.)

A role of the surfactant in the foaming process is to reduce surface tension. As surfactant content is increased, water removal from the mixture is eased (Touchette and Jenness. 1960, 484, 486). Surfactants have a molecular structure that consists lyophobic (hydrophobic) group that has little attraction towards the solvent and lyophilic (hydrophilic) group that has a strong attraction towards the solvent. If surfactant is dissolved into a medium such as water, hydrogen bonds between water molecules are broken and the structure of water is deformed. Due to this, surfactant molecules cover the water by a single layer directing their hydrophobic groups mainly toward the air. When hydrophobic groups and air are both nonpolar, the interface between similar phases reduces the surface tension of water. (Rosen 2004, 2-3.)

In the foam forming process, as much water as possible must be removed from the product to achieve as good quality as possible. Water removal usually includes two parts that are dewatering and thermal drying. In the dewatering part gravity makes water flow downwards through Plateau borders in the fiber-laden foam and consequently, water removes from the bottom of the sample. The dewatering part can be enhanced by using a vacuum or by heating the foam sample. Water viscosity decreases by the effect of increased temperature, which lowers the water flow resistance in fiber-foam structure and water can flow through the structure more easily. Dewatering is usually performed on a wire and when producing paper-like thin materials, fiber foam is wet-pressed before thermal drying. When producing thicker porous materials material must contain air and pressing is not used. In the thermal drying part, evaporation is used to remove the rest of the water after the dewatering part by using non-contact drying methods. Drying methods are discussed closely in chapter 4. Compared to papermaking mechanical pressure towards the sample during thermal drying is not allowed to avoid the collapsing of the fiber network and to maintain the porous structure of the sample. (Alimadadi and Uesaka 2016, 663; Pöhler et al. 2017, 368; Koponen et al. 2020, 9638, 9641.)

2.1.3 Advantages

Compared to water-laid forming, foam forming enables the production of highly porous structures with densities < 10 kg/m^3. This is because the bubbles in the foam support the fibrous composition during manufacturing. This allows using of higher consistencies, which signifies energy and water savings compared to water-laid forming. (Koponen et al. 2020, 9638.) Foam forming increases the bulk, softness and uniformity of the material but decreases its strength properties. Due to this, for example, nonwoven fabrics can be manufactured with less man-made fibers, which are expensive. (Radvan and Gatward. 1972, 750.) The strength properties of foam formed material can however be overcome by beating the fiber mass used in the mixture. High reachable viscosity compared to water-laid forming prevents flocculation of fibers in the mixture. Also, the formation of the end product is improved with the possibility to use various fiber lengths in the mixture. (Smith et al. 1974, 107, 110.)

2.2 Application of the process

2.2.1 Pilot-scale process examples

At VTT Technical Research Center of Finland, a pilot-scale environment for foam forming investigation has been built, located in Jyväskylä. Two pilot machines called VTT SUORA and VTT SAMPO exist there. SUORA was built in 2006 and SAMPO in 2017. (Asikainen et al. 2020, 532.)

SUORA contains forming and press sections followed by a reeler. It was originally designed for the investigation of water-laid products such as paper and board but can be used in foam forming experiments as well after modifications made in 2013. The web width of SUORA is 300 mm and its maximum machine speed is 2000 m/min. The press section consists of a long nip wet pressing unit and cylinder drying is used in the drying section. (Asikainen et al. 2020, 532; Heikkilä et al. 2020, 7.) The structure of SUORA's forming section is described in Figure 2.

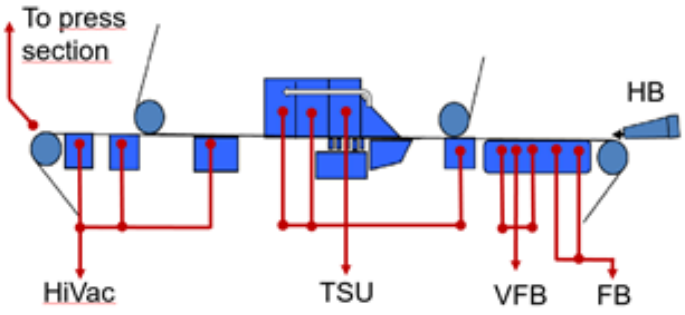

Figure 2: Forming section of SUORA. (HB = headbox, FB = forming board, VFB = vacuum foil boxes, TSU = top suction unit, HiVac = high vacuum section.) (Asikainen et al. 2020, 562.)

When the foam-laid process is run with SUORA, foam can be formed in a tank, with the in-line generation or with the combination of these two. Generated foam is injected into a former section from the headbox. The former section includes forming board (FB) that is equipped with vacuum foil boxes (VFB), followed by a top suction unit (TSU), consisting of three vacuum boxes with loadable blades against one box, and a high vacuum section (HiVac) with three chambers. Suction levels at different parts of the forming section are: VFB: -15 kPa, TSU: -25-(-10) kPa, HiVac: -45-(-15) kPa. (Figure 2.) (Asikainen et al. 2020, 562; Koponen et al. 2018, 483-484.)

The other pilot machine SAMPO was built for better investigation of foam-formed bulky and porous materials. It is manufactured for non-pressed materials and it contains an approach system, forming and drying sections followed with a reeler. SAMPO uses the same process computer and approach system as the older pilot SUORA, which prevents their simultaneous use. SAMPO has a vertical headbox and web width of 600 mm with a maximum machine speed of 200 m/min. The drying section consists of impingement and through-air dryers. (Asikainen et al. 2020, 532; Heikkilä et al. 2020, 7.) SAMPO pilot line setup is shown in Figure 3.

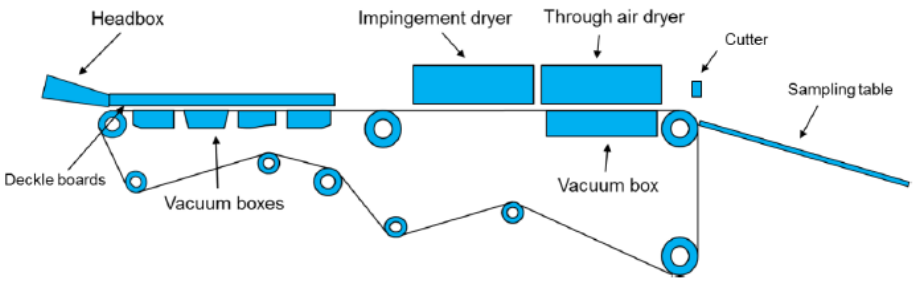

Figure 3: VTT SAMPO foam forming pilot line. (Asikainen et al. 2020, 241.)

Forming section of SAMPO has vertical and horizontal (fourdrinier) (Figure 3) geometry options for forming. When the vertical forming mode is in use 18 vacuum boxes, of which one is a high vacuum box, can be used. This enables better drainage capacity compared to the fourdrinier mode that uses only four vacuum boxes. From these two modes, the fourdrinier mode is designed for thick and porous structures. Vacuum boxes have maximum suction pressure of -20 kPa and one high pressure box has maximum suction of -70 kPa. (Asikainen et al. 2020, 532, 535; Heikkilä et al. 2020, 7.)

2.2.2 Product examples

In the traditional papermaking process, the fiber network has a highly two-dimensional (2D) in-plane orientation, which makes the product's structure layered. Foam forming allows producing of three-dimensional (3D) fiber networks, where fibers can be oriented in an out-of-plane direction (Z-direction). This enables the production of bulky and porous structures. To create these bulky structures, there must be as little in-plane fiber orientation as possible. This can be done by suitable drainage and drying methods that minimize the pressure directed to foam. Compared to layered 2D fiber structures like paper, foam formed 3D structures can have 100 times higher bulk with the same amount of fibers. Less connections are created when 3D porous structure is compared to 2D layered fiber networks. (Alimadadi and Uesaka 2016, 661, 662, 665; Pöhler et al. 2017, 368.)

Foam formed, porous and bulky structures are suitable for example in construction materials, thermal insulations, sound absorption, packaging and filtration. Especially, in thermal insulation, sound absorption and gas filtration, bulky and porous biobased foam formed materials have great potential to be used alongside already commercial products. (Jahangiri et al. 2014, 591; Pöhler et al. 2017, 368.) Examples of structures of bulky and porous foam-formed fiber materials are shown in Figure 4.

Figure 4: Examples of biobased porous foam-formed structures. (Asikainen et al. 2020, 252.)

Pöhler et al. 2017 investigated thermal insulation abilities of foam-formed hardwood (HW), softwood (SW) and thermomechanical pulp (TMP) samples with bulk densities between ~23-89 kg/m^3. Samples were compared to commercial products that were glass wool in two different bulk densities and cellulose wadding product consisting of recycled newsprint, recycled cotton fibers and thermofusible textile fibers. Glass wool had bulk densities of 18 and 29 kg/m^3 and cellulose wadding product had a bulk density of 42 kg/m^3. Better thermal insulation abilities than cellulose wadding products were achieved with foam-formed samples, but the best properties were reached with glass wool. However, when bulk density was close to 45 kg/m^3, foam-formed samples reached their lowest thermal conductivity values that were comparable with glass wool. TMP was the closest of the glass wool in comparison of properties. Air flow resistance was found to increase as bulk density increased and it was at the same level as glass wool.

3 RAW MATERIALS

In this chapter, the raw materials needed for the process are discussed in detail. The specific raw materials are pulp, surfactant and water. Basic information of these raw materials is gone through. Also, their physical features that are involved in the foam forming and drying process are explained.

3.1 Pulp

Pulping is a process that can be done mechanically, chemically, thermally and by combining these methods (Smook 1982, 35). The focus in this chapter is directed to chemical and chemimechanical pulps that are bleached softwood kraft pulp (BSKP) and chemithermomechanical pulp (CTMP), which are also used in the laboratory experiments of the experimental part. More precisely pulp qualities under examination are Metsä Pine (AKI) BSKP, which is pulp quality produced by Metsä Fibre Oy and CTMP, bleached ISO-75%, spruce, CSF (Canadian standard freeness) 600 ml produced by Rottneros. CSF 600 ml is the freeness rate of the pulp, which is the rate of drainage of a dilute suspension of pulp. (T 227 om-94: 1984, 1.) Pulping processes for these pulp qualities are gone through briefly, together with some properties of these pulps.

In chemical pulping, wood chips are cooked at a certain temperature and pressure in a mixture of suitable chemicals and an aqueous medium. The purpose of the chemical pulping process is to dissolve the lignin and retain most of the cellulose and hemicellulose. Two main chemical pulping methods are the kraft process and sulfite process.

In a kraft process, white liquor is used as a cooking (digestion) solution for wood chips. White liquor consists of sodium hydroxide (NaOH) and sodium sulfide (Na_2S) that are the cooking chemicals. As cooking or bleaching is completed, about half of the feedstock material, mostly lignin, is dissolved in the spent cooking liquor, also known as black liquor. Black liquor is then separated from the pulp and concentrated with the evaporators to 65-80 % dry solids content. Concentrated black liquor is then burned in the recovery boiler to recover the cooking chemicals and to produce energy. Inorganic smelt is produced via the combustion of black liquor. This smelt consists mostly of sodium carbonate (Na_2CO_3) and Na_2S. The

smelt is then formed into green liquor by dissolving it into water. To convert Na_2CO_3 into NaOH to recover the white liquor for the new cook, causticizing must be done. In the causticizing process, green liquor is reacted with quick lime (CaO). In the kraft process, cooking temperatures are usually 170-180 °C and cooking time is 2-4 h. The yield of the process is ~35-60 % of dry wood. (Forestbiofacts; Smook 1982, 38-39, 66-67.)

BSKP is made of kraft pulp by bleaching it. The purpose of bleaching is to make pulp brighter. For bleaching, the pulp is treated with different chemicals in varying conditions in many stages. Washing is carried out between every stage to prevent the moving of possible dissolved organic materials that can contain bleaching chemicals, to the next stages. The most common bleaching stages are reaction with Cl in acidic solution, dissolution of reaction products with NaOH, reaction with hypochlorite in alkaline solution, reaction with chloride dioxide (ClO_2) in acidic solution, reaction with peroxides in alkaline solution, high-pressure reaction with elemental oxygen in alkaline solution and mixing of chloride (Cl_2) and ClO_2. (Smook 1982, 154.)

BSKP is known for its long, thin and strong fibers with good tensile and bonding properties. Example of product, Metsä Fibre Oy Metsä Pine (AKI) BSKP has a typical fiber length of 2,1 mm. It is made out of pine and spruce with the quantities of 50-80 % pine and 20-50 % spruce. The pH of the pulp varies between 5-7. When pulp is refined with higher specific energy, the tensile index and density of the pulp are increased, whereas tear index and freeness value (CSF) are decreased. When specific refining energy is increased from 0 kWh/t to 100 kWh/t tensile index of manufactured sheet is increased from 23 Nm/g to 75 Nm/g and the density of the pulp is increased from 570 kg/m^3 to 713 kg/m^3. The tear index is decreased from 16,4 mNm^2/g to 14,2 mNm^2/g and CSF is decreased from 704 ml to 553 ml. These values are based on Metsä Fibre Oy pulp testing measurements. Typical end uses of BSKP are specialty papers, wood-free papers, tissue papers and board products. (Metsä Fibre Oy 2021.)

Chemimechanical pulping is a process where chemical treatment is combined with mechanical refining. Wood chips are used as a raw material in the process. Chemimechanical pulps can be split into two different groups that are chemimechanical pulp (CMP) and chemithermomechanical pulp (CTMP). Now focus is directed to CTMP. CTMP is thermomechanical

pulp that is nourished with chemicals (Rottneros 2019). First, in the CTMP process, wood chips are washed, after which the impregnation stage takes place. The most common impregnation methods are steaming and then soaking the wood chips in a sulphite solution and mechanically compressing the chips, followed by expanding them in a sulphite solution. With chemical treatment, lignin is swollen to make it soluble and easier to remove. After the chemical pretreatment stage, the refining stage takes place. Refining can be done in one- or two stages, depending on the specific energy needed to achieve desired properties for pulp. A two-stage refining process with separate reject refining is the most common chemimechanical pulping method for CTMP. After the refining stage, the screening stage takes place. In the screening stage, harmful particles are removed from good fibers (Smook 1982, 99). The screening stage is followed by possible bleaching before drying and baling of the pulp. CTMP process allows chemical treatment to be performed in various possible stages during mechanical refining. For example, in two-stage refining, chemicals can be added before the first refining stage and/or between the two stages. For softwoods, the most used chemical is sodium sulphite (Na_2SO_3) and for hardwoods - sodium hydroxide and/or sodium sulphite. The yield the in CTMP process is ~90 %. (Lönnberg et al. 2009, 248-262.) Typical production conditions for softwood and hardwood CTMP are given in Table 1.

Table 1: Typical production conditions for softwood and hardwood CTMP. Chemical doses are informed as a % of wood dry matter. (Lönnberg et al. 2009.)

CTMP type	Na_2SO_3 dose [%]	NaOH dose [%]	pH	Reaction temperature [°C]	Reaction time [min]
Softwood	2-4	-	9-10	120-135	2-15
Hardwood	0-4	1-7	12-13	60-120	0-30

CTMP pulps with high CSF values have fiber lengths close to kraft pulps. The typical fiber length of Rottneros CTMP, bleached ISO-75%, spruce, CSF 600 ml is 1,9-2,0 mm. For CTMP that has CSF of 600 ml, the typical tensile index of sheet manufactured from it is 19-21 Nm/g and the tear index is 8-11 mNm^2/g. Comparison of the properties of CTMP and BSKP with CSF of 600 ml are given in Table 2. Typical end uses of CTMP with high freeness are tissue papers and board products.

Table 2: Typical properties of BSKP and softwood CTMP pulps with freeness of 600 ml. (Lönnberg et al. 2009, 274, 276; Metsä Fibre Oy 2021.)

Pulp	Tensile index [Nm/g]	Tear index [mNm^2/g]	Density [kg/m^3]	Fiber length [mm]
BSKP	67	15	690	2,1
CTMP	20	10	400	1,9

3.2 Surfactant

As was discussed earlier, the role of surfactant is to reduce the surface tension of the liquid to aid the bubble formation. Now the focus is on sodium dodecyl sulphate (SDS), which is the surfactant that is used in the laboratory experiments of the experimental part. As SDS concentration is increased, surface tension is decreased. For example, in phosphate buffer solution SDS increase from 10 µmol/L to 1 mmol/L decreases surface tension from 70 mN/m to 40 mN/m. (Gimel and Brown. 1996, 8114.) SDS is an anionic surfactant, which makes it very suitable for foam forming because of its good foamability, stability, solubility, and small needed dose. SDS is a synthetic organic compound that has an amphiphilic structure, which means it has hydrophobic and hydrophilic parts. It consists of anionic organosulphate attached to a sulfate group. SDS can be made by first reacting dodecyl alcohol (dodecanol) with sulfuric acid, which results in dodecyl sulphate. Then, mixing the dodecyl sulphate with sodium hydroxide. The chemical formula of SDS is $CH_3(CH_2)_{11}SO_4Na$ and it is presented in Figure 5. The application of SDS is in industry and fundamental studies. It is used for example in detergents and toothpastes. It also has a low price, which is beneficial in the market. (Wołowicz and Staszak. 2020, 1-2.)

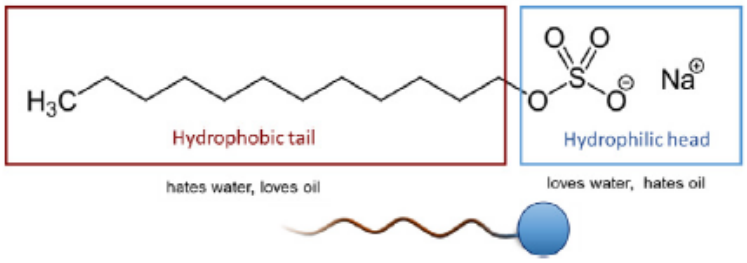

Figure 5: Chemical structure of SDS. (Wołowicz and Staszak. 2020, 2.)

3.3 Water

Water molecules have a polar covalent bond that have a tetrahedral arrangement between oxygen atom and two hydrogen atoms. To form bonds, energy is needed and breaking bonds releases energy. Electrons are not evenly shared between the oxygen atom and hydrogen atoms in the water molecule. Due to this charge separation, momentary dipoles are induced which makes water a good solvent. Also, small molecule size of water is favorable property for solvent. An example of bond forming is foam forming, where water works as a solvent when the bond is formed between fibers, surfactant and water by using mechanical energy for mixing. (Hanslmeier 2011, 7, 11-12.)

From a drying perspective, water must be evaporated to remove it from the substance. The energy is needed first to heat water to boiling point and second to vaporize it. Specific heat capacity for water at 25 °C is c_p = 4,18 kJ/kgK. It means that to increase water temperature by a certain temperature interval this amount of energy is needed. The heat of vaporization of water is h_{ev} = 2260 kJ/kg. (Hanslmeier 2011, 13-15.)

In the drying of porous fibrous materials, water must flow through fiber-foam structure to be removed. As was discussed earlier, water viscosity decreases as the temperature increases. Due to viscosity decrease, the flow of water is eased. At 20 °C and atmospheric pressure, the mean viscosity of water is ~1,0016 mPa·s (Gupta 2014, 221). Dynamic viscosity as a function of temperature for water at atmospheric pressure is illustrated in Figure 6.

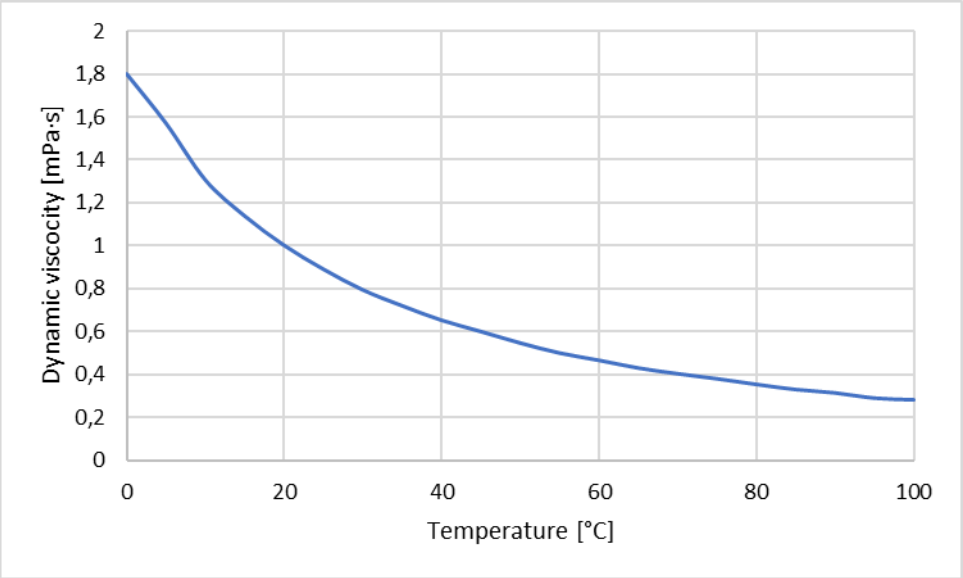

Figure 6: Water dynamic viscosity as a function of temperature at 1 atm. (Gupta 2014, 224; Souza and König. 2012, 156.)

It can be seen from Figure 6 that the dynamic viscosity of water is decreased from ~1,8 mPa·s to ~0,28 mPa·s when the temperature rises from 0 to 100 °C. Temperature increase also decreases the surface tension of water, which makes water molecules more active by increasing their movement (Vargaftik et al. 1983, 819). For the drying perspective, it means that when water reaches its boiling point and starts to evaporate, dynamic viscosity is much lower, and water can flow through matter more easily.

4 DRYING

In this chapter, the drying process fundamentals are discussed. Heat transfer methods are reviewed, and the principle of the drying process is explained. Drying technologies that are the most relevant for thick porous materials are presented, while the unsuitable drying methods are excluded. Drying methods that could use renewable electricity as a power source and will not apply mechanical pressure on the product are selected.

4.1 Fundamentals of drying

4.1.1 Heat transfer methods

Three main heat transfer methods are usually used in the drying of paper and other fiber products. These methods are conductive, convective, and radiative heat transfer. (Karlsson et al. 2000, 68.) Basic equations for these heat transfer methods in their boundary conditions, are reviewed.

In conduction drying, the drying energy is produced by pressing the heated surface against the web. The conductive heat transfer can be solved from Equation 1 (Karlsson et al. 2000, 68.):

$$q_{\mathrm{cond}} = \alpha_{\mathrm{cond}} \cdot (T_{\mathrm{s}} - T_{\mathrm{web}}) \quad (1)$$

where q_{cond} is conductive heat flow [W/m^2], α_{cond} is contact heat transfer coefficient [W/m^{2}K], T_{s} is hot surface temperature [K] and T_{web} is the temperature of the web surface [K].

In convective drying, heat energy is transferred to the web by convection through the air. Heat transfer from air to the web can be solved from Equation 2 (Karlsson et al. 2000, 68.):

$$q_{\mathrm{conv}} = \alpha_{\mathrm{conv}} \cdot (T_{\mathrm{a}} - T_{\mathrm{web}}) \quad (2)$$

where q_{conv} is convective heat flow [W/m^2], α_{conv} is the convective heat coefficient [W/m^{2}K] and T_{a} is air temperature [K].

Radiative heat transfer transfers heat to the material by electromagnetic radiation. Radiation penetrates the material and absorbs gradually while passing through. Absorption in the web can be indicated in several ways, but a simple way is by using empirical absorption efficiencies. This way, absorbed heat flux can be solved from Equation 3 (Karlsson et al. 2000, 69.):

$$q_{\text{abs}} = q_{\text{input}} \cdot \eta_{\text{rad}} \cdot \eta_{\text{abs}} \quad (3)$$

where q_{abs} is absorbed heat flux [W], q_{input} is input energy converted by radiator [W], η_{rad} is radiator efficiency [-] and η_{abs} is absorption efficiency of the radiation to the web [-].

In practice, the conductive drying method is not suitable for drying of thick, porous materials as the conduction through porous web becomes limited as soon as surface facing drying side becomes dry. Woody materials are good insulators when dry as their thermal insulation abilities are at the same level as mineral wool and fiberglass. (Ecostar Insulation 2019).

4.1.2 Drying process

As a process, drying is based on heat transfer and mass change by evaporating the water from a solid material (Asikainen et al. 2020, 388.). The drying process can be distributed into three different phases. These phases are the heating, constant drying rate phase and falling drying rate phase. Depending on conditions all these phases will not necessarily occur during drying. (Karlsson et al. 2000, 62.)

In the heating phase, the drying rate, and the temperature of the web increase gradually until they reach the constant rate conditions. In the constant drying rate phase, the drying rate and the temperature of the web are constant. This happens due energy that is consumed for water vaporization is equal to the energy that is put into the web. In this phase, the resistance for water vapor diffusion can be overridden, so evaporation can happen in the web and on the surface of the web. When moisture content decreases in the material, vapor diffusion resistance starts to increase from the interior to the surface, drying rate starts to decrease and falling rate phase occurs. Resistance increase happens because the thermal conductivity of the web decreases and the hygroscopic nature of pulp fiber decrease vapor partial pressure. The falling drying rate phase can be divided into two components. These components are the first and second falling rate phases. The transition between the first and second falling rate phases is the point where the web has lost all its free water. The point where the constant

drying rate phase changes to the falling drying rate phase is called critical moisture content (CMC). When the basis weight of the material increases, the CMC also increases. This happens because the material surface dries earlier with the thicker materials. Faster surface drying happens due to earlier stopping of capillary flow that keeps the surfaces saturated. (Karlsson et al. 2000, 62-63.)

4.2 Different drying methods

4.2.1 Microwave drying

Microwaves are electromagnetic waves. Range of microwave wavelengths is 1 mm to 1 m. Microwave drying or heating takes place between frequencies 300 MHz-300 GHz. (Schiffmann 2014, 286.)

When an electromagnetic wave goes through the medium the frequency of the wave stays the same. The speed of wave that is equivalent to the speed of light in air or vacuum also slows down. Due to these, the wavelength of the electromagnetic wave changes. These occurrences are demonstrated in Equations 4 and 5. The frequency of the electromagnetic wave can be solved from Equation 4 (Schiffmann 2014, 289.):

$$f = \frac{V_\mathrm{p}}{\lambda} \tag{4}$$

where f is the frequency of the wave [1/s], V_p is the velocity of propagation [m/s] and λ is the wavelength [m].

The velocity of propagation can be solved from Equation 5 (Schiffmann 2014, 288.):

$$V_\mathrm{p} = \frac{c}{\sqrt{\varepsilon'}} \tag{5}$$

where c is the speed of light in the air [m/s] and ε' is the dielectric constant of the material which wave is piercing [-].

Microwave systems operate on nominal fixed frequencies that are 915 MHz and 2450 MHz. These frequencies have been found to be the most favorable for water to absorb microwaves and convert them to heat (Asghari 2015, 9). To create these frequencies from alternate currencies (AC) of 50 or 60 Hz, generators must be used. Generators used in microwave

systems, include a direct current (DC) power supply and a magnetron or a klystron tube. Tubes are constant output power devices and power is usually controlled by indirectly changing the DC anode voltage. Generated microwave energy must be transferred to the applicator, which focuses the energy load to the destination. Waveguides, brass or aluminum channels of rectangular shape are usually used to transfer this energy. Materials used in applicators are always metals, so waveguides can also be used as applicators by themselves. These are called traveling wave applicators. In these applications, waveguides are assembled by connecting several waveguides for example to slotted form. This form allows multiple heating points to the material as the waveguide makes several turns back and forth. (Schiffmann 2014, 296-297.) An example of slotted waveguide is expressed in Figure 7.

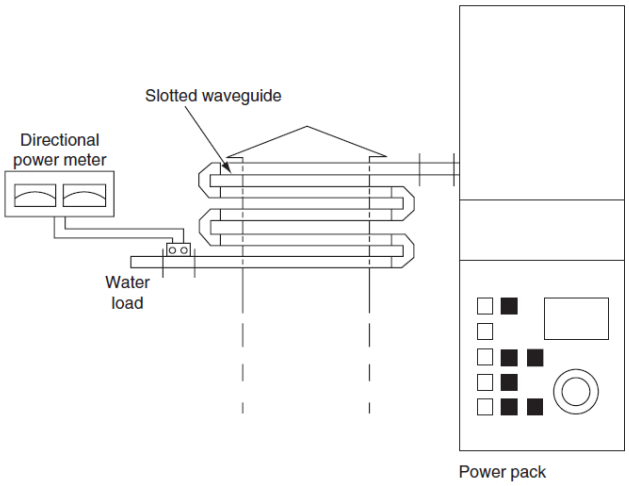

Figure 7: Slotted waveguide. (Schiffmann 2014.)

One advantage of microwave heating is that it penetrates the material and can heat the material very fast also from the inside. This also enables lower heating temperatures. Another advantage is that it can be adjusted easily for different purposes. Control of heating can be very accurate and efficient with fast controlling with a power generator. Surface temperatures stay usually that low that surface damages can be avoided, which leads to better product quality. However, specific parameters affect to the heating speed. These are the output power of the microwave system, power generated in the material, the mass of material, the specific heat of the material, dielectric properties, the geometry of material, heat loss mechanisms and coupling efficiency. (Schiffmann 2014, 293-294.)

Microwave heating can reduce costs in many ways. These are for example reduced material, maintenance and labor costs, speed and efficiency of the process, energy savings due to less heat load of the plant and less space that is needed for the process. (Schiffmann 2014, 302.)

Microwave drying can effectively evaporate water from inside of the structure, whereas conventional drying methods efficiently remove water from the surface of the structure with hot air. These two different drying techniques combined can enhance the drying efficiency and reduce drying costs. (Schiffmann 2014, 293-294.)

4.2.2 Impingement drying

Impingement drying is used for various purposes in industry. Rapid drying of thin sheets in continuous production, such as paper making, is utilizing impingement drying. Also, thicker sheets like veneer or lumber are dried with impingement dryers. Most of the heat transfer happens via convection, but a small amount happens via radiation. (Karlsson et al. 2000, 127, 134; Mujumdar 2014, 385.)

The main process parameters in impingement drying are air temperature, jet velocity, air moisture content and nozzle geometry. Other factors that affect the heat transfer in impingement drying are evaporation from the web, pressure difference over the dried product, surface under the dried product, movement of the surface and radiation heat from the nozzle plate. (Karlsson et al. 2000, 127-128.)

There are two main methods for impingement drying. These methods are direct impingement and indirect impingement. Direct impingement enables the most efficient drying rate and energy efficiency when the air jet is directed straight towards the surface that is dried. Indirect impingement is usually done by using fabric between the dryer and the dried material. It lowers the energy efficiency and drying rate a lot, but it is sometimes used for example in papermaking when there is a need to lower the risk of observation due to broke. Air temperatures must be lower (close to the web temperature) in indirect impingement, because of the temperature limits of fabrics. Due to this, dried material cannot absorb any energy from impingement air and most of the heat is released to the surroundings. (Karlsson et al. 2000, 137-138.)

In impingement drying, heat flow that arrives from nozzles to surface of the web via convection can be solved from Equation 6:

$$q_{\text{web}} = -\alpha \cdot (T_{\text{a}} - T_{\text{s}}) \cdot \frac{E}{e^E - 1} \tag{6}$$

where q_{web} is heat flow to the surface of the web [W/m^2].

Heat flow arriving at the surface of dried material can be solved from Equation 7:

$$q_{\text{mat}} = -\alpha \cdot (T_{\text{a}} - T_{\text{s}}) \cdot \frac{E}{1 - e^E} \tag{7}$$

where q_{mat} is heat flow to the surface of the dried material [W/m^2].

In Equations 6 and 7, factors $\frac{E}{e^E - 1}$ and $\frac{E}{1 - e^E}$ are Ackerman's factors. E can be solved from Equation 8:

$$E = \frac{\dot{m_{\text{ev}}}}{A} \cdot \frac{c_{p,\text{v}}}{\alpha} \cdot \frac{T_{\text{ex}} - T_{\text{s}}}{T_{\text{a}} - T_{\text{s}}} \tag{8}$$

where $\dot{m_{\text{ev}}}$ is the mass flow of evaporated water [kg/s], A is the area of dried surface [m^2], $c_{p,\text{v}}$ is the specific heat of vapor [J/kgK] and T_{ex} is the exhaust air temperature [K].

Illustrative presentation of heat transfer of air impingement drying, and evaporation are shown in the Figure 8 below. As can be seen, most of the heat transfer happens via convection of hot impingement air, but some heat radiation happens from hot surfaces.

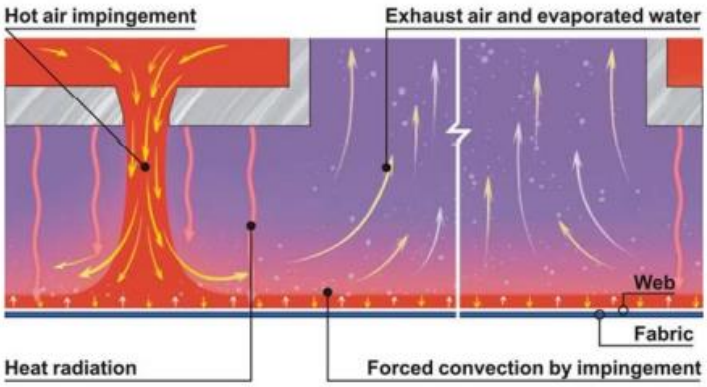

Figure 8: Heat transfer of air impingement drying and evaporation from the web. (Valmet 2012.)

5 PRIMARY ENERGY TRENDS

In this chapter primary energy use, its development for the future due to energy revolution, and its effect on microwave and impingement drying methods are discussed. Steam has been the primary energy source in drying, but nowadays electricity could be utilized as a drying energy source directly or indirectly. Possible energy sources in the future for these drying methods are examined. The potential of usage of high-temperature heat pumps in impingement drying and the utility of renewable electricity for microwave drying are examined briefly.

5.1 Primary energy development

During the next 30 years, electricity consumption will increase, and renewable energy sources will reach the same or even larger share as coal has nowadays in power generation. Solar and wind energy capacity will increase most out of renewable energy sources by 2050, because of growing investment in these sources. (British Petroleum 2020, 7.)

High-temperature heat pumps currently have a temperature limit of 180 °C, which might limit their drying efficiency compared to dryers using electricity directly (Sintef 2021). For example, new porous biobased fiber structures require novel approaches for drying. In practice, suitable drying methods could be impingement drying for indirect electricity use and microwave drying for direct electricity use. Primary energy consumption by source in 2018 and 2050 (estimated) globally is illustrated in Figure 9. It is noticeable that renewable energy consumption is estimated to increase over ten times growing from 27 EJ (2018) to 277 EJ (2050). This makes it the highest consumed energy source. Hydro power consumption is estimated to increase about 20 EJ. Oil consumption is estimated to drop in half from 2018 to 2050 and coal consumption is estimated to be only 15 % of 2018 consumption in 2050. Natural gas will remain its consumption in the same level while nuclear power will be almost doubled.

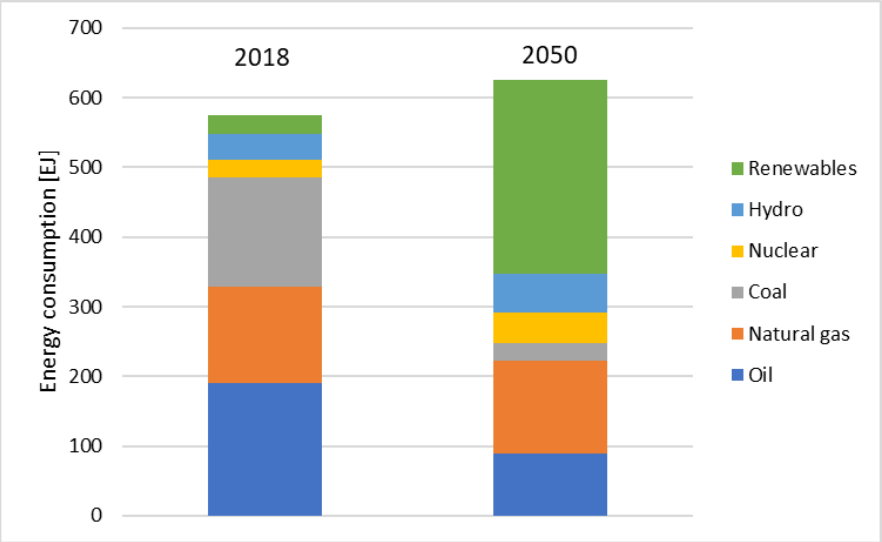

Figure 9: Global primary energy consumption by source in 2018 (left) and estimated 2050 consumption (right). (British Petroleum 2020, 64.)

5.2 Impingement drying

The air impingement drying method that uses high-velocity hot air jets to dry products makes it possible to use indirect electricity as an energy source (Karlsson et al. 2000, 73). One possible technique that could be exploited is high-temperature heat pumps. These heat pumps can use low-temperature waste heat to produce high-temperature process heat by using electricity as an added energy source. In the case of impingement drying, for example solar energy could be used as an indirect electricity source to heat impingement air with waste heat received from some cooling process. The coefficient of performance (COP) describes the efficiency of a pump and is the ratio of heat output to electrical input. These high-temperature heat pumps can have COP of 2-5. (Ahrens 2021.) COP value's theoretical maximum for the heat pump operating with constant temperatures can be determined with the Carnot process. Carnot process is described in the Equation 9 (Ahrens et al. 2021, 4.):

$$COP_{\text{carnot}} = \frac{T_{\text{sink}}}{T_{\text{sink}} - T_{\text{source}}} \tag{9}$$

Where COP_{carnot} is theoretical maximum for coefficient of performance [-], T_{sink} is process heat temperature [K] and T_{source} is waste heat temperature [K].

To calculate true COP, Carnot efficiency must be considered. If COP of 5 is wanted when produced process heat is 180 °C and Carnot efficiency is 50 %, waste heat temperature of

~135 °C is needed. If Carnot efficiency is increased to 60 %, waste heat temperature can be ~126 °C.

A simple illustration of the most common heat pump process, the vapor compression cycle, is shown in Figure 10. In the vapor compression cycle, refrigerant circulates in a closed circuit. State of refrigerant changes during the circuit giving out heat to the low-temperature waste heat converting it to high-temperature process heat. First, refrigerant is in a low temperature state at low-pressure side and is heated to low-pressure vapor by waste heat in the evaporator. Then added electricity is used to run the compressor increasing the vapor pressure and temperature making it high-temperature vapor. High-temperature vapor is then transferred through the condenser giving out heat to heat up the waste heat to process heat. After the condenser, the circulating refrigerant condenses back to a liquid state and it is expanded back to low pressure and temperature state in the expansion valve. (Ahrens 2021.)

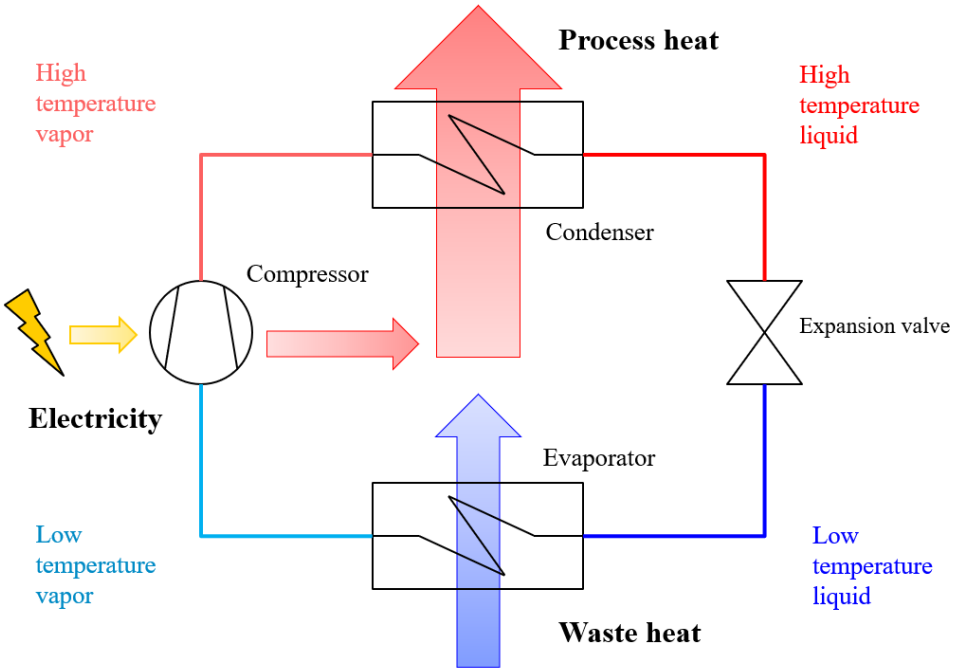

Figure 10: High-temperature heat pump process. (Ahrens 2021.)

5.3 Microwave drying

The microwave drying process that uses electricity directly as a source of power has variety of possibilities to use amongst renewable energy sources. When process steam is not needed, it can use any type of electricity. As renewable energy sources take over most of the energy consumption in the future (Figure 9), they will probably be primary energy sources for

microwave drying as well. Energy system transition to lower carbon system opens possibilities to use energy more versatile, which allows consumers to have more options. Energy markets will be more localized, which is advantageous for energy sources like solar and wind power that are under high development. Localized energy markets enable smaller areal production amounts, which is also beneficial for solar and wind power. This also favors microwave drying because of its low operating heat loads and high process efficiency. Microwave drying has an on-off heating nature with rapid heating and fast controllable output power adjusting, which makes it a highly suitable drying method, powered by renewable electricity, in the future. (British Petroleum 2020, 7; Schiffmann 2014, 293.)

EXPERIMENTAL PART

6 MATERIALS AND METHODS

To achieve the most energy-efficient and cost-efficient process for the manufacturing of thick porous fiber structures, the drying part of the process must be optimized. The quality of the product must be considered when the drying process is been designed. This means that structural or visual damage to the product during drying is to be prevented.

In this study, two different drying methods were investigated experimentally on a laboratory scale. Drying methods using conductive heat transfer were ruled out, so one drying method using convective heat transfer and one using radiative heat transfer were chosen. These drying methods were impingement drying and microwave drying. Experiments took place in VTT Jyväskylä, Central Finland. Foam forming was used as a technology to produce porous samples for drying experiments. Used fiber raw materials were Metsä Pine (AKI) pre-refined BSKP pine pulp from Metsä Fibre Oy, Äänekoski Bioproduct Mill Finland, and bleached spruce chemi-thermomechanical pulp (CTMP, CSF 600 ml) from Rottneros AB, Rottneros Mill, Sweden. Drying was examined by observing the mass change of the samples during drying in the form of removing water. Also, temperature measurements were made.

6.1 Sample preparation

Pine pulp and CTMP samples were formed in the laboratory using sodium dodecyl sulphate (SDS) as a surfactant of the foam. SDS that was diluted to 10 % was used in these experiments. The dosage of the 10 % SDS was 6 mL/L.

To determine what kind of fibers used masses consist, fiber analysis was made for both pine pulp and CTMP. Analysis was made with L&W Fiber Tester Code 912 Plus -measurement system (Figure 11). Analysis was performed by following the work instruction based on the modified ISO 16065-2 Pulps- Determination of fibre length by automated optical analysis, Unpolarizsed light method -standard.

Figure 11: L&W Fiber Tester Code 912 Plus -fiber analyzer.

Two fiber analyses were made for both raw materials to ensure the correctness of the results. The average mean length of pine pulp fibers was 2,025 mm and the average mean width was 29,3 µm. CTMP had an average mean length of 1,900 mm and average mean width of 38,4 µm. As can be seen, pine pulp had longer but on average thinner fibers than CTMP. It was also noticeable that CTMP had average mean fines 56,3 % when pine pulp had 27,6 %.

Samples that had pine pulp as a raw material were prepared by using pre-refined pine pulp from Metsä Fibre Äänekoski mill. The consistency of pine pulp was about 4 %. Consistency was increased before foaming by removing water by pressing the mass against the wire and decreased by adding water to the mass. CTMP samples were prepared from over 90 % dry content CTMP and from 25-26 % consistency screwed CTMP by wet dissolving them to lower consistencies. Wet dissolving was performed by following the work instruction based on the standards: EN-ISO 5263-2 Pulps-Laboratory wet disintegration. Part 2: Disintegration of mechanical pulps at 20 degrees °C and SFS-EN ISO 5263-1 Pulps-Laboratory wet disintegration. Part 1: Disintegration of chemical pulps. Instructions for mechanical mass were

followed in the pre-treatment part and instructions for chemical mass were followed after soaking. First, a decided amount of high consistency CTMP was weighed and put in a measuring vessel. After that, analysis pure water was added to get the volume of the 1 or 2 liters for the mixture. Then, the mixture had to be soaked minimum of 4 hours with over 60 % consistency pulp. After soaking, the mixture was poured into a wet dissolver (Figure 12) and mixed 30 000 rounds with a mixing blade. After the disintegration, the fiber mixture was ready for foam generation.

Figure 12: CTMP in ~2,5 % consistency after wet disintegration.

The samples were foam formed in the 5-liter cylindrical foaming vessel. The foam was generated with Netzsch mixer (Figure 13). A mixing rate of 3800 rpm was used and mixing was completed after the vortex was closed. Mixing time varied depending on the raw material and consistency of the fiber mixture but was typically 1,5 to 3 minutes. It was noticed that when the consistency was higher, mixing time also raised and vice versa. Depending on the consistency of the fiber mixture, the air content of the foam varied. Lower consistency mixtures reached higher volume after foaming, which meant higher air content. Air contents of 29-67 % were obtained during experiments.

Figure 13: Netzsch mixer that was used in foam generation.

When the foam was generated it was poured into the mold to drain immediately after forming. Drainage of the samples was a minimum of 15 minutes to get the most of free water out of the samples via gravity before drying. After drainage, samples were transferred to dryers, weighed, and drying could start. Molds that were used in the experiments were spherical in shape, to avoid possible corner effects during drying. In impingement drying experiments two different sizes of molds were used, 30 mm and 60 mm deep molds with 163 mm diameter. These molds were both made of metal. In microwave drying experiments, three different sizes of molds were used, i.e. 39 mm, 49 mm and 79 mm deep molds with 150 mm diameter. These molds were made of plastic. To make drainage and drying possible, there were a wire on the bottom of the sample and other supportive structures (Figure 14). Different kinds of drying setups were used during experiments. Weights of these setups were taken into account when samples were weighed during experiments. Weights of the setups varied from about 415 g to 585 g in impingement drying and from about 276 g to 371 g in microwave drying.

Figure 14: Examples of drainage and drying setup for impingement (left) and microwave (right) drying.

The moisture ratio of the foam formed samples before impingement drying was 12,2-14,6 kg/kg and dry solids content varied between 6,4-7,6 %. Before microwave drying moisture ratio of the samples was 7,0-19,3 kg/kg and dry solids content varied between 4,9-12,5 % (Section 6.3). Trial point set was wider in microwave drying experiments than in impingement drying experiments, which explains the variation in moisture ratios and dry solid contents after drainage.

6.2 Drying equipment

6.2.1 Impingement drying

Impingement drying experiments were executed at “Combo” air impingement dryer, which is built at VTT Jyväskylä. This dryer consists supportive table that has a movable platform for dried samples, a mounted air impingement box with round 2,5 mm diameter nozzles consisting 1,5 % of the area of impingement box, a frequency-controlled fan and electric resistance heating elements to heat impingement air (Timofeev and Jetsu. 2021, 5). The air impingement box with the table and controlling unit can be seen in the Figure 15. Distance from nozzles to the movable platform was 75 mm and kept constant in all the experiments. Distance to sample surface was ~15 mm with 60 mm mold and ~47 mm with 30 mm mold as samples shrank during drainage.

Figure 15: Air impingement box mounted to supportive table.

Jet velocities of 30 m/s and 50 m/s, which was maximum with existing fan-setup, and air temperatures of 150 ºC and 200 ºC were used in the experiments. Air jet velocities were monitored with Mikor TT4702 air pressure meter (Figure 16), which was connected to the air impingement box with a pitot-tube and wire to get a signal to the device. Mikor pressure meter has pitot-tube velocity range calibrated for air at 16 ºC and 1000 mbar. For other conditions, true velocity could be calculated by multiplying the reading of the meter with the velocity factor. Density of air decreases as temperature increases. Due to that and effect of the velocity factor, reading in the device had to be a little lower than target velocity. The impingement air temperature was monitored from Fluke 52 II thermometer (Figure 16) that was attached to the air impingement box with thermocouple wires. Thermocouples are made from two wire leads that are welded together to create a junction. These wire leads are made from different metals and when temperature changes between junction and end of the wires, voltage that changes over temperature is generated. This junction is called a hot junction. Another junction is an isothermal block that stays at a known constant temperature, known as a cold junction. These junctions create a thermoelectric circuit. Usually, an analog-to-digital converter (ADC) is connected to the isothermal cold junction to monitor the

temperature. (Wu 2018, 3.) The principle of thermocouple can be seen from Figure 17. Wire type A illustrates the +lead and wire type B illustrates the -lead.

Figure 16: Mikor TT4705 pressure meter (left) for jet velocity monitoring and Fluke 54 II thermometer (right) for jet temperature monitoring.

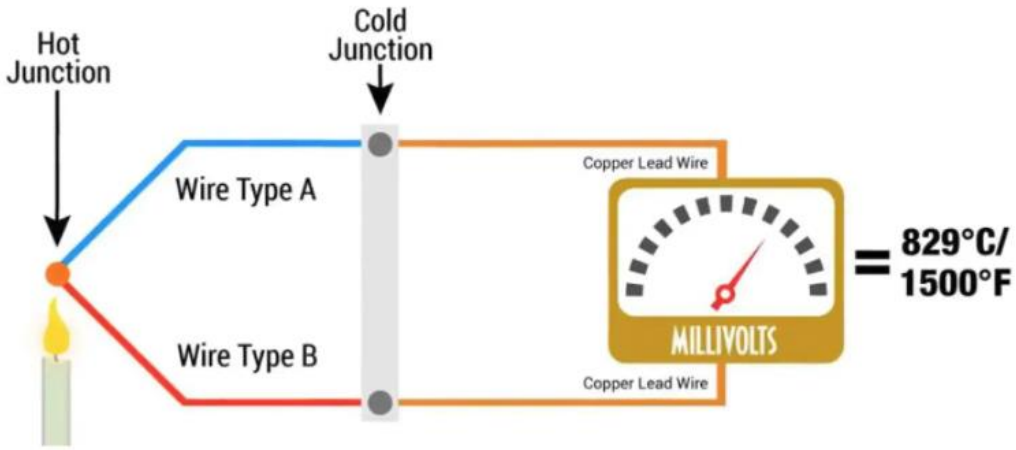

Figure 17: Working principle of the thermocouple. (Omega Engineering 2019.)

There are different types of thermocouples depending on the metal pairs that create the junction. Temperature range and accuracy are the most important factors that alter between different thermocouple types. Thermocouple types are designated with one letter to denote the

used metals. (Wu 2018, 4.) Used thermocouples were K-type. Alloy combination for this type is nickel-chromium for +lead and nickel-aluminum for -lead. Maximum temperature range of K-type thermocouple is from -200 ºC to 1250 ºC. (National Institute of Standards and Technology (NIST). 2000, 214.)

To start up the dryer, power had to be put on by pressing the “emergency stop offset”-button at the bottom of the control panel (Figure 18). After that, the fan was turned on. The speed of the fan could be read from the monitor of the blue panel (Figure 18), which is the control panel of the fan. The velocity of the air jet could be changed by adjusting the rounds of the fan from the control panel of the fan (Figure 18). The impingement air heaters were turned on first from the main switch of the heaters and after that heating power was adjusted with 3 kW and 9 kW switches (Figure 18). Air temperature could be monitored from the screen on the panel above (Figure 18).

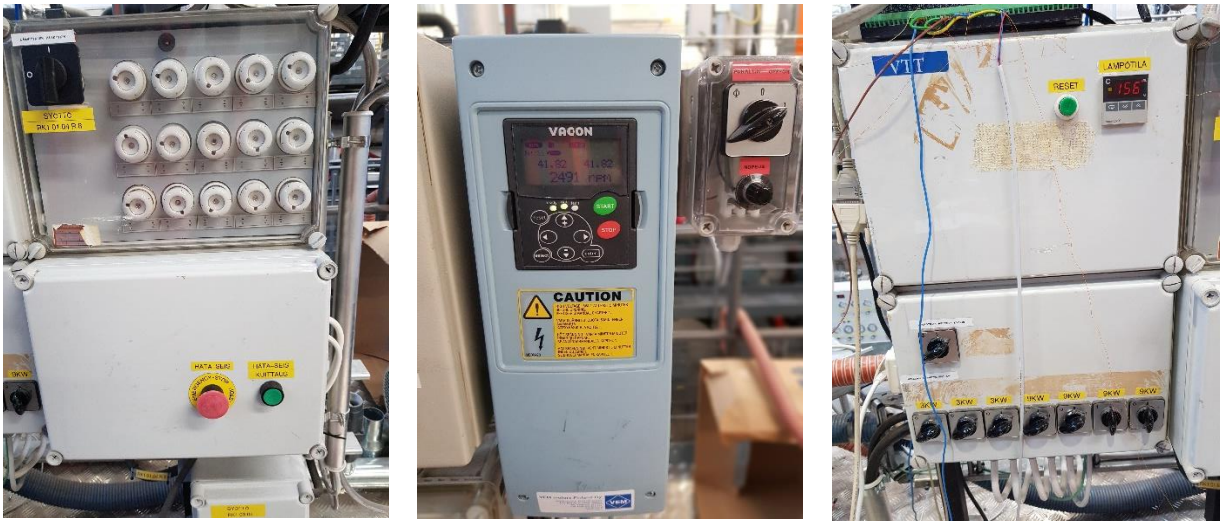

Figure 18: Control panels of air impingement dryer: Emergency switch and “emergency stop offset”-button (left), the control panel of the fan (middle), the main switch of the air heater and heating power control switches (right).

Drying efficiency was examined by following the water evaporation via mass change of the samples during drying. The mass change was measured by weighing the sample between a certain drying time to receive a sufficient amount of data. In impingement drying, samples were weighed between 1 to 4 minutes of drying. The weighing was performed by moving the platform, where the sample was placed, away from the dryer and moving the sample on the scale as fast as possible (Figure 19). The average weighing time was 20-30 seconds.

Teopal Precica 3100 C scale was used for sample weighing. The accuracy of this scale was 0,01 grams. Continuous drying experiments without weighing during the drying were also completed with 50 m/s jet velocity and with air temperatures of 150 ºC and 200 ºC. These air temperatures were chosen because of high temperature heat pumps operate already at 150 ºC and probably will operate at 200 ºC in the future. Both measurements were performed with 60 mm deep mold.

Along with mass change experiments, temperature measurements were made during drying. These measurements were performed by placing three thermocouple wires to different heights in the mold where fiber foam was poured (Figure 20). Foam had to be carried to the dryer from the laboratory and poured there to start the drainage, because thermocouples were connected to the mold, and from the other end, to the control panel of the dryer.

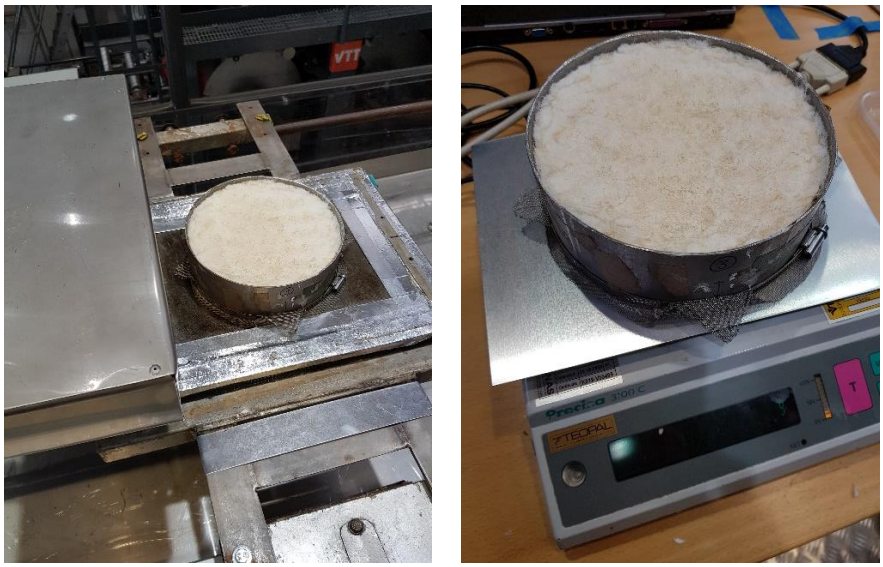

Figure 19: Sample taken away from the dryer (left) and sample weighing (right).

Figure 20: Thermocouple wires connected to sample mold.

Thermocouple wires were connected to the instruNet Model 100 Analog/Digital Input/Output System, which was connected to the control panel of the dryer and the computer. Measurement data was collected to the instruNet World computer program. InstruNet Model 100 Input/Output system has channels where wires could be connected. In this case, thermocouple wires were connected to channels 1, 4 and 7. Names of the channels in the instruNet World along the position of the thermocouples, measured from the bottom, are given in Table 3.

Table 3: Names of the thermocouples in the instruNet World program and positions of the thermocouples before pouring of the foam.

Name of the thermocouple	Position [mm]
Ch1 Vin+	11-12
Ch4 Vin+	23-25
Ch7 Vin+	38

Data was collected with the time steps of 2 seconds and InstruNet World program plotted temperature curves as a function of time for every channel. Surface temperatures of the samples were also measured after every 5 minutes during drying. These measurements were performed with OS425-LS Omega non-contact infrared thermometer (Figure 21) by moving the platform, where the sample was placed, quickly away from the dryer (for 1-2 sec).

Figure 21: OS425-LS Omega non-contact infrared thermometer.

In impingement drying experiments only pre-refined Äänekoski pine pulp was used as a raw material for fiber foam. The consistency of the foam was kept constant at about 4 %. In mass change investigations, drying was ended when the mass change was < 1g/min. Temperature measurements were ended when all three thermocouples reached the impingement air temperature. After samples were taken out from the molds they were weighed and then put in the oven to 105 ºC temperature overnight to find out the dry mass. Sample on the platform under the dryer can be seen in Figure 22.

Figure 22: Sample getting dried under the air impingement box.

6.2.2 Microwave drying

Microwave drying experiments were executed at BP-211/50 process microwave oven designated for laboratory scale (Figure 23). This microwave oven is manufactured at Microwave Research and Applications, Inc. The microwave oven has an IR-heat sensor and stepless True-To-Power power control. Magnetron of this microwave oven works continuously, which means that sample is being emitted with microwave radiation for the whole drying process. Maximum power of the microwave oven is 3,2 kW and frequency 2,45 GHz.

Figure 23: BP-211/50 process microwave oven.

The experiments were started by first checking the interior of the oven in case if there could be anything harmful and making sure that “microwave power” switch was switched off. After that, powers were switched on from the main power switch from the wall and the manual mode was selected. Then “main power” switch from the oven was switched on. At this point, any radiation is not emitted. The working of the microwave oven was then tested by placing a porcelain mug filled with water in the oven, switching on the “microwave power” switch, adjusting the desired power level from the power control and pressing “timer reset” button to start emitting microwaves. Microwave stops emitting the radiation when the timer runs out of time, “timer reset”-button is pressed or the door of the oven is opened. During this test leak radiation was measured with TROTEC BR15 radiation meter (Figure 24) from a working distance (about 0,5 m). This procedure must be made before any drying or heating experiments. Power density should never be over 5 mW/cm^2 at the working distance.

Figure 24: TROTEC BR15 radiation meter.

The drying efficiency of the microwave oven was investigated by following a mass change of the samples during evaporation. Samples were weighed with the scale next to the oven as quickly as possible when the microwave's timer ran out and no more microwaves were emitted. The used scale was Kern PLS with an accuracy of 0,01 grams. After weighing, the sample was put back in the microwave oven and weighed again after a certain time. This procedure was repeated until the sample was dry enough and a desirable amount of data points were gained. One-minute drying time between weightings was used in these experiments. Weighing had to be performed with the setup as pictured in Figure 14, otherwise the sample might have collapsed during experiments. Masses of the used supportive structures have been taken into account in calculations by subtracting them from the weighed total mass of sample and structures.

Thermocouples could not be used in temperature measurements with the microwave because they consist of metals, which conduct electricity and sparks as they absorb microwaves. Due to this temperature measurements were performed by using OS425-LS Omega non-contact infrared thermometer (Figure 21) and microwave's own infrared (IR) temperature sensor. IR sensor was connected to the microwave by following the Microwave Research and Applications, Inc. Processing Microwave BP-211/50 installation and Operation Manual. It was mounted from the top of the microwave to one of three available mounts to point down to the middle of the bottom of the microwave. The target area of the sensor is about 25 mm in diameter and the sensor will measure this whole area (Microwave Research and

Applications, Inc., 12). Due to this samples were tried to put as middle as possible under the sensor to get as accurate results as possible. Neither of these temperature measurement devices could measure the inside temperature of the samples, so only surface temperature could be examined during microwave experiments. IR sensor's measured reading could be monitored from the controller screen (Figure 23).

In the surface temperature measurements, where OS425-LS Omega was used, measurements were made at the same time when weighing took place. As soon as the timer of the microwave ran out of time, the door of the oven was opened, and infrared was pointed straight on the surface of the sample to get the surface temperature. This method was noticed to be complicated when the mold size changed. After noticing that, the IR sensor was connected to the microwave and the rest of the surface temperature measurements were made by using this method. IR sensor was in the microwave pointing to the same spot all the time, so surface temperature could be monitored for the whole drying time. Surface temperatures measured with an IR sensor were written down at the beginning and at the end of every drying minute to investigate how much the surface temperature drops during weighing. Also, continuous drying experiments, where the sample was not taken out of the oven, were made to see surface temperature development during drying.

After drying was completed, samples were taken out from the molds, weighed, and then put in the oven to 105 ºC temperature overnight to find out the dry mass.

6.3 Calculations

Based on mass change measurements, calculations were made to gain more information about the drying efficiencies. Dry solids content, moisture ratio and drying rate development during drying were clarified. The dry solids content was solved from Equation 10 (Karlsson et al. 2000, 61):

$$d.s.c. = \frac{m_{\mathrm{d}}}{m_{\mathrm{i}}} \cdot 100\ \% \tag{10}$$

where $d.s.c.$ is the dry solids content [%], m_{d} is the dry mass of sample [g] and m_{i} is the measured sample weight during drying [g].

When the dry mass of a sample was known, the moisture ratio could be solved by knowing the mass of a sample at this point. The moisture ratio was solved from Equation 11:

$$X = \frac{m_{\mathrm{i}} - m_{\mathrm{d}}}{m_{\mathrm{d}}} \tag{11}$$

where X is the moisture ratio of a sample [kg/kg].

When moisture ratios between two trial points were calculated, by knowing the time gap between these points, the drying rate was solved from Equation 12:

$$DR = \frac{m_{\mathrm{d}}}{A} \cdot \frac{X_0 - X_{\mathrm{i}}}{t} \tag{12}$$

where DR is the drying rate [kg/m^2/h], A is the surface area of a sample [m^2], X_0 is the moisture ratio of a sample in previous trial point [kg/kg], X_{i} is the moisture ratio in the current trial point [kg/kg] and t is the time gap between measurements [h].

7 RESULTS

7.1 Impingement drying

7.1.1 Mass change measurements

Air impingement drying experiments were executed by using ~4 % consistency pre-refined pine pulp as a raw material of foam formed samples. Consistency was kept constant in all experiments. Mold depths of 30 mm and 60 mm were used, and both had a diameter of 150 mm. Jet velocities of 30 m/s and 50 m/s were used with impingement air temperatures of 150 ºC and 200 ºC. Distance from the air impingement box to the sample platform was constant 75 mm.

During weightings of mass change experiments, some moisture was condensed on the surface of the scale from the bottom of the samples. This happened until 28-40 % dry solids content was reached. After that, all the water removal happened via evaporation. Masses of this condensed water have been considered during calculations. Mass of the sample in certain trial point was calculated by subtracting the mass of condensed water, used mold and other supportive frames from the total mass that was weighed with the scale. Mass change as a function of drying time with different jet velocities, drying temperatures and mold heights is shown in Figure 25.

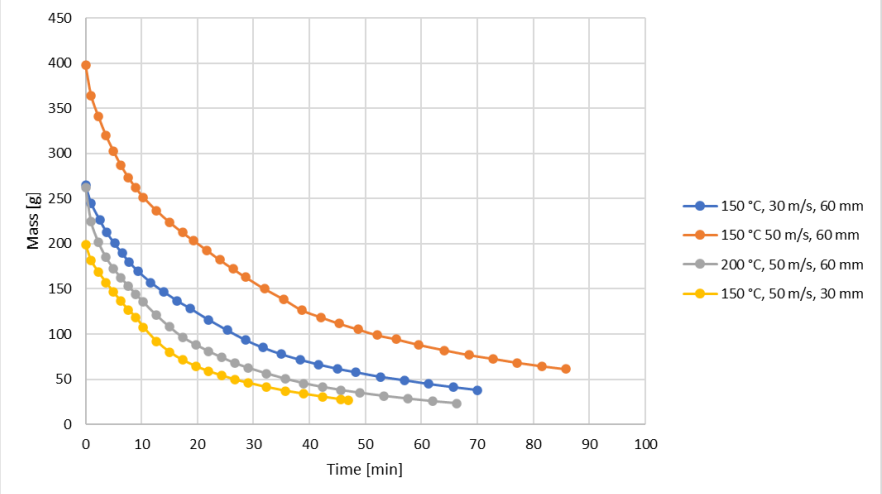

Figure 25: Mass change of pine pulp samples as a function of drying time in impingement drying. Air temperature, jet velocity and mold height are shown on the right.

The drying curves are quite similar in shape. It can be also seen that when mold height drops in half, but jet velocity and impingement air temperature stay the same (50 m/s and 150 ºC), the mass change curve is almost identical. Starting weight of the sample is doubled and weight after drying is nearly doubled when drying time is almost twice as long. The effect of the impingement distance to the sample surface between 30 mm and 60 mm mold in these circumstances can be said negligible. The average shrinkage of the samples in thickness direction during drainage was 9 mm with 60 mm mold and 2 mm with 30 mm mold. Before drying, the dry solids content varied between 6,4-7,6 %. The increase of jet velocity from 30 m/s to 50 m/s and increase of air temperature from 150 ºC to 200 ºC can be seen as enhanced drying efficiency (Figure 25). Drying time was shorter with lower mold height, but also mass before drying was less.

Moisture ratios in the trial points were calculated with Equation 11. Moisture ratio as a function of drying time with different jet velocities, drying temperatures and mold heights is shown in Figure 26. Noticeable was that mold height had the biggest effect on moisture ratio decrease (Figure 26). This makes sense, since water has a shorter distance to reach the surface of the sample when the thickness is decreased. Curves also show that the moisture ratio decreases faster with increased air temperature. The reason for faster drying with 30 m/s jet velocity compared to 50 m/s, when both samples dried with 150 ºC air temperature, is most likely that the mass difference between the samples after drainage was 132,8 g (Figure 25). As expected, the most efficient drying was reached when air temperature was 200 ºC and jet velocity was 50 m/s. With these parameters, and 60 mm mold, the moisture ratio was dropped from 12,79 kg/kg to 0,27 kg/kg in 66 minutes and 20 seconds of drying. True drying time would be shorter when there is no sample weighing during drying.

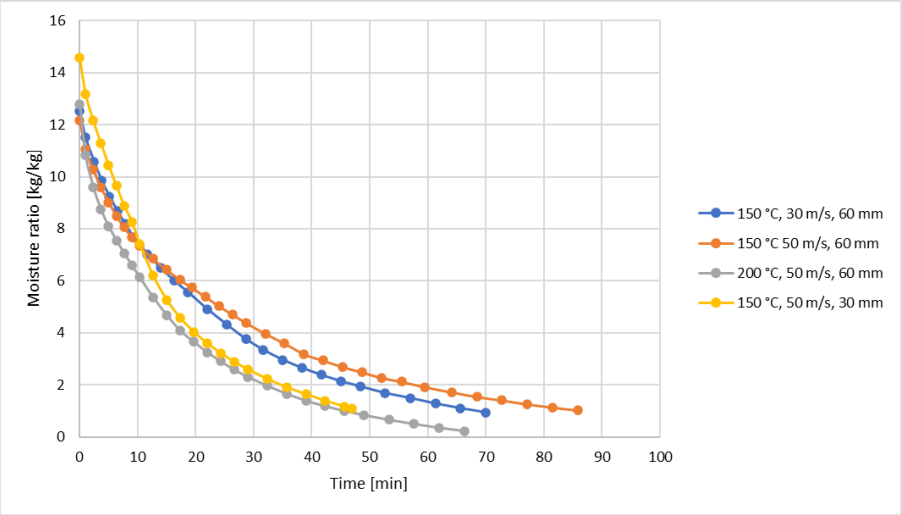

Figure 26: Moisture ratio of pine pulp samples as a function of drying time in impingement drying. Air temperature, jet velocity and mold height are shown on the right.

The development of dry solids content of the samples during drying was calculated with Equation 10. As mentioned before, in air impingement drying experiments dry solids content of the samples did not vary a lot before drying. Due to this different parameters can be compared more reliably. Dry solids content as a function of drying time with different jet velocities, drying temperatures and mold heights is shown in Figure 27.

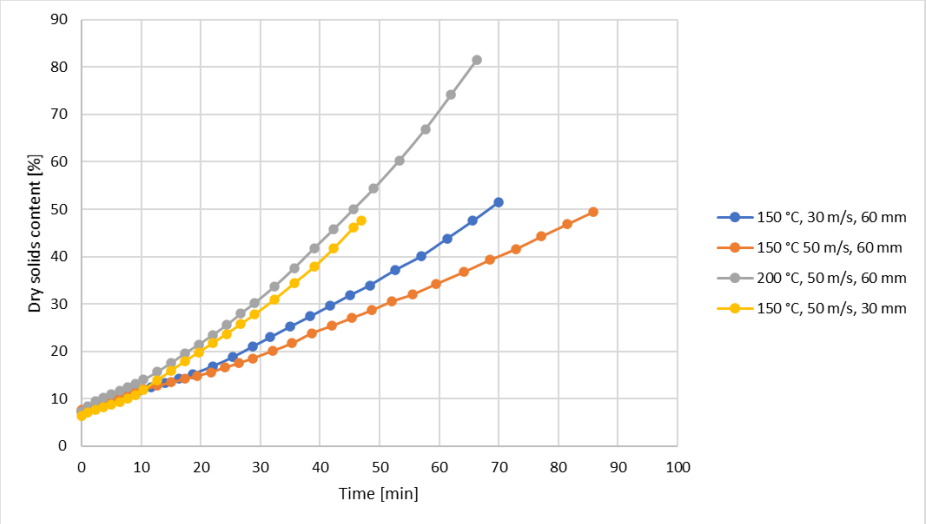

Figure 27: Dry solids content of pine pulp samples as a function of drying time in impingement drying. Air temperature, jet velocity and mold height are shown on the right.

The increased jet velocity and impingement air temperature increased the drying performance. With about 4 minutes shorter drying time and maximum variation of 1,2 % in dry solids content before drying, almost 30 % higher dry solids content was reached when jet

velocity was increased from 30 m/s to 50 m/s and temperature was raised from 150 ºC to 200 ºC (Figure 27). This dry solids content was 81,5 %, with a drying time of 66 minutes and 20 seconds. Because of long drying times and difficult estimation of dry solids content at the end of drying, other samples were not dried to higher dry solids contents. Lower mold height seemed to also have a positive effect on drying speed. This might however be misleading because the size of the sample is smaller, and the mass is lower. Due to its smaller size, the sample consists of less mass in a form of water, which leads to shorter drying times.

The drying rate was calculated with Equation 12. Drying rate as a function of moisture ratio, with different jet velocities, air temperatures and mold heights is shown in Figure 28.

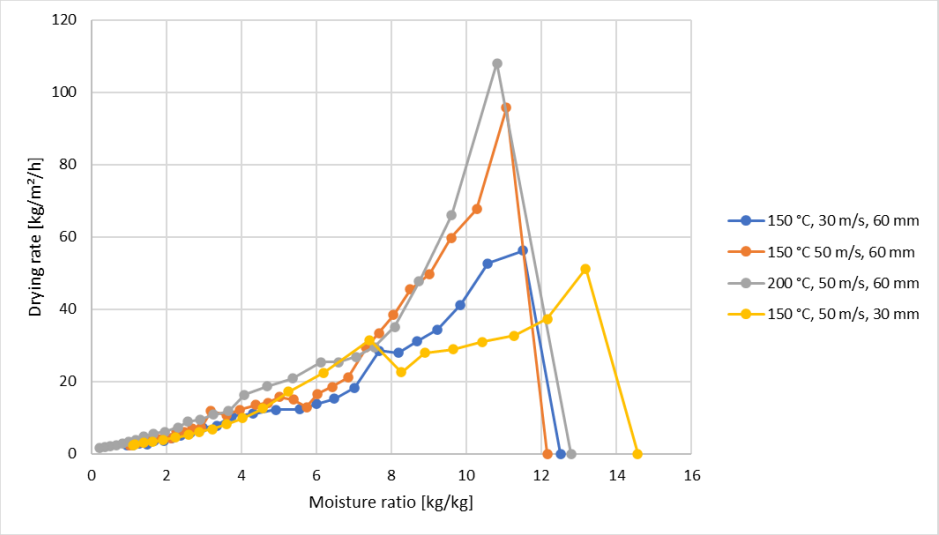

Figure 28: Drying rate of pine pulp as a function of moisture ratio. Air temperature, jet velocity and mold height are shown on the right.

As can be seen from Figure 28 with the mold heights of 60 mm the highest drying rates were reached when the moisture ratio was between 10-12 kg/kg. These moisture ratios were achieved between first 1-3 minutes of drying (Figure 26). With the air temperature of 200 ºC and jet velocity of 50 m/s, the best drying rate reached with air impingement drying was 108 kg/m^2/h. With the 30 mm mold highest drying rate 51,2 kg/m^2/h was obtained when the moisture ratio was 13,18 kg/kg and drying was taken 1 minute. The highest drying rates were reached when samples consist still a lot of water. Dry solids contents were between 7-9 % at these points. When mold height was 60 mm, jet velocity was raised from 30 m/s to 50 m/s and air temperature from 150 ºC to 200 ºC, drying rate at the highest point was almost

doubled. The highest average drying rate reached was 11,3 kg/m^2/h and the lowest was 7 kg/m^2/h, both with the air temperature of 150 °C and jet speed of 50 m/s.

By examining drying rate curves from Figure 28 it is noticeable that with 60 mm mold height only the heating phase and falling rate phase were obtained during drying. Mutually of moisture ratio 8 kg/kg short constant drying rate phase can be seen with 30 m/s jet velocity and 150 ºC air temperature (Figure 28). With 30 mm mold height, almost constant drying rate phase can be seen between moisture ratios 7,4-11,3 kg/kg. However small slope, where the drying rate drops momentarily, is noticed near the 8 kg/kg moisture ratio. After the slope, the beginning of the falling rate phase can be seen clearly. During the falling rate phase, when about 5 kg/kg moisture ratio is reached, drying rate values start to be almost equal regardless of the drying parameters (Figure 28).

7.1.2 Temperature measurements

Temperature measurement experiments were executed by placing thermocouple wires into sample mold to monitor the temperature development in the sample during drying. Two temperature measurement experiments were made with impingement drying. Both were made using the mold depth of 60 mm. Impingement air temperatures of 150 ºC and 200 ºC were used and jet velocity was kept at a maximum of 50 m/s in both measurements. Temperature data measured with thermocouples were collected from the instruNet World program. The surface temperature was measured with an infrared thermometer (Figure 21) between every 5 minutes of drying. Based on instruNet World's data, the measured temperature of thermocouples as a function of drying time is presented in Figure 29.

As can be seen from Figure 29, the temperature first rose from near 20 ºC to 40-50 ºC and stayed constant before it started increasing rapidly towards impingement air temperature with both air temperatures. After this constant rate period, temperature obviously started raising first in the point closest to the surface of the sample. This refers that temperature raised as water was evaporated and sample was dry in that point. Dried parts then worked as heat insulators that grew thicker the drier the sample was. With lower air temperature, there was a bigger time gap between different depths, when temperature started increasing. It can also be seen that as soon as the temperature started rising in the deeper points, air

impingement temperature was reached faster the deeper the point was. Temperature rise peak in the 200 ºC air temperature measurement most likely result from some current peak.

Although surface temperature measurements took approximately 1-2 seconds, surface temperature was measured to drop about 10 ºC/s when sample was taken out of the dryer. Cooling of the surface can be seen as slopes in the temperature curves (Figure 29). Surface temperature measurements as a function of drying time can be seen in Figure 30. To see the difference between surface temperature and temperature in different depths of the sample, thermocouple measurement data between 5 minutes is plotted to the same figure.

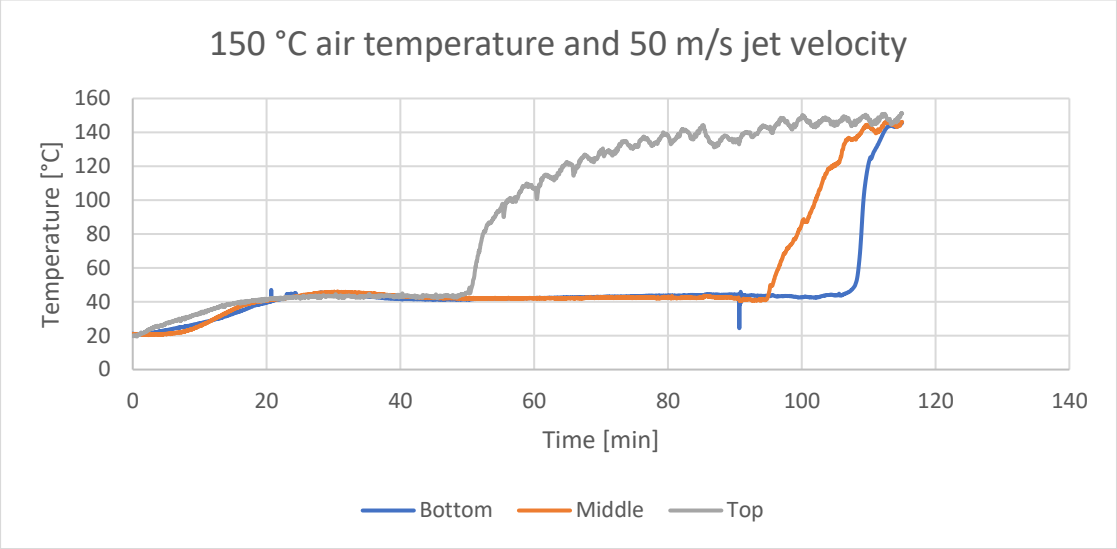

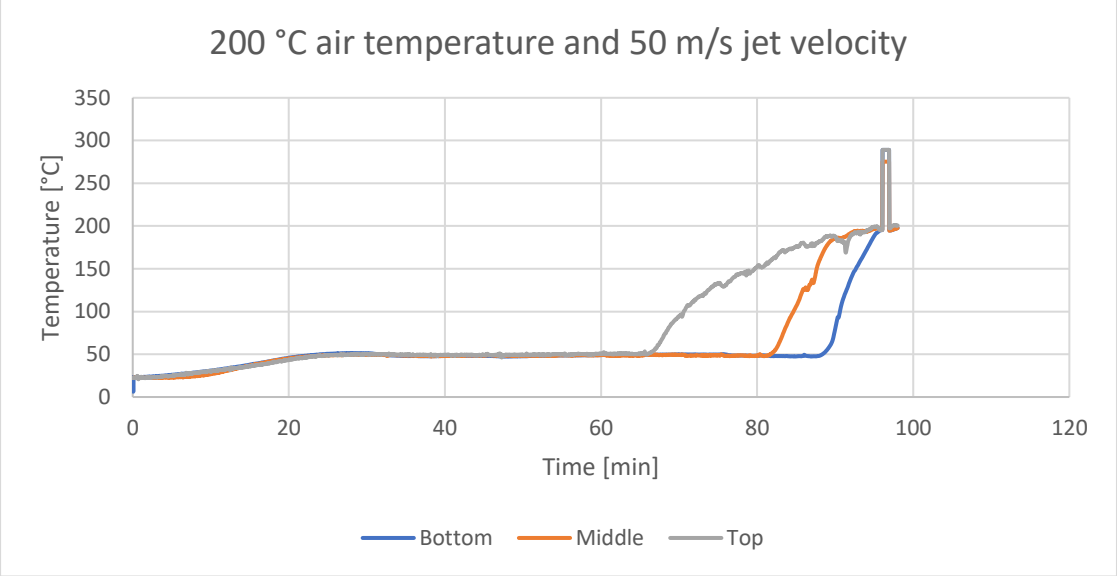

Figure 29: Temperature of pine pulp sample as a function of drying time for jet velocity of 50 m/s and air temperatures of 150 ºC and 200 ºC. Thermocouple positions (Bottom, Middle, Top) are shown below the curves.

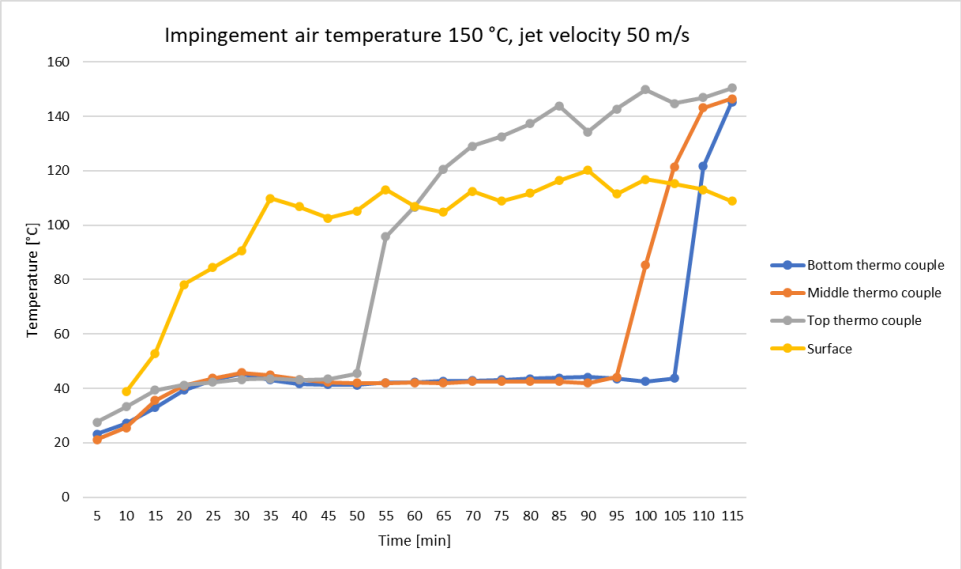

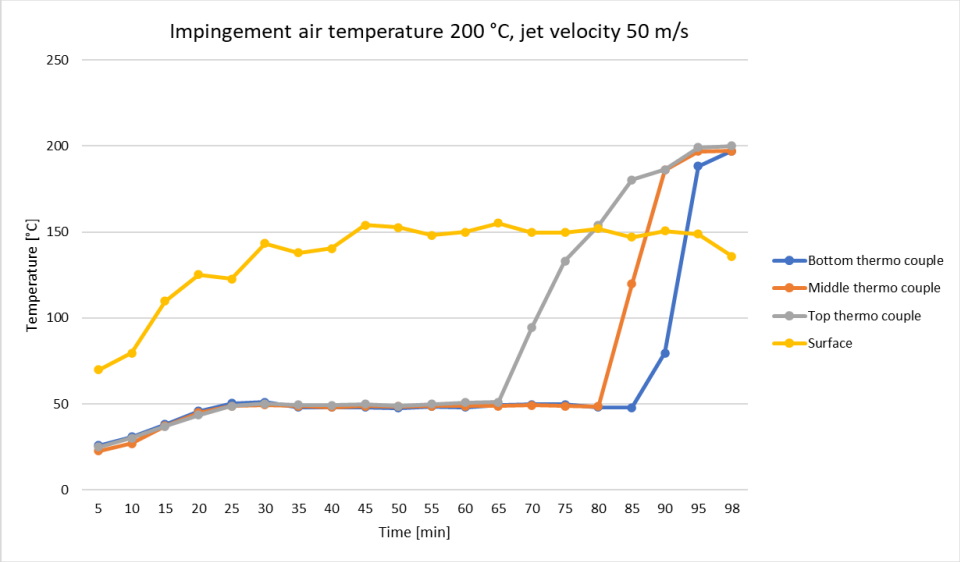

Figure 30: Surface temperature and temperature of pine pulp in different depths as a function of drying time.

Figure 30 illustrates that surface temperature raised fast during drying and stayed at between certain range. This also illustrates that surface dried fast and started to reduce moisture removal from deeper points of the samples. The surface temperature never reached the impingement air temperature, which can be justified by a temperature drop of about 10 ºC/s during measurements. If the surface temperature could be measured during the sample was dried, temperatures would have been closer to the impingement air temperature.

Positions of the thermocouples, measured from the bottom, before foam was poured into the mold are shown in Table 3. During the pouring of the foam, the positions of the thermocouples moved slightly. After drying, samples were split to specify the positions of the thermocouples. Specific positions after splitting were difficult to define but movements were not major (~1-2 mm in thickness direction).

The visual quality difference between the samples was noticed when the impingement air temperature was raised. With an air temperature of 150 ºC, the sample surface turned a little brownish, whereas, with 200 ºC air temperature, the sample surface was totally brown. When temperature rises over 40 ºC, SDS decomposes, which causes the darkening of the surface (Sigma- Aldrich). Figure 31 pictures the visual effect of air temperature on the samples.

Figure 31: Impingement air temperature effect to the surface of the samples. 150 ºC (samples 6 and 7) and 200 ºC (sample 8) air temperatures.

In impingement drying, this burning phenomenon is hard to avoid because of long drying times and uneven drying. Air meets first the surface of the sample, which is under the impingement temperature for the whole drying time. In the deeper spots of the sample structure, it takes more time to reach this temperature (Figure 29), when air has to penetrate through the fiber network. Due to this, the sample receives the greater heat load the closer the surface gets.

7.2 Microwave drying

7.2.1 Microwave power correction

Reading in the microwave power control tells the percentage of the power from the maximum. This power adjustment, however, is not linear and a specific power level cannot be signified only by taking into account the percentage from the maximum power. Directional calculations were made to gain information from the most used power levels in the experiments. These calculations were made by testing how much time took to heat about one liter of 25 ºC water to boiling point (100 ºC) with power levels 20 %, 40 %, 60 %, 80 % and 100 %. Water temperature was measured, with thermocouples that were connected to the Fluke 54 II thermometer (Figure 16), after every one or two minutes of heating until water started boiling. Water was heated in a 2000 mL cylindrical measure vessel with 125 mm diameter, made out of glass. To get about the same amount of water before every test, the vessel was filled to the 1000 mL mark and weighed before heating. Water temperature as a function of time, in power levels mentioned above, can be seen in Figure 32.

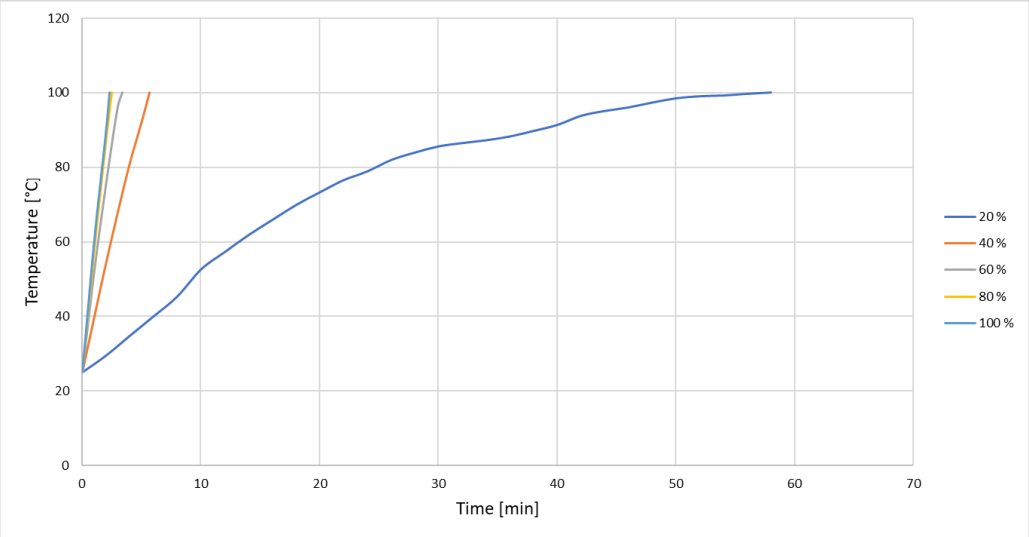

Figure 32: Water temperature as a function of time with various microwave power levels.

As can be seen from Figure 32, there is a big difference in the heating times between 20 % and 40 % power levels. With 20 % level to heat water to boiling point took 58 minutes when with 40 % power it took only 5 minutes and 40 seconds. With power levels 80 % and 100 % difference was not that significant. With 80 % level to heat water to boiling point took 2 minutes and 30 seconds when with 100 % power it took only 2 minutes and 20 seconds. By

examining these results can be said that power adjustment is not linear, and it seems to be accelerating to power level 60 % and after that increment of the power is not large.

To figure out how much microwave power different levels emit to water, calculations were made based on elapsed time from water to reach the boiling point. First, energy demand to heat water from 25 ºC to 100 ºC was calculated from Equation 13:

$$Q = m_{\mathrm{w}} \cdot c_{p,\mathrm{w}} \cdot \Delta T \tag{13}$$

where Q is the energy demand [kJ], m_{w} is the mass of water [kg], $c_{p,\mathrm{w}}$ is the specific heat capacity of water [kJ/kgK] and ΔT is the temperature change [K].

When the heating time was known, emitted microwave power to water in certain power level could be solved from Equation 14:

$$P = \frac{Q}{t} \tag{14}$$

where P is the microwave power [W] and t is the heating time [s].

Specific heat capacity at 25 ºC was used for water during these calculations. Amount of this is $c_{p,\mathrm{w}}$(25 ºC) = 4,18 kJ/kgK (Hanslmeier 2011, 15). For example, when the test was run for a 60 % power level, the mass of water was 1,034 kg. From Equation 13, energy demand is:

$$Q = 1{,}034\ \mathrm{kg} \cdot 4{,}18 \frac{\mathrm{kJ}}{\mathrm{kgK}} \cdot 75\mathrm{K} = 324{,}27\ \mathrm{kJ}.$$

The heating time for 60 % power level was 3 minutes and 25 seconds. From Equation 14, emitted microwave power to water for this power level is:

$$P = \frac{324{,}27\ \mathrm{kJ}}{205\ \mathrm{s}} = 1581{,}81\ \mathrm{W}.$$

Calculated microwave powers for tested power levels and corrected power levels based on these results are tabulated in Table 4.

Table 4: Emitted microwave powers to water at power levels 20 %, 40 %, 60 %, 80 % and 100 % and corrected microwave power levels.

Power level [%]	Microwave power [W]	Corrected power level [%]
20	90,3	3,9
40	940	40,7
60	1580	68,5
80	2150	93,1
100	2310	100

As mentioned before, the maximum power of microwave should be 3,2 kW and with 100 % power level, emitted microwave power to water was only 2,3 kW (Table 4). Also, these results confirm that the microwave's power adjustment is not linear. The difference between 80 % and 100 % should be bigger and 20 % power is only about 4 % of 100 % power level based on these measurements. As can be seen 40 % power level is almost correct. After that, a quick increase in power can be noticed and the gap between power levels shrinks towards 100 % power level. Emitted microwave power to water as a function of microwave power level can be seen from Figure 33.

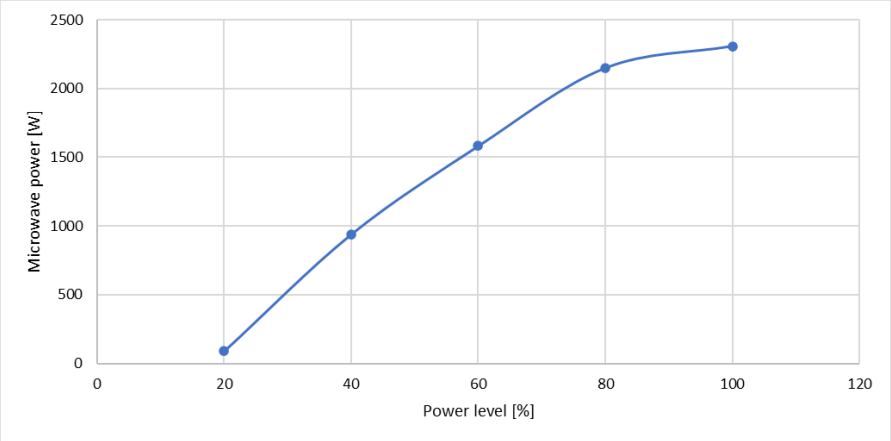

Figure 33: Emitted microwave power to water as a function of microwave power level. Heating from 25 ºC to 100 ºC.

Errors in measurements can be possible such as the exact starting time of boiling. This was challenging to see when the microwave oven's door glass was quite dark (Figure 23). Water temperature could not be measured with the microwave's mounted IR sensor, which complicated this even more. Varying measurement time with thermocouples could also affect the results and cooling of water might occur during measurements. Due to thermocouple measurements, heating could not be continuous from the beginning to the boiling point, which also decelerated the heating and calculated power levels are most likely lower than they should. Most of the radiation is emitted to the water, but some is also emitted to other surroundings such as plastic equipment and fibers of the samples. This reduces the measured power levels somewhat but is difficult to determine.

To gain information about the power density that can be achieved with the most used microwave power levels for different sample thicknesses, directional calculations were made based on corrected power levels. These calculations take account the power that is emitted to water. Let's assume that the average shrinkage of samples on thickness direction was ~5 mm regardless of the sample mold height. Mold heights of 39 mm, 49 mm and 79 mm were used, so in these examples sample thicknesses are 34 mm, 44 mm and 74 mm. Let's also assume that sample thickness is even and there is no variation. Let's use 74 mm sample thickness and 60 % microwave power level for example calculations. The average volume of the sample during drying was solved from Equation 15:

$$V = H \cdot A \tag{15}$$

where V is the volume of the sample [m^3] and H is sample height [m].

Emitted power densities for different sample volumes were solved from Equation 16:

$$\dot{P} = \frac{P}{V} \tag{16}$$

where $\dot{P}$ is power density [kW/m^3].

From Equation 15, volume of the sample is:

$$V = 0{,}074\ \text{m} \cdot 0{,}0177\ \text{m}^2 = 0{,}0013\ \text{m}^3.$$

From Equation 16, power density is:

$$\dot{P} = \frac{1{,}58\ \text{kW}}{0{,}0013\ \text{m}^3} = 1209{,}6\,\frac{\text{kW}}{\text{m}^3}.$$

Power densities for all three sample thicknesses are plotted as a function of most used power levels in Figure 34.

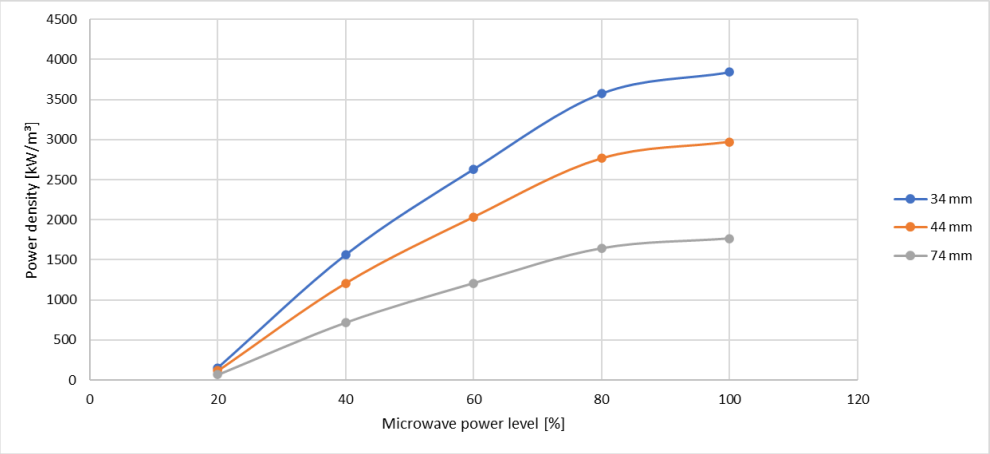

Figure 34: Power density as a function of microwave power level. Sample thicknesses are shown on the right.

As can be seen from Figure 34, the difference in power density between different sample thicknesses starts to increase when the microwave power level is increased. With 20 % power level all thicknesses have almost same power densities, whereas with 100 % power, power densities vary a lot. It is also noticeable that when a sample is thinner and has a smaller volume, reached power density is higher. Figure 34 presents that with a 100 % microwave power level, the thinnest samples can a reach power density of over 3800 kW/m^3 when the under 1800 kW/m^3 can be reached with the thickest samples. This makes sense as sample volume is more than doubled when thickness changes from 34 mm to 74 mm. About 3000 kW/m^3 power density can be reached with the middle thickness (44 mm) (Figure 34). With the thinnest samples, almost the same power density is reachable with a 40 % power level as is reachable with the thickest samples with a power level of 80 %. Although the power densities vary a lot with different sample sizes, drying times were still in the same range. During experiments it was found that thicker samples reached higher drying rate values (Section 7.2.2), which must be one reason for similar drying times. Specific surface area relative to mass of the sample inhibits the evaporation, which increases the drying time. This means that if different diameters of molds have been used, more variation in drying times would probably occur.

7.2.2 Mass change measurements

Mass change experiments in microwave drying were executed by using pre-refined pine pulp and CTMP as raw materials of foam-formed samples. Altogether 48 samples (32 for pine pulp and 16 for CTMP) were made, and several starting consistencies were applied being between 2-10 %. Samples were dried in three different mold heights of 39 mm, 49 mm, and 79 mm with a constant diameter of 150 mm. Microwave power levels were all tested from 20 % to 100 % with 10 % increases. Most used levels were 20 %, 40 %, 60 %, 80 % and 100 %. These power levels were selected for the plot examples of drying curves. Consistencies selected for plots were between 3-5 %, so that differences between power levels and used fibers can be perceived more easily. Microwave drying as a drying method for thick and porous fibrous samples was noticed to be workable and more efficient than air impingement drying. For this reason, more experiments were performed for microwave drying than air impingement drying.

Like in air impingement drying experiments, during sample weighing, some water was condensed on the scale. Condensation occurred in almost every weighing and the amount of condensed water was bigger the moister the sample was at that point. The mass of condensed water is considered in drying rate calculations by reducing it from the weighed total mass of the sample. Mass of used mold and other supportive structures (Figure 14) was also subtracted from the total weighed mass. An example plot of a mass change as a function of drying time for selected samples is shown in Figure 35.

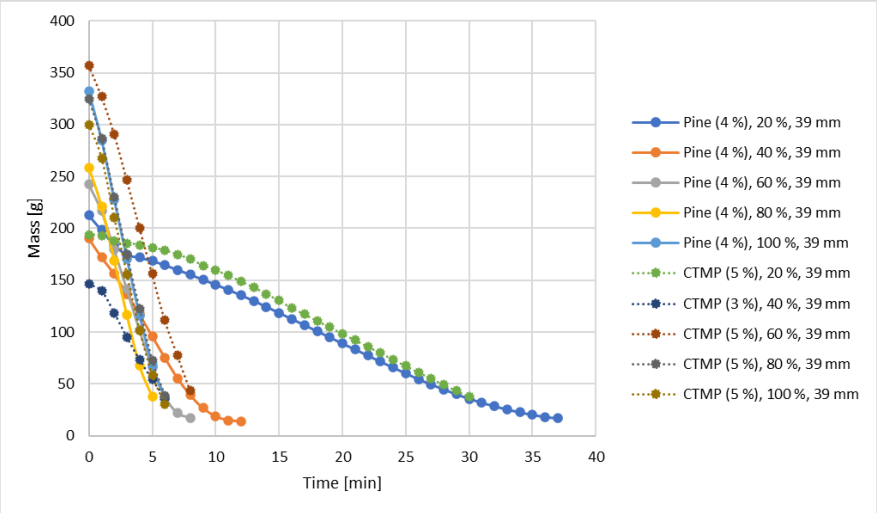

Figure 35: Mass change as a function of drying time in microwave drying. Fibers and consistency of the sample, microwave power level and mold height are shown on the right.

As can be seen from Figure 35, mass change was notably slower with 20 % than with other power levels. With higher power levels such a significant difference was not noticed. With power levels of 80 % and 100 %, difference in mass change was almost equal. This can be explained with corrected microwave power calculations (Table 4). There was no significant difference in mass change between pine pulp and CTMP with the same power levels with these consistencies.

It was noticed after about 10 samples that during the first drying minutes, especially with higher power levels, some water dribbled from the sample to the bottom of the microwave oven. This means that all removed water during drying was not evaporated purely. The noticed amounts of dribbled water were between ~2-35 g. To illustrate the effect of dribbled water on the mass change, an example is shown in Figure 36. Another graph takes dribbled water into account and presents the mass change due to evaporation and another graph presents the weighed mass change of the sample.

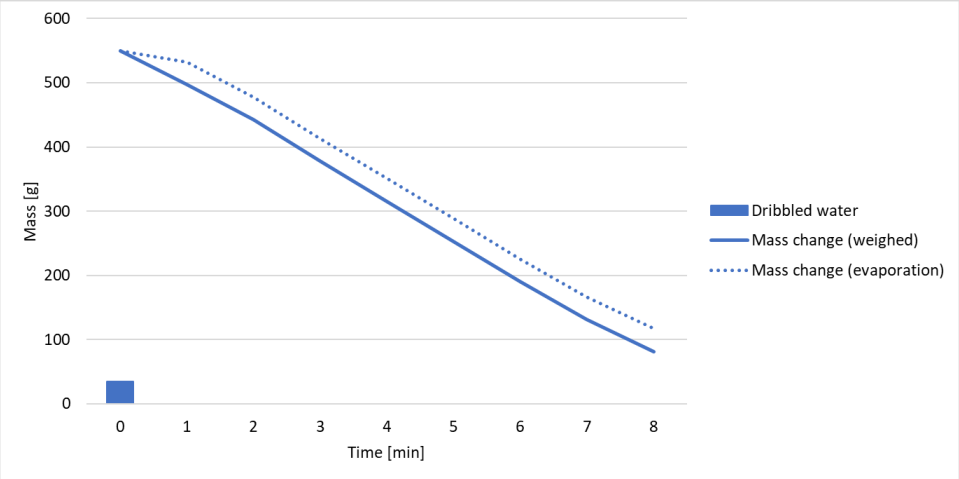

Figure 36: An example of weighed mass change compared to mass change due to evaporation as a function of drying time in microwave drying.

In Figure 36, dribbled water is drawn as a column. In this example, the mass of dribbled water was ~35 g, which was found to be the biggest. In the drying rate calculations it is assumed that dribbled water is not evaporated, which explains the gap between the two graphs. This helps to illustrate the mass change that happened via evaporation. The sample in this example was pine pulp with the 4 % consistency dried in the 79 mm high mold. It was noticed that more water was dribbled when mold height and microwave power were increased. It was also found out that when sample consistency was higher, dribbled water amount decreased. Differences between used fibers were not found.

Dry solids content during drying was calculated with Equation 10. An example plot of dry solids content as a function of drying time for selected samples is shown in Figure 37.

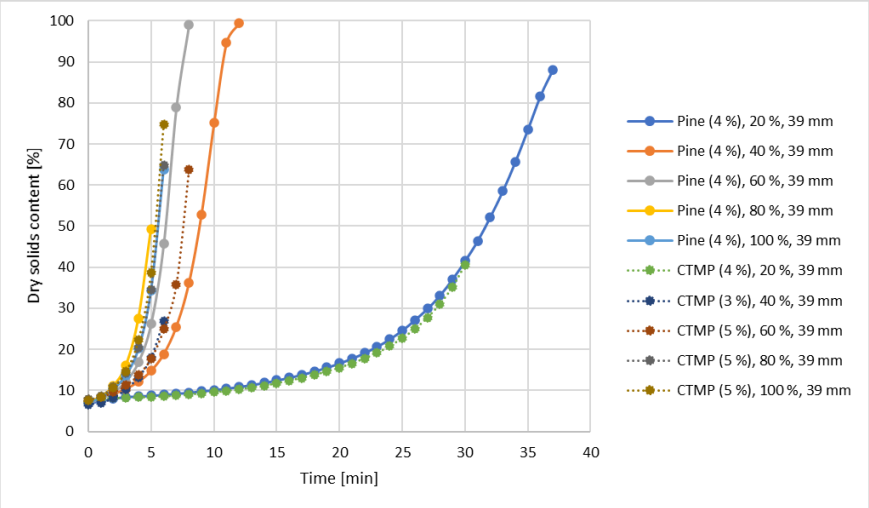

Figure 37: Dry solids content as a function of drying time in microwave drying. Fibers and consistency of the sample, microwave power level and mold height are shown on the right.

Figure 37 presents that drying is easier to control with low power when a change in dry solids content between measurement points is not that huge. This makes it easier to reach higher dry solids content without over-drying the sample. Some samples and supportive structures were damaged during experiments by drying samples too much. Damages occurred were burning damages to the sample and to the mold (Section 7.2.4). It was then assumed that this phenomenon will happen with every sample. Especially with higher power levels drying was stopped early enough to avoid these damages as much as possible. A significant difference between 20 % power level to other used power levels can be seen clearly in Figure 37. For example, with pine pulp to reach dry solids content of 40 % with 20 % power level, took about 30 minutes of drying, when with 40 % power level it took a bit over 8 minutes. With higher power levels, differences diminish. For example, 4 % consistency pine pulp samples dried for 6 minutes with power levels of 60 % and 100 %, dry solids contents of 45,7 % (60 % power) and 63,9 % (100 % power) were reached (Figure 37).

Moisture ratios in the trial points during drying were calculated with Equation 11. An example plot of moisture ratio as a function of drying time for selected samples is shown in Figure 38.

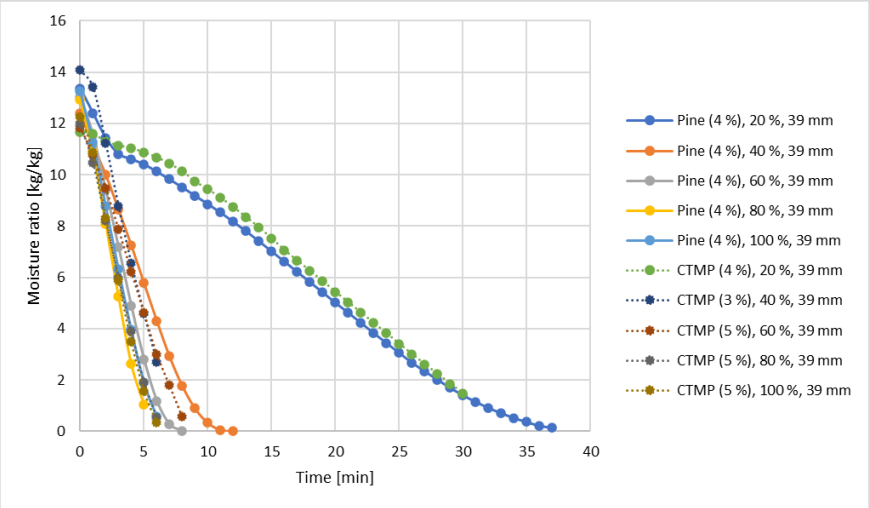

Figure 38: Moisture ratio as a function of drying time in microwave drying. Fibers and consistency, microwave power level and mold height are shown on the right.

As Figure 38 illustrates, drying time was found to reduce with higher power levels. Development of moisture ratio during drying with 20 % power level was poor compared to higher power levels (Figure 38). With 40 to 100 % power levels, drying curves are mostly shaped like slopes, whereas with 20 % power drying was stable and slow. With 80 % and 100 % power levels maximum drying time was 6-7 min despite the fibers. Based on the correction calculations, this result appears valid considering the real power that is emitted to water inside the sample (Table 4).

When the development of moisture ratio during drying was solved, the momentary drying rate in the trial points could be solved with the Equation 12. Dribbled water was not considered as evaporated water. An example plot of drying rate for selected samples as a function of moisture ratio is shown in Figure 39.

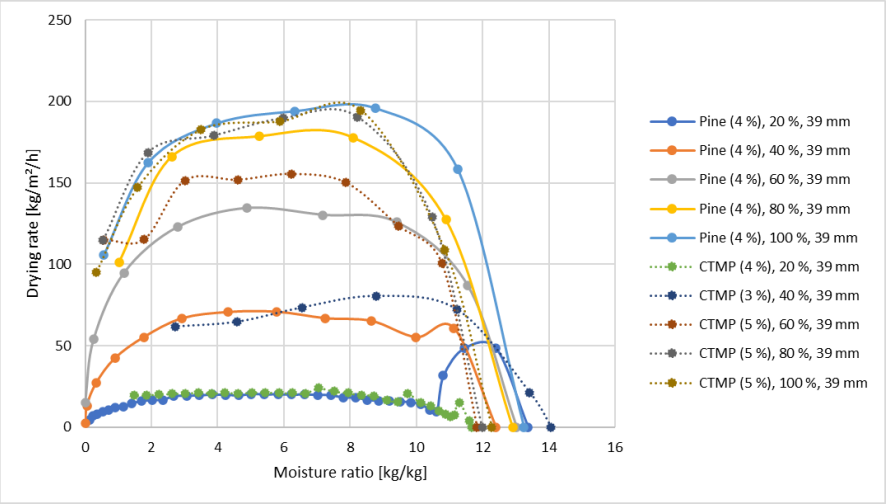

Figure 39: Drying rate as a function of moisture ratio in microwave drying. Fibers and consistency, microwave power level and mold height are shown on the right.

As Figure 39 illustrates, higher momentarily drying rates were reached when the used power level was higher. With 80 % and 100 % power levels highest drying rates were observed between moisture ratios of 6-8 kg/kg. Regardless of the power level, the highest momentarily drying rate was reached with CTMP samples. These differences seemed to be more significant with lower power levels. However, an interesting peak in drying rate can be noticed with pine pulp sample with 20 % power level, when at the beginning of drying, the drying rate of 81,3 kg/m^2/h was reached.

Drying curves for every power level, especially levels above 60 %, show that the heating phase, constant rate phase and falling rate phase occurred during microwave drying (Figure 39). A very rapid heating phase occurred, which led to a rather unstable constant rate phase. The constant rate phase was more stable with lower power levels when less amount of water was evaporated between the measurement points. When higher power was used, samples lost a huge amount of mass due to evaporation between measurement points (Figure 35) and the constant rate phase could not stabilize. Falling rate phases occurred between moisture ratios of 2-4 kg/kg (Figure 39). Falling rate curves can be seen more radical with higher power levels (Figure 39) and the drying rate was found to drop as much as ~50-65 kg/m^2/h between one-minute period.

During the experiments, the highest momentarily drying rate of 223 kg/m^2/h was reached with 100 % power level and 79 mm mold height when pine pulp sample with the consistency

of 6,5-7 % was dried. The moisture ratio at this point was 6,2 kg/kg. The highest average drying rate over the whole drying time, where the sample was not destroyed at the beginning, was 199 kg/m^2/h. This was reached with the ~4 % consistency pine pulp sample that was dried with a 100 % power level in a 79 mm deep mold. The highest reached average drying rates for most used power levels are tabulated in Table 5. Used fibers, their consistencies and mold heights are mentioned.

Table 5: Highest average drying rates reached by most used microwave power levels.

Power level [%]	Fibers	Consistency [%]	Mold height [mm]	Drying rate [kg/m^2/h]
20	CTMP	~3	49	26,0
40	Pine	~2,5-2,8	49	81,8
60	Pine	~6,5-7	79	146
80	Pine	~4	79	189
100	Pine	~4	79	199

It is noticeable from Table 5 that average drying rates are increased along with increased power levels. Samples dried with a mold height of 79 mm were found to have a better average drying rate in higher power levels (60-100 %). As microwaves emit power to the whole sample and the power level is high enough, it is possible that larger samples due to their bigger volume can evaporate more water, and higher drying rates can be reached. It was noticed earlier with the example measurements that usually CTMP samples had higher momentarily drying rates (Figure 39). However higher average drying rates were reached with pine pulp samples. Major of the experiments were performed with pine pulp and CTMP was not used in 79 mm mold height measurements, which might be the reason that the best results were achieved with pine pulp. With the most used mold height (39 mm), pine pulp sample of 4 % consistency and CTMP sample of 5 % consistency were drier with 100 % power giving the average drying rates of 167 kg/m^2/h for pine pulp and 153 kg/m^2/h for CTMP. With lower power levels CTMP was found to reach higher average drying rates. Also, the most used consistency (~4 %) gave the best results with the higher power levels. With the amount of data that were gained during the experiments it is difficult to estimate which consistency is the best for a certain power level to make drying as efficient as possible. Drying

rate curves of the samples, as a function of moisture ratio, with the highest average drying rates are plotted in Figure 40.

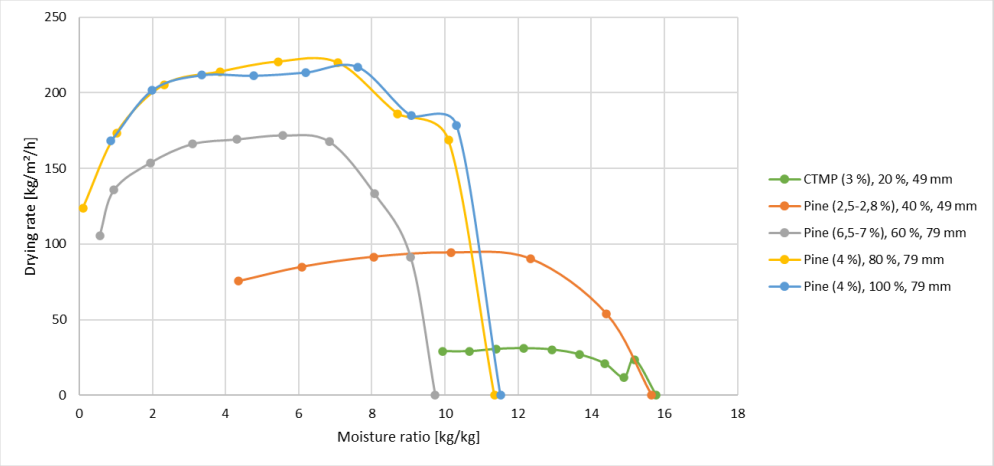

Figure 40: Drying rate as a function of moisture ratio in microwave drying. Highest average drying rates for most used power levels. Fibers and consistency, microwave power level and mold height are shown on the right.

Figure 40 shows that the highest average drying rates for power levels 20 % and 40 % were reached probably due to shorter drying times than normally used for these power levels. Curves show that the proper falling rate phase did not even take place (Figure 40), which increased the average drying rate. The structure of the CTMP sample, dried with 20 % power, collapsed during the drying, which led to a high moisture ratio at the end of the drying (Figure 40). Dry solids content of under 10 % was reached with this sample. The pine pulp sample dried with 40 % power was also left moist, to under 20 % dry solids content, which increases the average drying rate. If higher dry solids content could be reached during drying, the average drying rates with these lower power levels would be more comparable to other results and would not be distorted. Dry solids contents of ~54-90 % were reached with power levels 60 %, 80 % and 100 %. Due to this, these average drying rates are more comparable to other measurements and can be found as valid results. Drying curves for 60 %, 80 % and 100 % power levels were not exceptional compared to other curves achieved and were similar in shape. When examining the microwave power correction results (Table 4), can be seen that power levels of 80 % and 100 % are very close to each other. The similarity of drying curves can be somehow explained with this.

7.2.3 Temperature measurements

Beside mass change measurements, surface temperature measurements of the samples were made during drying experiments. The most accurate measurements were made by using microwave oven's own IR temperature sensor. It was noticed that surface temperature dropped dozens of degrees during weighing of samples and it took few seconds of time for surface to heat up again. One experiment was performed, where pine pulp sample with consistency of ~4 % was dried 6 minutes with 100 % power level in the 79 mm mold and behavior of surface temperature was monitored by filming the whole drying process. Figure 41 illustrates the surface temperature behavior during the drying of the sample.

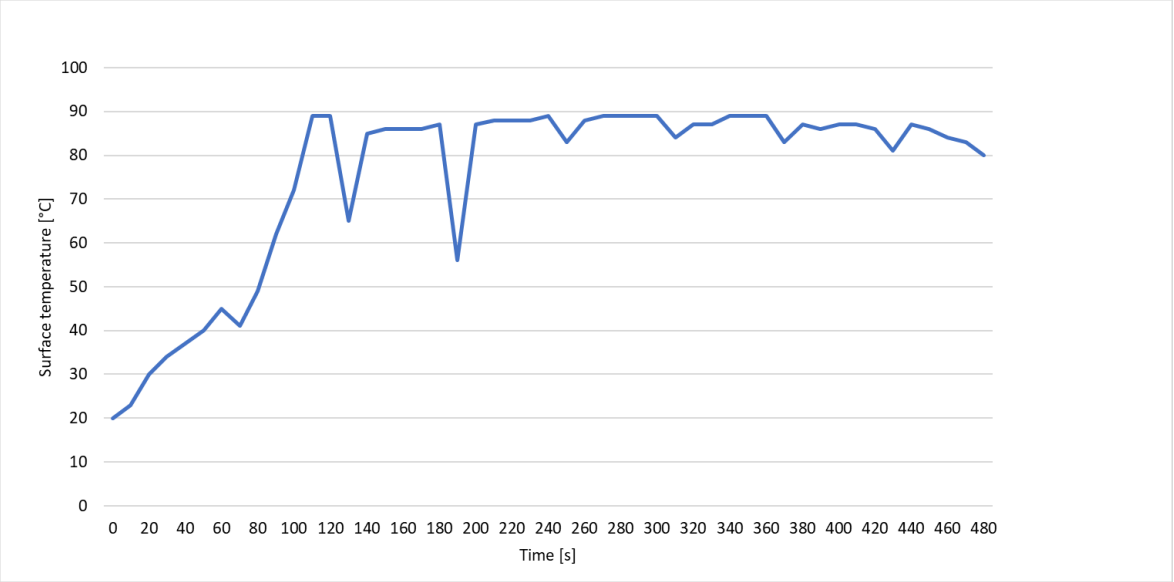

Figure 41: Surface temperature behavior as a function of drying time. 4 % consistency pine pulp sample dried with 100 % power in a 79 mm mold.

The weighing of the sample during drying took place every minute and the effect of it is noticeable as the temperature drops in Figure 41. It can be also seen that drying was still in the heating phase during the first weighing and surface temperature reached about half of the maximum. In the beginning, the surface temperature seemed to drop more during the weighing. This happened probably because the sample was still heating from the inside and was not reached the constant rate phase yet. After the constant rate phase was reached, the surface temperature did not drop as much during weighing. Since the constant rate phase was reached it took about 10 to 15 seconds for surface to heat back up to maximum temperature. Cooling of the surface during weightings could have some effect on drying efficiency

when compared to continuous drying. The behavior of the internal temperature of the sample could not be examined, which makes estimation more difficult.

Higher surface temperatures were reached with higher microwave power levels. Same example samples as in the mass change measurement plots are used to illustrate the behavior of surface temperature during drying. Temperatures were measured beside the mass change measurements. Surface temperature as a function of drying time is shown in Figure 42. 20 % power level measurements for both fibers have been omitted from the figure due to their long drying times to make plots clearer. Both used measurement techniques are presented.

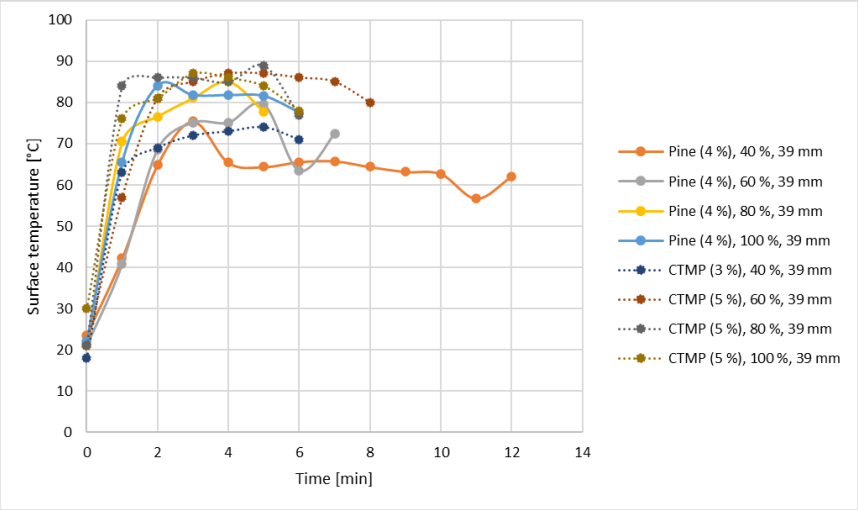

Figure 42: Surface temperature as a function of drying time. Fibers and consistency, microwave power level and mold height are shown on the right.

The increased microwave power level causes higher surface temperatures. Surface temperatures of every example pine pulp sample were measured with OS425-LS Omega non-contact infrared thermometer (Figure 22), whereas CTMP samples were measured with microwave oven's mounted IR sensor. The difference between measurement techniques can be seen from the shape of the temperature plots (Figure 42). Measurements made with IR sensor are more stable whereas OS425-LS Omega measurements are unstable due to difficult measurement conditions. CTMP samples seemed to reach higher maximum surface temperatures during experiments and temperatures rose faster (Figure 42). Measurement technique surely has an impact on this. Maximum surface temperatures reached for most used microwave power levels are given in Table 6. All the maximum surface temperatures were measured with a mounted IR sensor.

Table 6: Maximum obtained surface temperatures of the samples and required time to reach for the applied power levels.

Power level [%]	Power [W]	Fibers	Consistency [%]	Maximum surface temperature [ºC]	Time [min]
20	90,3	Pine	~2,5-2,8	68	5
40	940	Pine	~2,5-2,8	83	2
60	1580	Pine	~6,5-7	84	2
80	2150	CTMP	~5	89	8
100	2310	Pine	~4	90	5

The maximum surface temperature reached during experiments was 90 ºC and it was reached with 100 % microwave power level in 5 minutes of drying when pine pulp sample with ~4 % consistency was dried. Excluding a 20 % power level, maximum surface temperatures reached with other power levels are rather close to each other. It is noticeable that the measurement technique had some impact on the results as most of the maximum temperatures were reached with pine pulp samples, unlike Figure 42 presents. The effect of the sample consistency to maximum surface temperature is difficult to estimate, as consistencies vary notably in the results (Table 6).

7.2.4 Sample quality

During microwave drying experiments some transformations in the sample structure were noticed. Unlike with air impingement drying, burning damage or color change were not noticed unless drying was carried too far. Burned sample structure and damaged sample mold can be seen in Figure 43. The dry solids content of this sample was ~99 % when damage occured.

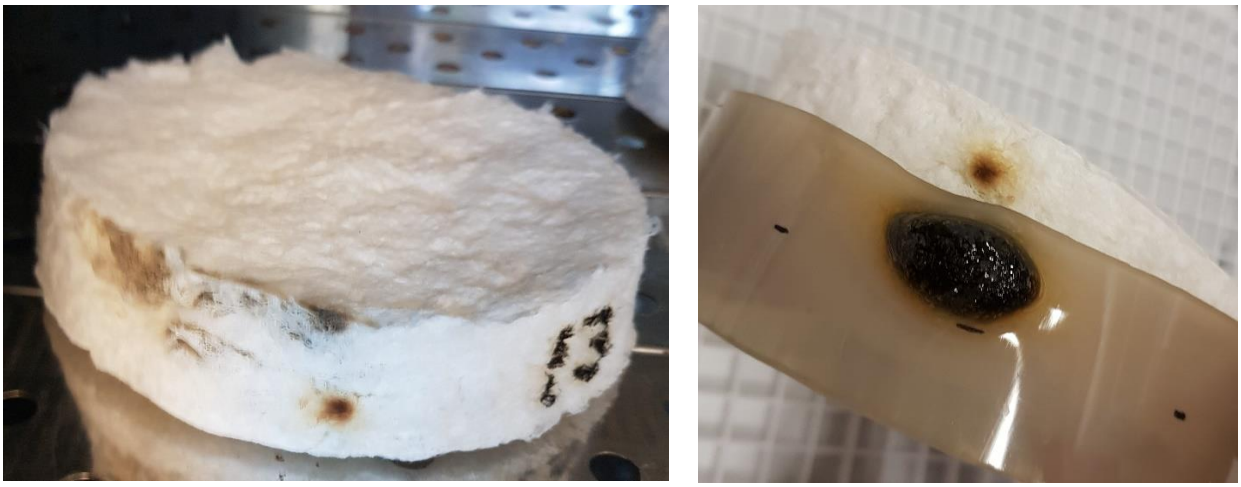

Figure 43: The effect of the burn damage to the sample and sample mold.

Shrinking and structural transformations were the most common changes that samples experienced. Structural transformations were mostly focused on the surface of the sample, but other parts also experienced transformations. With lower consistencies, the surface transformation from smooth to concave was a typical effect. The rugged or bumpy structures were most common with higher consistencies. Multiple samples gain some kind of air pockets or bulges to the center of the surface during drying. These appeared probably from the effect of bubbling that was noticed during drying as a swelling of the sample surface. This surface swelling happened most likely because of the volumetric heating of microwaves that caused the fast increase in initial temperature and vapor pressure. Evaporated water then strove to push through the sample structure and porous fiber composition could not last the stress of this effect. Usually, if this swelling happened, it took place during the first minutes of drying, when samples consisted still of a lot of water. The surface expanded over the height of mold edges in a shape of a dome and started collapsing after a certain period of time, which varied with different sample parameters. The structure of CTMP samples tended to collapse more after the expansion. The expansion lasted a longer time with lower microwave power when the sample heating took more time. In these cases, the expansion was noticed to happen during several drying minutes but was seen to be calmed the further the drying went. Expansion happened rapidly immediately at the beginning of drying with higher power levels, and usually, it took about 20-30 seconds for the surface to set. From these observations, it can be concluded that the surface expansion effect happened during the heating phase of drying. It was also noticed that water dribbling tended to happen at the same time with surface

expansion. Water was most likely able to flow through the sample structure easier due fast temperature rise during the first minutes of drying. Increased temperature decreases water viscosity (Figure 9), which lets water flow through the matter easier. After surface expansion ended, no more water was dribbled through the sample structures. As was mentioned earlier, samples with higher consistencies (> 7 %) did not experience as strong surface expansion as samples with lower consistencies. Higher consistency samples also let less water through their structures during the drying. This refers that structures of lower consistency samples that consisted of more water at the beginning of drying could not resist water to flow through due to fast viscosity drop.

Samples with lower consistencies (< 7 %) were more vulnerable to expansion and their structure tended to collapse. Figure 44 presents dry solids contents as a function of the moisture ratio of several example samples to illustrate the starting points of surface expansion during drying. All these points are the trial points gained from the first drying minute.

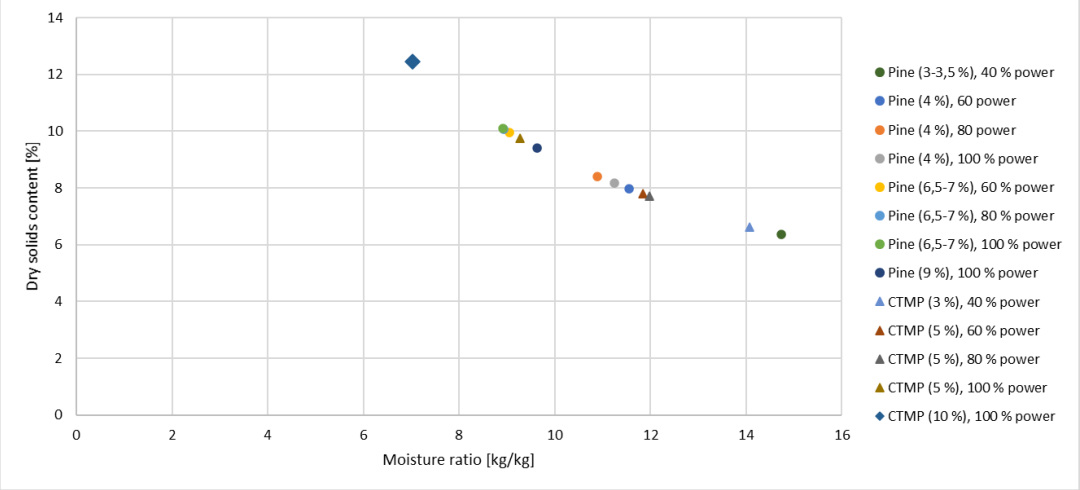

Figure 44: Dry solids content as a function of moisture ratio. Plotted points show the beginning of the surface expansion. Fibers, sample consistency and microwave power level are shown on the right.

It can be seen from Figure 44 that even though dry solids content at the beginning of the drying was around 10 %, surface expansion happened with the microwave power level of 60 % and 100 %. CTMP sample with ~10 % foam consistency is plotted in the shape of diamond to differentiate from other samples because no surface expansion was noticed during the drying of this sample. The moisture ratio of this sample was ~7 kg/kg and dry solids content was ~12,5 % at the beginning of the drying (Figure 44). 100 % microwave power was used to dry this sample which indicates that efficient drying of which the sample

structure lasts can be performed at least with these sample parameters. The drying time of this sample was 6 min and 30 sec, which is desirable. The surface temperature of over 80 ºC was reached during the first drying minute, but still, surface expansion was not noticed. Even higher consistency foams could not be generated with the circumstances of these experiments.

To investigate structural modifications caused by microwave heating, tomography pictures were taken from several samples. Tomography pictures were taken horizontally and vertically. Samples with different consistencies and used power levels were graphed to gain as much information about structural modifications as possible.

The effect of bubbling during drying is clearly noticeable from the tomography pictures. When consistency was kept constant and power level was raised, sample structure tended to change from concave and bent form to flatter or even dome shape. This effect can be seen from Figure 45, where tomography pictures of ~4 % consistency pine pulp samples dried with 30 % and 80 % power levels, are shown.

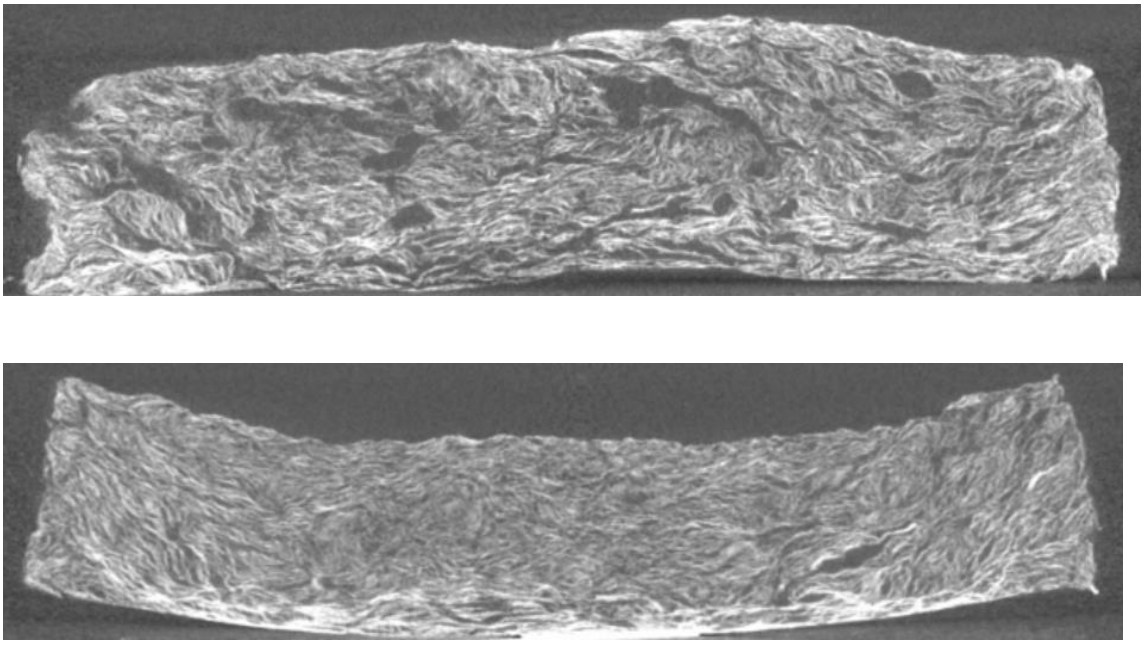

Figure 45: The effect of microwave power level to sample shape. Pine pulp samples of ~4 % consistency dried with power levels of 30 % (bottom) and 80 % (top). Tomography pictures were taken from the sides.

Sides were more bent upwards when drying was performed with lower power level or lower consistency existed. Edges of the samples tended to form ruggeder, and the surface got

bumpier when drying power was increased (Figure 45). Higher power levels created a bigger dome effect due to bubbling. This phenomenon created bulges to the middle of the sample surfaces and with the highest power levels, hollow air pockets were noticed. Tomography pictures of ~4 % consistency pine pulp sample dried with 100 % microwave power level are shown in Figure 46 to illustrate the formed hollow air pockets.

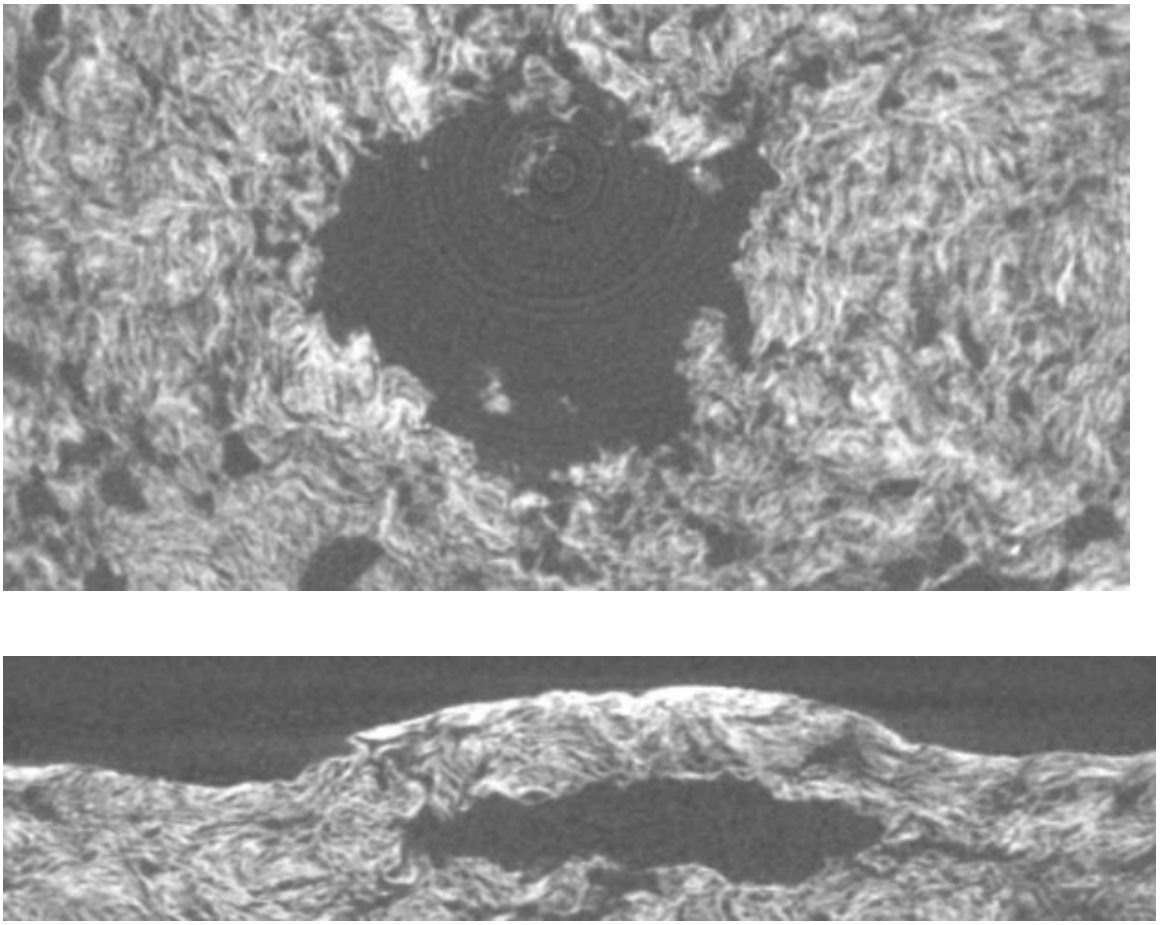

Figure 46: Formed air pocket to the sample surface due to bubbling. The sample was 4 % consistency pine pulp sample dried with 100 % power. Tomography pictures of the sample from the top (top) and the side (bottom).

As can be seen from Figure 46, expansion of the sample surface caused a clear hollow air pocket to the center. The shape of the surface for most of the samples was on the same type unless a dome shape (Figure 45) appeared. Some tomography pictures revealed that even though surface expansion happened, and bulges were formed, they were not hollow every time.

It was noticed that more fibers were organized close to the edges of the samples when higher drying power was used. This happened probably because of the bigger dome effect due to bubbling. A spherical and symmetric shape of the used sample molds explains why fibers tended to organize to the edges after the expanded surface collapsed. When the dome effect ended and the surface collapsed, surface mass continued its movement away from the center towards the edges of the mold. The moving mass lost its kinetic energy due to colliding with the mold edges and transferred fibers settled to the edges of the sample. Lower power levels did not cause as big surface expanding which appeared as a more stable fiber organization. Also, higher consistency samples, even with higher power levels, withstood the drying better and surface expansion was not noticed. This led to more stable surface and fiber orientation. An illustrative example of 5 % and 10 % consistency CTMP samples dried with 100 % microwave power in the 39 mm mold are shown in Figure 47.

Figure 47: 5 % (left) and 10 % (right) consistency CTMP samples dried with 100 % microwave power and 39 mm mold.

The amount of air gaps formed inside the samples was increased due to the power raise. These air gaps were originated probably due to fast water evaporation that happened between Plateau borders. More air space in the sample structure originated when consistency was lower, but these gaps are different in shape. However, there was not a significant difference between pine pulp and CTMP fibers, but the consistency was the biggest factor affecting fiber orientation. The increased amount of formed air gaps made structure and fiber orientation more unstable. More porous samples with fewer air gaps had stable fiber orientation.

7.2.5 Compressibility strength measurements

To gain information about compressibility strengths of foam formed samples, compressibility strength tests were performed in a laboratory. Both, pine pulp and CTMP samples were tested with different consistencies. All tested samples were dried in the 39 mm high mold. Tests were performed with Lloyd LR10K universal tester (Figure 48). Conditions during tests were 23 ± 1 °C and relative humidity of 50 ± 2 %.

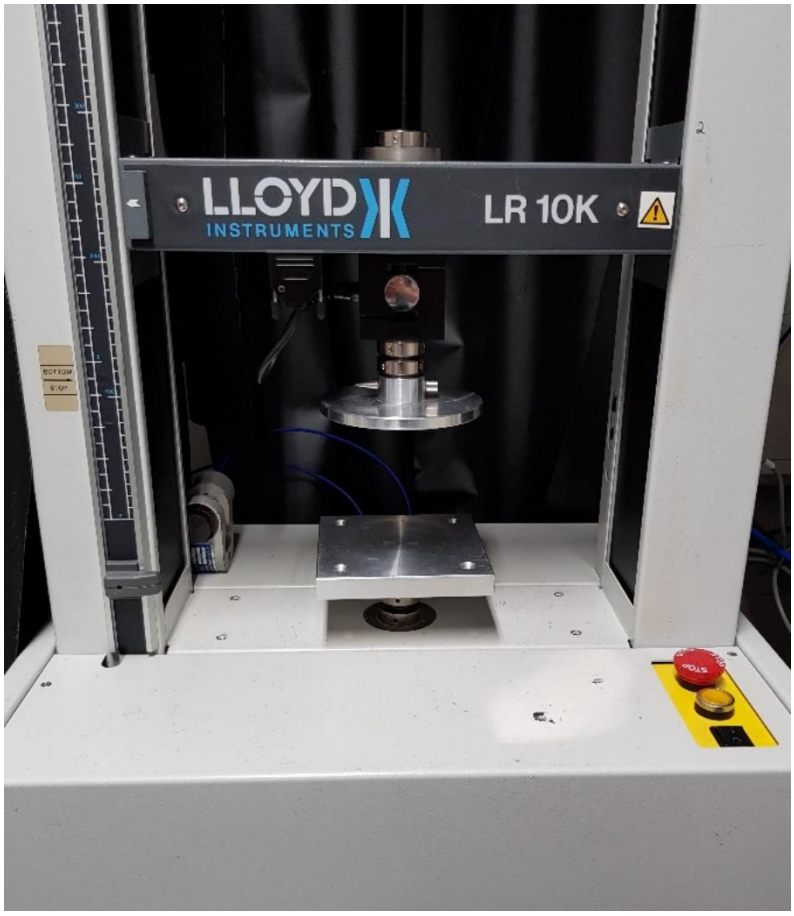

Figure 48: Lloyd equipment for compressive strength measurements.

In Figure 48, a circular plate that is connected to a measuring sensor is compressing tip with diameter a of 14 cm. Under that is a thicker square bottom plate (15x15 cm). Lloyd testing equipment is connected to a computer and data is collected to a program called NEXYGEN.

Samples were prepared for testing by cutting them into smaller sizes. Samples were cut from the middle into shapes of a square. Two sizes applied: 7,5x7,5 cm (56,25 cm^2) and 10x10 cm (100 cm^2). 9 samples were tested of which 7 were pine pulp and 2 were CTMP. Samples were weighed before and after measurements. One compressing per sample was made.

Samples were pressed until they were compressed to 50 % of their starting thickness. The reversibility of the samples was not examined during measurements.

Before compression, starting force had to be directed to the sample. This force is based on a surface area of the sample and pressure of 250 Pa. Starting force before compression was solved from Equation 17:

$$F = p \cdot A_s \tag{17}$$

where F is the force [N], p is the pressure [Pa] and A_s is the surface area [m^2].

From Equation 17, starting forces applied during experiments were:

$$F = 250 \text{ Pa} \cdot 0{,}005625 \text{ m}^2 = 1{,}44 \text{ N}$$

and

$$F = 250 \text{ Pa} \cdot 0{,}01 \text{ m}^2 = 2{,}50 \text{ N}.$$

Compressing speed until starting force is reached is determined based on starting thickness of the sample. It can be solved from Equation 18:

$$v_c = 0{,}1 \frac{1}{\text{min}} \cdot H \tag{18}$$

where v_c is compressing speed mm/min and H is sample thickness [mm].

Starting thicknesses of the samples were determined by lowering the compressing tip of Lloyd to the level where it started to touch the sample surface and a small load amount (~0,20-0,40 N) was applied. Sample thickness and the current load were then watched from the screen of Lloyd's control panel (Figure 49). "Extension" that is shown on the screen in Figure 49 presents the distance between compressing tip and bottom plate. When there was a sample between the tip and the bottom, and a small load was applied, starting thickness of the sample could be determined. Based on starting thicknesses of samples, until starting forces were reached, compressing speeds between 1,50-4,20 mm/min were applied during the experiments. When the starting forces were reached, compressing speed increased and the average compressing time was ~30 seconds.

Figure 49: Control panel of Lloyd.

Figure 50 illustrates compression load as a function of compression for tested samples. Compression percentage presents the amount of how much the sample is compressed from its original thickness. Graphs end to 50 % compression because data collection was set to that point.

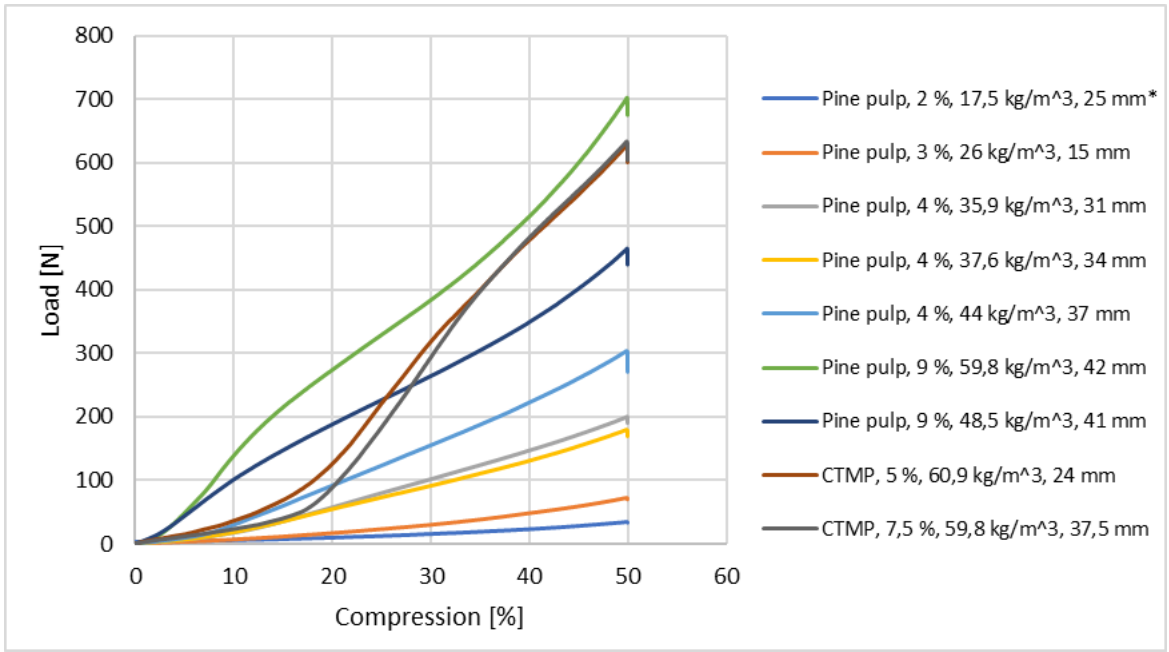

Figure 50: Compressing load as a function of compression from original thickness (* = 10x10 cm sample. Other samples were 7,5x7,5 cm.). Fibers, consistency, density and sample thickness before compressing are shown on the right.

It can be seen from Figure 50 that as sample consistency increased, higher loads were applied during compressing. However, CTMP samples had almost identical graphs even though consistencies were 5 % and 7,5 % and the thickness difference between these samples was 13,5 mm and mass difference ~4 g. They reached almost the same load at the end of compressing. These loads were 628 N with 5 % consistency and 634 N with 7,5 % consistency. During drying of these samples, 7,5 % consistency sample experienced huge surface expansion when 5 % consistency sample did not. The surface expansion created a hollow air pocket to the middle of the sample and the sample structure was also rugged compared to others, which could affect compression results. CTMP graphs were also steeper than pine pulp graphs, which refers that CTMP structures are more elastic and need more force to be compressed. Pine pulp graphs are quite similar in shape together and gentler than CTMP graphs. With consistencies lower than 9 %, load tended to grow smoothly when compression increased with pine pulp samples. With 9 % consistency, load change increased fast till 5-8 % compression, then increased slowly till ~30 % compression, and started to increase faster again till 50 % compression. This can be seen as rising and stable shapes in the graphs (Figure 50). Load change with both CTMP samples can be seen increasing slowly till 20 % compression and after that growing quickly between 20 % and 30 %, then slowly decreasing till 50 % compression (Figure 50). The lowest reached load with pine pulp samples was 33,7 N with 2 % consistency and the highest was 702 N with 9 % consistency. This was also the highest load measured during the experiments. Two measurements were made with 9 % consistency pine pulp samples with starting thicknesses of 41 mm and 42 mm, but measured loads are different and the difference at the end of compressing was ~237 N (Figure 50), which is a quite significant difference with almost identical sample parameters. The sample from 9 % consistency samples that reached lower load was dried with 100 % microwave power when another was dried with 80 %. The sample that was dried with 100 % power experienced more structural stress during drying, for example, higher surface expansion, which could affect compressing load values. There were three 4 % consistency pine pulp samples with different thicknesses (Figure 50) and the thickest of those (37 mm) experienced higher loads during compressing than the other two (31 mm and 34 mm). Every sample from these three experienced surface expansions in the drying experiments and had that unstable surface with a formed air pocket in the middle of the sample. 31 mm and 34 mm samples were dried with 70 % and 80 % microwave power levels when 37 mm sample was dried

with 100 %. Mass of the 37 mm sample was higher than the other two thinner samples. Also, with 9 % consistency pine pulp samples, 42 mm thick sample, which reached higher compressing load values, was heavier and had the density of 59,8 kg/m^3 (Figure 50). This refers that pine pulp samples gain higher loads when consistency and mass are increased. Based on the measurements, CTMP samples did not behave the same way and more measurements would have to be done to estimate their structural behavior more accurately.

Slopes were also calculated for every sample from the measurement data. The slope illustrates the steepness of the graph at a certain measurement point and is determined here as a force of the steepest point of the rising graph divided with a change in sample thickness. The highest slope values and compression loads in those points for every sample are given in Table 7.

Table 7: The highest reached slopes and compression loads of the tested trial points. Fibers, consistency and starting thickness of samples are shown on the left column.

Sample	Slope [N/mm]	Load [N]
Pine pulp, 2 %, 25 mm	5,70	32,3
Pine pulp, 3 %, 15 mm	18,2	70,2
Pine pulp, 4 %, 31 mm	19,0	196
Pine pulp, 4 %, 34 mm	17,0	175
Pine pulp, 4 %, 37 mm	25,4	297
Pine pulp, 9 %, 41 mm	33,9	453
Pine pulp, 9 %, 42 mm	53,0	688
CTMP, 5 %, 24 mm	86,2	197
CTMP, 7,5 %, 37,5 mm	60,7	294

It is noticeable that the highest slope values were reached with CTMP samples. The highest slope value was 86,2 N/mm and it was reached with 5 % consistency CTMP sample at the

point where compression load was 197 N and 23,8 % of sample thickness was compressed. With pine pulp samples, the highest slope value was 53 N/mm and it was reached with a 9 % consistency sample at the point where the load was 688 N and 49,3 % of sample thickness was compressed. Pine pulp samples tended to gain their highest slope values at the end of compressing with greater load forces when CTMP samples reached them about halfway through compressing. The highest slopes can be seen in Figure 50 where graphs are the steepest.

7.2.6 Energy consumption

Energy consumption calculations were made based on the calculated corrected microwave powers (Table 4). Calculated powers were powers that microwave radiation emits to water during drying. Due to this only energy that is consumed for water removal could be clarified. Consumed energy depends on drying time and used power level. Average drying time for every power level amongst the most used power levels was used in calculations. Dry solids contents at the end of drying were not the same in a group of compared samples, which distorts the results. The average dry solids content at the end of drying for pine pulp samples was 59,8 % and for CTMP samples 53,6 %. These averages were calculated from the average dry solids contents reached for the most used power levels. Reached average dry solids contents for different power levels are presented in Table 8.

Table 8: Average dry solids contents reached for the most used microwave power levels and average drying times for pine pulp and CTMP samples.

Power level [%]	Average drying time (Pine) [min]	Average DSC (Pine) [%]	Average drying time (CTMP) [min]	Average DSC (CTMP) [%]
20	30,5	83,1	20,8	50,2
40	7,3	39,4	6,0	27,0
60	6,2	58,7	8,0	63,8
80	6,3	63,8	6,0	67,1
100	6,9	53,8	5,1	60,1

Table 8 illustrated that with power levels 60 %, 80 % and 100 % average dry solids contents reached are quite close to each other and the total average for used fibers including an average of CTMP dried with 20 % power. However, with lower power levels (20 % and 40 %), average dry solids contents had more spread. In the circumstances where drying experiments were performed, it was difficult to forecast the dry solids content at the end of drying.

When average drying time and microwave power emitted to water were known, average energy consumption for drying could be solved from Equation 19:

$$E_{\mathrm{avg}} = P \cdot t_{\mathrm{avg}} \tag{19}$$

where E_{avg} is average energy consumption [kWh] and t_{avg} average drying time [h].

From Equation 19, average energy consumption for example pine pulp samples dried with 80 % power is:

$$E_{\mathrm{avg}} = 2{,}15\ \mathrm{kW} \cdot 0{,}11\ \mathrm{h} = 0{,}226\ \mathrm{kWh}.$$

Based on average dry masses of samples with most used power levels, average energy consumption per produced dry kilo can be solved from Equation 20:

$$E_{\mathrm{avg/kg}} = \frac{E_{\mathrm{avg}}}{m_{\mathrm{d,avg}}} \tag{20}$$

where $E_{\mathrm{avg/kg}}$ is energy consumption per produced dry kilo [kWh/kg] and $m_{\mathrm{d,avg}}$ is average dry mass [kg].

From Equation 20, the average energy consumption per produced kilo for example for pine pulp samples dried with 80 % power is:

$$E_{\mathrm{avg/kg}} = \frac{0{,}226\ \mathrm{kWh}}{0{,}028\ \mathrm{kg}} = 8{,}1\ \frac{\mathrm{kWh}}{\mathrm{kg}}.$$

Figure 51 illustrates average energy consumptions per produced dry kilo for the most used power levels for pine pulp and CTMP samples. Average drying times for different power levels are also plotted to the same figure.

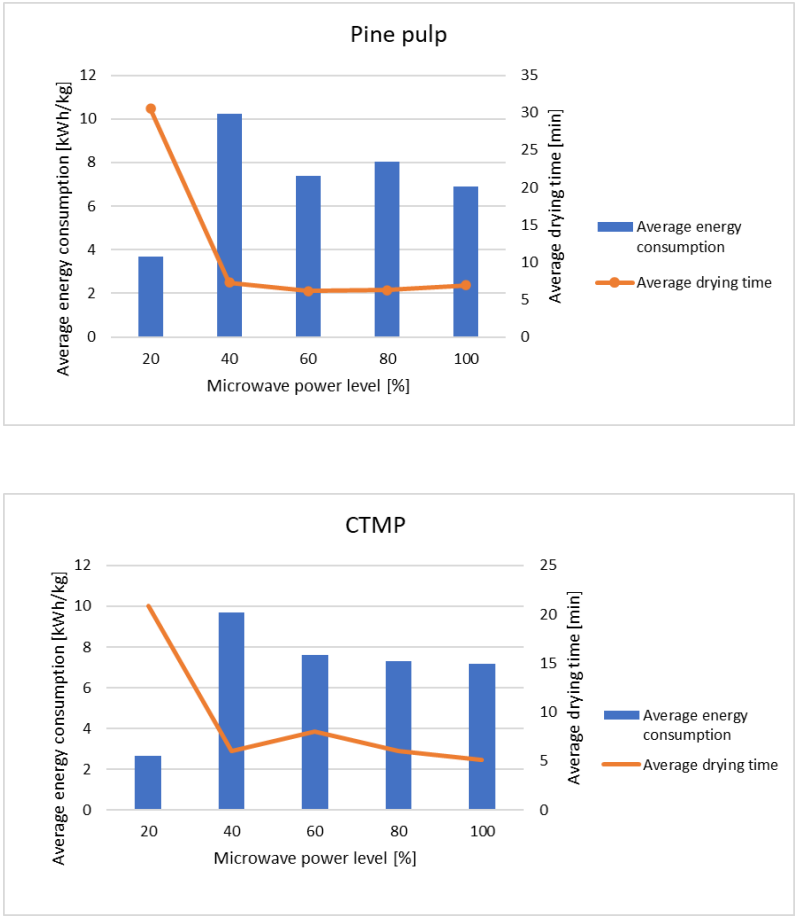

Figure 51: Average energy consumption and drying time for the most used microwave power levels.

It can be seen from Figure 51 that the average energy consumption for both fibers with a 20 % power level (0,09 kW) was low, but average drying time was lot longer than with higher power levels. With a 20 % power level, for pine pulp average energy consumption was 3,7 kWh/kg and average drying time was 30,5 min and for CTMP 2,6 kWh/kg and 20,8 min. Starting consistencies of samples dried with 20 % were low (~2,5-4 %), but the structure of most of the samples withstood the drying and due to that average drying time was long and average dry solids content at the end of drying was moderate. It is also noticeable that the average drying time with a 40 % power level (0,94 kW) was short and in the same range with higher power levels. Average energy consumption was the highest amongst the most used power levels for both fibers. 10,2 kWh/kg for pine pulp and 9,7 kWh/kg for CTMP. Starting consistencies of samples dried with 40 % power level were low (~2,5-4 %) for both fibers and drying had to be ended early to avoid quality damage to samples and other supportive structures, which caused the low average dry solids content at the end of

drying. If higher starting consistencies were used also for 40 % power level, average drying time, and average dry solids content at the end of drying would have been higher and more comparable. Average energy consumption was lower with 100 % than with 60 % and 80 % for both fibers (Figure 51). However, consumptions were similar with these power levels and were between 6,9-8,1 kWh/kg. Higher average sample dry masses with these power levels resulted from use of thicker sample molds. A bigger total amount of pine pulp samples compared to CTMP samples could affect the results and due to that bigger spread between results is occurred with CTMP samples. It was also found that CTMP samples behaved more versatile during drying, and it was difficult to perceive the relation between the microwave power level and the sample with different parameters. With power levels of 60 %, 80 % and 100 %, starting consistencies of 2-9 % were applied with pine pulp samples and 5-10 % with CTMP samples. With these power levels, higher dry solids contents, with similar energy consumption, were obtained with CTMP. Sample thickness was not found to have magnitude on drying times.

8 COST CALCULATIONS

Calculations were made to estimate possible operation expenses. The considered expenses include labor, raw material and energy costs. Taxes were not included in the calculations. Also, investment costs were disregarded. Calculations were made assuming that drying equipment is fitted to a 40 ft container to make it movable. Sizes of the 40 ft container are 12,192 m (length) X 2,352 m (width) X 2,591 m (height), where 2,352 m is inner width (iContainers 2013). Length and height are outer dimensions. It was assumed that the container has openable side walls, so extra space across the container is not needed when there is no need to get inside the container. This allows necessary maintenance tasks to be performed from outside. The width of the container enables a track width of 2 m, which was used in the example calculations.

Most of the drying experiments were performed with pre-refined pine pulp as a raw material of the foam, so it was used also in these cost calculations. It was assumed that foam was formed near drying equipment. It was also assumed that foam was available all the time and no production delays occurred because of foaming. The average drying time of pine pulp samples dried with 100 % microwave power was used in dimensioning. The consistency of the foam was assumed to be ~4 %. Sample thickness was decided to be 34 mm according to the most used mold size of 39 mm and assuming that average shrinkage in thickness direction during drainage was ~5 mm. Based on the dry masses gained in the laboratory experiments, a basis weight of the dry product for calculations is selected to be 1320 g/m^2 (t/km^2).

8.1 Dimensioning of the process

As mentioned, drying process is sized to one 40 ft container. This allows track width of 2 m. According to the dimensions of a 40 ft container, a 12 m long dryer is possible to fit into one container. This means that the drying area would be 24 m^2 for straight (not bended) product. For 4 % consistency pine pulp sample with thickness of ~34 mm that was dried with 100 % power, drying time in laboratory experiments was found to be ~6 minutes, so it is selected to be drying time. With a 12 m dryer length and 6 minutes drying time, a machine speed maximum is 2 m/min. The process also needs extra containers for drainage. They are assumed to be connected to the drying part. Let’s consider that drainage is performed on a

moving wet wire, which is run at the same speed as a dryer to avoid possible structural damages that could happen if machine speed is changed between drainage and drying parts. The drainage time of samples in the laboratory experiments was found to be around 15 minutes. If machine speed is 2 m/min, a 30 m long drainage part is necessary. The drainage part is also considered to be fitted in containers. To reach a long enough track for drainage, three 40 ft containers are required.

When the basis weight of the product, machine speed and track width are known, production speed can be solved from Equation 21:

$$\dot{m} = BW \cdot v \cdot w \cdot 60 \frac{\text{min}}{\text{h}} \tag{21}$$

where $\dot{m}$ is production speed [kg/h], BW is basis weight of product [kg/m^2], v is machine speed [m/min] and w is track width [m].

From Equation 21, production speed is:

$$\dot{m} = 1{,}32 \ \frac{\text{kg}}{\text{m}^2} \cdot 2 \ \frac{\text{m}}{\text{min}} \cdot 2 \ \text{m} \cdot 60 \ \frac{\text{min}}{\text{h}} = 316{,}8 \ \frac{\text{kg}}{\text{h}}.$$

8.2 Costs

According to production speed, it is assumed that two workers can run the process. It is also assumed that the machine is running 5 days a week, 8 hours a day and 45 days per year are reserved for machine maintenance and adjustments. This means about 10,5 working months per year. If the average days per month is 30,5 and working days per week is 5, working days per month is ~21,8. When there are ~21,8 working days per month, about 10,5 working months per year and daily working hours are 8, there will be 1828,6 working hours per year. Based on the Eurostat 2020 Finland Labor cost level for industry, the hourly salary cost of 37 €/h, which comes from the compensation of employees plus taxes minus subsidies, is used in the cost calculations (Eurostat b). Annual labor costs can be solved from Equation 22:

$$C_{\text{labor}} = s \cdot t_{\text{h}} \cdot n \tag{22}$$

where C_{labor} is annual labor costs [€], s is worker's hourly salary [€/h], t_{h} is annual working hours [h] and n is the number of work personnel [-].

From Equation 22, labor costs per year are:

$$C_{\text{labor}} = 37\ \frac{€}{\text{h}} \cdot 1828{,}6\ \text{h} \cdot 2 = 135\ 314\ €.$$

When production speed and annual working hours are known, annual dried production can be solved from Equation 23:

$$m_{\text{dry}} = \frac{\dot{m} \cdot t_{\text{h}}}{1000\ \frac{\text{kg}}{\text{t}}} \tag{23}$$

where m_{dry} is the mass of dried product [t].

From Equation 23, annual dried production is:

$$m_{\text{dry}} = \frac{316{,}8\ \frac{\text{kg}}{\text{h}} \cdot 1828{,}6\ \text{h}}{1000\ \frac{\text{kg}}{\text{t}}} = 579{,}3\ \text{t}.$$

When considering raw material costs, fiber costs can be determined from dried production, but surfactant and water costs must be solved by considering the change in moisture ratio of the product during the drying. This, because water and surfactant are raw materials needed for foam forming before drying. Annual production including water that is evaporated can be solved from Equation 24:

$$m_{\text{wet}} = m_{\text{dry}} \cdot \Delta X \tag{24}$$

where m_{wet} is mass the of wet product [t] and ΔX is the moisture ratio change during drying [kg/kg].

The value of moisture change during drying is based on the laboratory experiments ΔX = 12,8 kg/kg. Then the mass of annual production including water is:

$$m_{\text{wet}} = 579{,}3\ \text{t} \cdot 12{,}8\ \frac{\text{kg}}{\text{kg}} = 7\ 414{,}9\ \text{t}.$$

Raw material costs were determined based on the unit values of 2020 Eurostat annual data. The price of fibers was chosen to be the unit price of chemical wood pulp in Finland and surfactant price was chosen to be the unit price of anionic organic surface-active agents in Germany (Eurostat c). The unit price of water was chosen to be 1 €/t and it is assumed that tap water is not used but process water is taken from the lake with own filtering for example. Unit prices of raw materials are given to Table 9.

Table 9: Unit prices for raw materials. (Eurostat b.)

Raw material	Unit price [€/t]
Fibers	446
Surfactant	1081
Water	1

Total annual raw material costs for the process can be solved from Equation 25:

$$C_{\mathrm{RM}} = C_{\mathrm{fiber}} + C_{\mathrm{surf}} + C_{\mathrm{w}} \tag{25}$$

where C_{RM} is annual raw material costs [€], C_{fiber} is annual fiber costs [€], C_{surf} is annual surfactant costs [€] and C_{w} is annual water costs [€].

As was mentioned earlier, annual fiber costs can be solved based on annual dried production. Annual fiber costs can be solved from Equation 26:

$$C_{\mathrm{fiber}} = c_{\mathrm{fiber}} \cdot m_{\mathrm{dry}} \tag{26}$$

where c_{fiber} is the unit value of fibers [€/t].

Annual surfactant and water costs can be solved based on the production that includes water evaporated during drying (Equation 24). These costs can be solved from Equations 27 and 28:

$$C_{\mathrm{surf}} = c_{\mathrm{surf}} \cdot m_{\mathrm{wet}} \cdot f_{\mathrm{surf}} \tag{27}$$

where c_{surf} is the unit value of surfactant [€/t] and f_{surf} is share of surfactant in the foam [-].

$$C_{\mathrm{w}} = c_{\mathrm{w}} \cdot m_{\mathrm{wet}} \cdot f_{\mathrm{w}} \tag{28}$$

where c_{w} is the unit value of water [€/t] and f_{w} is share of water in the foam [-].

Surfactant content in the foam with 10 % SDS, which was used in the experiments, was 6 mL per 1 L of the mixture. When foam consistency was ~4 %, share of SDS was 0,6 % and the share of water was 95,4 %. From the Equations 26, 27 and 28, annual costs of fiber, surfactant and water are:

$$C_{\mathrm{fiber}} = 445{,}43\ \frac{€}{\mathrm{t}} \cdot 579{,}3\ \mathrm{t} = 258\ 034\ €,$$

$$C_{\mathrm{surf}} = 1081{,}27\ \frac{€}{\mathrm{t}} \cdot 7414{,}9\ \mathrm{t} \cdot 0{,}006 = 48\ 105\ €,$$

$$C_{\mathrm{w}} = 1\ \frac{€}{\mathrm{t}} \cdot 7414{,}9\ \mathrm{t} \cdot 0{,}954 = 7\ 074\ €.$$

From Equation 25, total annual raw material costs are:

$$C_{\mathrm{RM}} = 258\ 034\ € + 48\ 105\ € + 7\ 074\ € = 313\ 213\ €.$$

Drying energy to the process is assumed to be produced only by electricity. This also allows the process to be movable when the conventional steam power plant is not needed for producing hot steam for drying.

Water removal from the product during drying includes water heating and evaporation, which should be calculated separately. It is assumed that water temperature inside the foam before drying is 25 °C, meaning that water must be heated from 25 °C to 100 °C. First, energy demand per ton of water has to be solved. Energy demand per ton of water for heating can be solved from Equation 29:

$$E_{\mathrm{heat}} = \frac{c_{p,\mathrm{w}} \cdot \Delta T}{3{,}6\ \frac{\mathrm{MJ}}{\mathrm{kWh}}} \tag{29}$$

where E_{heat} is energy demand for heating of water [kWh/t].

Specific heat capacity for water is $c_{p,w}$(25 ºC) = 4,18 kJ/kgK = 4,18 MJ/tK. When ΔT = 75 K, from Equation 29, energy demand for heating is:

$$E_{\text{heat}} = \frac{4{,}18\,\frac{\text{MJ}}{\text{tK}} \cdot 75\ \text{K}}{3{,}6\,\frac{\text{MJ}}{\text{kWh}}} = 87{,}1\ \frac{\text{kWh}}{\text{t}}.$$

Latent heat of evaporation of water is h_{ev} = 2260 kJ/kg = 2260 MJ/t (Datt 2011, 702). Energy demand for evaporating ton of water can be solved from Equation 30:

$$E_{\text{ev}} = \frac{h_{\text{ev}}}{3{,}6\,\frac{\text{MJ}}{\text{kWh}}} \tag{30}$$

where E_{ev} is energy demand for water evaporating [kWh/t].

The energy demand for water evaporation is then:

$$E_{\text{ev}} = \frac{2260\,\frac{\text{MJ}}{\text{t}}}{3{,}6\,\frac{\text{MJ}}{\text{kWh}}} = 627{,}8\ \frac{\text{kWh}}{\text{t}}.$$

Total energy demand for removing ton of water can be solved from Equation 31:

$$E_{\text{tot,w}} = (E_{\text{heat}} + E_{\text{ev}}) \cdot (1 + loss) \tag{31}$$

where $E_{\text{tot,w}}$ is total energy demand for removal of ton of water [kWh/t] and $loss$ is total losses [-].

Losses during drying was chosen to be 20 %. From Equation 31, total energy demand for water removal of ton of water is:

$$E_{\text{tot,w}} = \left(87{,}1\ \frac{\text{kWh}}{\text{t}} + 627{,}8\ \frac{\text{kWh}}{\text{t}}\right) \cdot (1 + 0{,}20) = 857{,}8\ \frac{\text{kWh}}{\text{t}}.$$

Total energy demand for water removal per ton of product can be solved when change in moisture ratio during drying is known. This can be solved from Equation 32:

$$E_{\text{tot}} = E_{\text{tot,w}} \cdot \Delta X \tag{32}$$

where E_{tot} is total energy demand for water removal per ton of product [kWh/t].

The total energy demand for water removal per ton of product is:

$$E_{\mathrm{tot}} = 857{,}8\ \frac{\mathrm{kWh}}{\mathrm{t}} \cdot 12{,}8\ \frac{\mathrm{kg}}{\mathrm{kg}} = 10\ 980{,}3\ \frac{\mathrm{kWh}}{\mathrm{t}}.$$

When annual production is known, total annual energy consumption can be solved from Equation 33:

$$E_{\mathrm{cons}} = \frac{E_{\mathrm{tot}} \cdot m_{\mathrm{dry}}}{1000\ \frac{\mathrm{kWh}}{\mathrm{MWh}}} \tag{33}$$

where E_{cons} is total annual energy consumption [MWh].

The total annual energy consumption is:

$$E_{\mathrm{cons}} = \frac{10\ 980{,}3\ \frac{\mathrm{kWh}}{\mathrm{t}} \cdot 579{,}3\ \mathrm{t}}{1000\ \frac{\mathrm{kWh}}{\mathrm{MWh}}} = 6\ 361\ \mathrm{MWh}.$$

Based on the total annual energy consumption, electricity price was selected from Eurostat. Electricity prices for non-household consumers with annual consumption of 2 000-20 000 MWh (no taxes involved). Price was selected from the second half of the year 2020 and the price was 0,0651 €/kWh. (Eurostat a.) Annual energy costs can be solved from Equation 34:

$$C_{\mathrm{E}} = c_{\mathrm{el}} \cdot E_{\mathrm{tot}} \cdot m_{\mathrm{dry}} \tag{34}$$

where C_{E} is annual energy cost [€] and c_{el} is electricity unit price [€/kWh].

From Equation 34, annual energy costs are:

$$C_{\mathrm{E}} = 0{,}0651\ \frac{€}{\mathrm{kWh}} \cdot 10\ 980{,}3\ \frac{\mathrm{kWh}}{\mathrm{t}} \cdot 579{,}3\ \mathrm{t} = 414\ 086\ €.$$

Labor-, raw material- and energy expenses were considered in the cost calculations. Total annual operational costs for the process can be solved from Equation 35:

$$C_{\mathrm{tot}} = C_{\mathrm{labor}} + C_{\mathrm{RM}} + C_{\mathrm{E}} \tag{35}$$

where C_{tot} is total annual operational cost [€].

From Equation 34, total annual operating costs are:

$$C_{\text{tot}} = 135\,314\,€ + 313\,213\,€ + 414\,086\,€ = 807\,434\,€.$$

Operational costs per produced dry ton can be solved from Equation 36:

$$C_{x,\text{prod}} = \frac{C_x}{m_{\text{dry}}} \tag{36}$$

where $C_{x,\text{prod}}$ is cost of variable *x* per produced dry ton [€/t] and C_x is annual cost of variable *x* [€].

The costs based on the production for labor, raw materials, energy, and total are then:

$$C_{\text{labor,prod}} = \frac{135\,314\,€}{579{,}3\,\text{t}} = 243\,\frac{€}{\text{t}},$$

$$C_{\text{RM,prod}} = \frac{313\,213\,€}{579{,}3\,\text{t}} = 541\,\frac{€}{\text{t}},$$

$$C_{\text{E,prod}} = \frac{414\,086\,€}{579{,}3\,\text{t}} = 715\,\frac{€}{\text{t}},$$

$$C_{\text{tot,prod}} = \frac{807\,434\,€}{579{,}3\,\text{t}} = 1489\,\frac{€}{\text{t}}.$$

To illustrate the shares of different cost factors, calculated annual operational costs are shown in Figure 52. The shares of costs are divided in such a way that energy 48 %, raw materials 36 % and labor 16 %. The cost distribution depends on many parameters and could be different if these parameters are changed. For example, labor costs would increase if more personnel are needed to run the process. If amount of removed water during drying would be less, drying time would be shorter, and less energy would be needed for larger scale production.

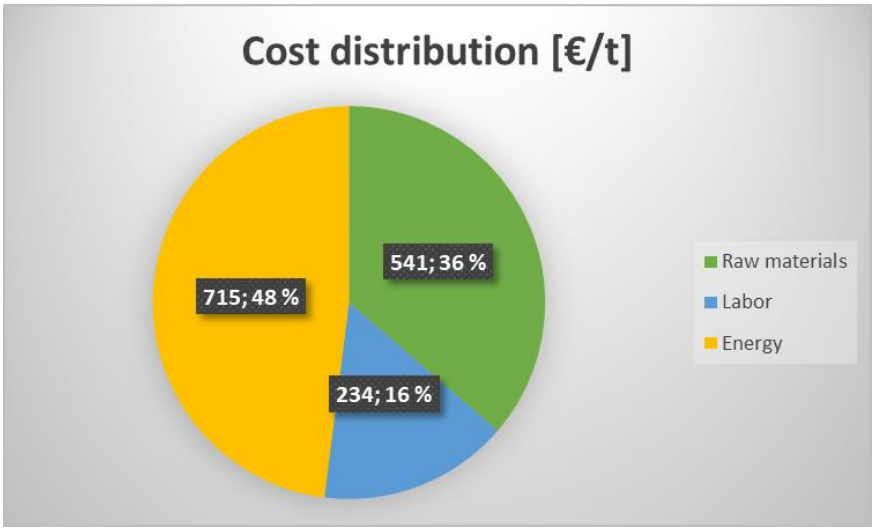

Figure 52: The shares of calculated annual operational cost for the process.

9 DISCUSSION

During the air impingement drying experiments that considered the mass change of the samples, the weighing took approximately 20-30 sec, which decelerated the drying speed. At the same time the weighing probably did not cause significant errors between the samples and the results are comparable between samples, but continuous process would be more efficient. Based on the mass change measurements and calculated data, as jet velocity and impingement air temperature were increased, drying time was decreased. Increased drying temperature (150 to 200 °C) led to sample surface darkening caused mainly by SDS. The surface was already darkened when the inner structure of the sample still contained lots of water. This happened due to decomposition of SDS, which happens when temperature is 40 °C or higher. Darkening can be reduced by reducing the SDS dose or using another surfactant. Sample surface also experienced transformations as increased jet velocity turned the flat surface into a concave form. Otherwise, samples maintained their smooth structures, which is favorable considering the quality parameters. Dry solids content at the end of drying was difficult to estimate, which led to variations between the samples. Calculations based on measured mass change data were processed after all experiments were executed and due to that dry solids contents during the experiments were not on record. Drying was continued until mass change was < 1 g/min, but it should have continued further as the highest dry solids content at the end of the drying was 81,5 %. Most of the samples reached the dry solids content of only around 50 % which is little (Figure 27).

During the drainage, thicker samples (60 mm mold) lost around 290 g of water when thinner samples (30 mm mold) lost only ~120 g of water. This explains the higher moisture ratio of the thinner sample at the beginning of the drying (Figure 28). Thicker samples also consisted of more water mass, so greater gravity forces were directed on them, which also explains greater drainage amounts. Drying rates fell greatly after the first drying minutes (Figure 28). This happened most likely because, the sample surface that was first under the effect of impingement air, dried fast and as much water could not be evaporated from the inside of the sample due to slow heat conduction into the inner structure. Drying rates tended to stabilize when the moisture ratio was under 8 kg/kg despite the drying parameters (Figure 28).

In the temperature measurement experiments, it was noticeable that as the temperature started to raise towards the impingement air temperature, the deeper the measurement point was the faster temperature reached the air temperature (Figure 29). At those points, the dry solids content of the samples was already over 50 % based on the mass change measurements. Due to that, water mass inside the sample was relatively small and as the heat transferred in the sample structure, decreased water mass was heated fast, which explains the faster temperature raise in the deeper measurement points. Based on the measurements, the surface temperature did not reach the impingement air temperature (Figure 30). If a sample consists of water, the evaporation from the surface of the sample cools down the surface and the evaporated water prevents temperature to increase over 100 °C. The larger the evaporation is the lower the surface temperature gets. Fast cooling of the surface happened as measurements had to be done by moving the sample away from the dryer. During temperature measurements, foam generated in the laboratory had to be carried to impingement dryer before pouring it to the mold, because thermocouples were connected to dryer and mold. Foam remained its structure and any major changes in the foam was not noticed due carrying. The impingement drying method by itself was not found fast enough to consider it for commercial use for such thick fiber products. However, it could work as a pre-dryer alongside some other drying method as it dries the surface of the fiber structure fast and favorable drying rates were reached at the beginning of the drying. Furthermore, the optimal geometry of 25 mm impingement distance from the sample surface was not used during drying experiments, but the distance varied due to mold size and sample thickness which probably affects to the results considerably.

Based on the microwave power correction calculations it was found that power adjustment was first growing and then decreasing (Table 4). As power level is increased, different power levels approach each other and the difference between power levels becomes smaller. Lost microwave power that is emitted to the surroundings is difficult to estimate, but it could reduce the microwave power emitted to fiber foam structure. The exact input power of the microwave for different power levels could be determined with suitable equipment, but they were not available during these experiments. In the power density measurements, exact thicknesses of the samples could not be determined, and more precise results would have been gained if power densities have been calculated for every sample and their averages for different thicknesses were used. However, the main purpose was to gain directional

information about the power densities for different sample sizes and power levels. In mass change measurements, it was noticed that evaporated water mass between weightings tended to be almost constant when power level was kept the same during drying. This confirms that most of the microwave power is emitted to water despite the amount of water structure consisted, because microwaves operate in the favorable frequencies for wavelengths of water. Dry solids content at the end of drying was difficult to control when samples consisted of only small amount of water and the over-drying was needed to be avoided. Over 30 % increases in the dry solids contents in one drying minute were found which made the exact ending point deciding very challenging. Due to this, there was a lot of variation between the final dry solids contents. Drying was ended before any damage to the surroundings and the mold happened. In future, experiments could be performed without the supportive mold to avoid these damages. However, some measurements were accomplished to end right on time when dry solids content was over 90 %, which helped to estimate the drying time more precisely and it could be helpful also in further investigations. Drying rates reached with higher power levels were at right level and they tended to remain stable to moisture ratios of 2 kg/kg (Figure 39). The average drying rates tended to be higher for pine pulp than CTMP with higher power levels (80-100 %). The sample porosity, the structure of fibers and their orientation might be the reasons for differences in drying rates. Either consistencies were not exactly the same between pine pulp and CTMP samples which might also affect on achieved drying rates. Based on the fiber analysis, CTMP had the average mean fines of 56,3 % when pine pulp had 27,6 %. Fines have an impact on pore sizes and increased fines hinder the water removal from the sample structure.

If considering a commercial dryer, it is important that water can be evaporated fast. Microwave drying was found to be fast, which opens possibilities for dryer design for example in the terms of dryer length and machine speed. At the beginning of microwave drying, it was found that samples were sensitive to fast temperature raise, which damaged the structure. During weigh measuring, sample had time to cool down, which might have impact to the results. Further investigation is needed to find the favorable power adjusting for microwave drying that fiber foam structures can take the emitted heat load without suffering structural damage. It was found that more stable surface temperature measurements were gained with the microwave oven’s mounted IR sensor, which measured the temperature during the whole drying. Surface temperature tended to reach its maximum during the first two drying minutes

(Figure 42). During sample weighing, the surface temperature dropped a lot, but it raised back to a maximum almost instantly when microwaves were emitted again. As microwaves penetrate to the structure generating stable heat load, the temperature inside the sample had to be higher than on the surface to evaporate the water because surface temperatures never exceeded 90 °C.

Samples experienced a lot of structural transformations, especially on the surfaces, due to fast initial water temperature and pressure increases. Other structural transformations such as bumpy and rugged sides came most likely from the movements of fibers in the fiber foam suspension due to high volumetric heat load during the drying. It was found that when the moisture ratio of ~7 kg/kg was reached sample did not experience the surface expansion even though 100 % power was applied. To avoid surface expansion, a drying program that would start with a lower power level and increase the power as drying goes further could be considered or some other drying method like impingement drying could be used as a pre-drying method. These adjustments could reduce the processing speed, but product quality would be better and cost savings would be received due to fewer reject. All the samples were dried in circular molds, which can affect the structural behavior.

When considering the commercial process, the production line would most likely produce continuously rectangular shaped thick fiber web and drying would also happen during the motion. This could affect the structural transformations. Based on the average drying times with different power levels, energy consumptions were calculated. The results only give directional information because drying could not be ended after certain dry solids content was reached and average end dry solids contents had lots of variation (Table 8). However, average drying times could have only increased little due fast development of dry solids content at the end of drying.

Based on operational cost calculations, it was found that electricity price affects significantly to the energy costs. Increased product thickness increases costs as longer drying time is needed and dryer must be lengthened. It will also increase the fiber expenses as basis weight is increased. The unit price of used fibers has the major effect on the raw material costs as it was found to be the highest expense amongst the raw materials. Due to this, it is important to consider the unit price of the fibers carefully.

Altogether, it was found that in the terms of drying efficiency, microwave drying is a better option for thick porous fiber materials than impingement drying. Quality parameters are still difficult to control as structures are quite sensitive to fast heat load of microwaves. More investigations should be carried out to find optimal power adjusting and sample consistency to avoid as much damage as possible. A combination of impingement drying and microwave drying would be interesting to investigate. In practice, in laboratory scale, it would not be easy because of different arrangements that these drying methods demand.

10 CONCLUSIONS

The main objective was to find the efficient drying methods for thick porous biobased materials. The main considered parameters were heat transfer and water evaporation capacity, the possibility to use renewable electricity as an energy source and adaptability in the near future. The additional objective was to investigate parameters affecting the quality of the structures during drying and the possible costs. Air impingement drying and microwave drying were investigated in a laboratory scale. From the investigated methods, the most promising method appears to be microwave drying.

The results of the drying experiments indicate that air impingement drying itself is not an effective drying technique for thick and porous foam formed materials. Drying times were from 45 min to over one hour for such a small laboratory samples, and due to this cannot be seen as a fast enough drying method. However, the surface of the sample dried quite fast. With 200 ºC impingement air temperature and 50 m/s jet velocity surface turned brown quickly when most parts of the sample had a high moisture content. The highest momentary drying rate reached was 51,2 kg/m^2/h and the highest average drying rate was 11,3 kg/m^2/h. The sample surface tended to suffer minor quality detriments, in a form of surface darkening, as SDS decomposes in temperatures over 40 °C. Increased jet velocities increased the concavity of the sample surface. In thickness direction, the temperature increase was slow.

Microwave drying was found to be fast drying method, especially with the higher power levels. With the 100 % power level, average drying time was ~6 min, despite the consistency or fibers. With microwave drying over 4-times higher momentarily drying rates and 18-times higher average drying rates were reached compared to impingement drying. The highest momentarily drying rate reached during experiments was 223 kg/m^2/h and the highest average drying rate was 199 kg/m^2/h. Both were reached with the thickest sample mold (79 mm) and pine pulp as fibers. However, there were no remarkable differences between pine pulp and CTMP. It was found that higher drying rates were reached with thicker sample molds. The highest dry solids content reached without any damage was 90 %. The sample surface tended to expand and collapse during the first drying minutes due to fast increase of initial temperature and pressure of volumetric heating of microwaves. Due to the surface

expansion, sample surfaces tended to collapse and turn into concave. Also, the whole sample structure bended either upwards or downwards. It was found that increased consistency decreased or even prevented the surface expansion. At the moisture ratio of 7 kg/kg (dry solids content of 12,5 %) the surface expansion did not occur even with 100 % microwave power level.

Directional operational cost calculations were made for microwave drying process that was designed to be fitted into 40 ft container. The machine speed of dryer was selected to be 2 m/min and drying time ~6 min based on the laboratory experiments. Considered costs were labor, raw materials and energy. Taxes nor investment costs were involved in the calculations. Two working personnel were considered to run the process. Raw materials consisted of fibers, surfactant and water. Drying energy was considered to be produced with electricity. After calculations the total operational costs were 1489 €/t divided into labor 234 €/t (16 %), raw materials 541 €/t (36 %) and energy 715 €/t (48 %). Base prices used in the directional calculations were found to affect to the results. For example, electricity price has a substantial effect to the energy costs. It was also found that product thickness affects on many variables such as machine speed, dryer length and raw material costs.

REFERENCES

Ahrens, M. U. et al. 2021. Integrated high temperature heat pumps and thermal storage tanks for combined heating and cooling in the industry. Applied Thermal Engineering, vol. 189.

Ahrens, M. U. 2021. High Temperature Heat Pumps as a Way to Decarbonise Norwegian Industry. Sintef. [network publication]. [referred 14.10.2021]. Available: High Temperature Heat Pumps as a Way to Decarbonise Norwegian Industry - #SINTEFblog

Alimadadi, M. and Uesaka, T. 2016. 3D-oriented fiber networks made by foam forming. Cellulose, 23(1), pp. 661–671. doi: 10.1007/s10570-015-0811-z.

Asghari, A. 2015. Fluid and Microfluidic Dielectric Measurement Using a Cavity Pertubation Method at Microwave C-Band. Thesis. Univeersity of Texas at San Antonio. College of Engineering. Department of Electrical and Computer Engineering.

Asikainen et al. 2020. FUTURE FIBRE PRODUCTS - FFP 2020. Final Report 2020. Reports 11, 18 and 23. Confidential.

British Petroleum. 2020. Energy Outlook 2020 edition explores the forces shaping the global energy transition out to 2050 and the surrounding that. BP Energy Outlook 2030. London. [statistical review]. [referred: 7.10.2021]. Available: https://www.bp.com/content/dam/bp/business-sites/en/global/corporate/pdfs/energy-economics/energy-outlook/bp-energy-outlook-2020.pdf.

Datt, P. 2011. Latent Heat of Vaporization/Condensation. Encyclopedia of Snow, Ice and Glaciers. Encyclopedia of Earth Sciences Series. ISBN: 978-90-481-2642-2.

Ecostar Insulation. 2019. The Importance of Insulation R Values. [network publication]. [referred 1.11.2021]. Available: Insulation R Values | Home Insulation | EcoStar (ecostarinsulation.ca)

Eurostat a. Data Browser. Electricity prices for non-household consumers – bi-annual data (from 2007 onwards). Band ID: 2000 MWh < Consumption < 20 000 MWh. Excluding taxes

and levies. Finland. 2020-S2. [network publication]. [referred: 21.9.2021]. Available: Statistics | Eurostat (europa.eu)

Eurostat b. Data Browser. Labour cost levels by NACE Rev. 2 activity. Statistical classification of economic activities in the European Community. Finland. Industry (except construction). [network publication]. [referred: 15.9.2021]. Available: Statistics | Eurostat (europa.eu)

Eurostat c. Procom – statistics by product. Data. Excel files (NACE Rev.2). [network publication]. [referred 16.9.2021]. Available: Excel files (NACE Rev.2) - Prodcom - statistics by product - Eurostat (europa.eu)

Forestbiofacts. Pulping and biorefining. Kraft pulping. [network learning environment]. [referred 22.9.2021]. Available: Kraft pulping – ForestBioFacts

Gimel, J. C. and Brown, W. 1996. A light scattering investigation of the sodium dodecyl sulfate-lysozyme system. The Journal of Chemical Physics 104(20), pp. 8112-8117. doi: 10.1063/1.471496.

Gupta, S.V. 2014. Viscometry for Fluids. Calibration of Viscometers. Volume 194. Delhi, India. ISBN: 978-3-319-04858.

Hanslmeier, A. 2011. Water in the Universe. Astrophysics and Space Science Library. ISBN: 978-90-481-9983-9.

Heikkilä. et al. 2020. Nonwovens from Mechanically Recycled Fibres for Medical Applications. [network publication]. [referred 20.10.2021]. Available at: https://cris.vtt.fi/en/publications/nonwovens-from-mechanically-recycled-fibres-for-medical-applicati.

Hjelt, T. et al. 2020. Foam forming of fiber products: a review. Journal of Dispersion Science and Technology 0(0), pp. 1–37. doi: 10.1080/01932691.2020.1869035.

iContainers. 2013. Containers & pallets. 40-foot Container - Dimensions, Measurements and Weight. [network publication]. [referred 21.10.2021]. Available: 40-foot Container - Dimensions, Measurements and Weight | iContainers

Jahangiri et al. 2014. On filtration and heat insulation properties of foam formed cellulose based materials. Nordic Pulp and Paper Research Journal, 29(4), pp. 584–591. doi: 10.3183/npprj-2014-29-04-p584-591.

Karlsson et al. 2000. Papermaking Part 2, Drying. Papermaking Science and Technology. Book 9. ISBN: 952-5216-09-8.

Kiiskinen, H. et al. 2019. Progress in foam forming technology. Tappi Journal, 18(8), pp. 499–510. doi: 10.32964/TJ18.8.499.

Knowpap. Tuotantoprosessit. Paperikoneen kuivatusosio – yleistä. Kuivatusosan sijainti paperikoneella. [network learning environment]. [referred 14.10.2021]. Available: KnowPap - Paperikoneen kuivatusosa - yleistä

Koponen, A. et al. 2018. The effect of in-line foam generation on foam quality and sheet formation in foam forming. Nordic Pulp and Paper Research Journal, 33(3), pp. 482–495. doi: 10.1515/npprj-2018-3051.

Koponen, A. I. et al. 2020. Drainage of high-consistency fiber-laden aqueous foams. Cellulose, 27(16), pp. 9637–9652. doi: 10.1007/s10570-020-03416-y.

Kouko, J. et al. 2021. Generation of aqueous foams and fiber foams in a stirred tank. Chemical Engineering Research and Design, 167, pp. 15–24. doi: 10.1016/j.cherd.2020.12.013.

Langevin, D. 2017. Aqueous foams and foam films stabilised by surfactants. Gravity-free studies. Comptes Rendus - Mecanique, 345(1), pp. 47–55. doi: 10.1016/j.crme.2016.10.009.

Lönnberg, B. et al. 2009. Mechanical Pulping. Papermaking Science and Technology. Book 5. Second Edition. ISBN: 978-952-5216-35-6.

Microwave Research and Applications, Inc. Processing Microwave BP-211/50. Installation and Operation Manual.

Metsä Fibre Oy. 2021. Metsä Pine AKI. Bleached Softwood Kraft Pulp. [technical datasheet]. [referred 23.9.2021]. Available: PowerPoint Presentation (metsafibre.com)

Mujumdar, A. 2014. Impingement drying. Handbook of Industrial Drying, Fourth Edition, pp. 385–394. doi: 10.1201/b17208.

National Institute of Standards and Technology (NIST). 2000. Revised Thermocouple Reference Tables: Type K. Monograph 175, 44(Revised to ITS-90), pp. 214–215.

Omega Engineering. 2019. Working principle of thermocouples. [website]. [referred 4.8.2020]. Available: How Do Thermocouples Work? Working Principles Of Thermocouples (omega.com)

Punton, V. W. 1975. The Use of an Aqueous Foam as a Fibre-Suspending Medium in Quality Papermaking. Foams. Proceedings of a Symposium organized by the Society of Chemical Industry, Colloid and Surface Chemistry Group, and held at Brunel University. Akers, R. J. Ed. Academic Press, pp. 179–193.

Pääkkönen, E. 2020. Packaking that does not cost the earth. VTT Technical Research Centre of Finland. [network publication]. [referred: 25.10.2021]. Available: Expanded polystyrene (EPS) alternatives in the making (vttresearch.com)

Pöhler, T. et al. 2017. Use of papermaking pulps in foam-formed thermal insulation materials. Nordic Pulp and Paper Research Journal, 32(3), pp. 367–374. doi: 10.3183/npprj-2017-32-03-p367-374.

Radvan, B. and Gatward, A. P. J. 1972. The Formation of Wet-Laid Webs by a Foaming Process. Tappi, 55(5), pp. 748-751.

Rosen, M. J. 2004. Surfactants and Interfacial Phenomena. Third Edition. Wiley-Interscience. A John Wiley & Sons, Inc., Publication. ISBN: 0-471-47818-0.

Rottneros. 2019. Pure Possibilities. [brochure]. [referred 2.11.2021]. Available: broschyr_allaprodukter_medel.pdf (rottneros.com)

Schiffmann, R. F. 2014. Microwave and dielectric drying. Handbook of Industrial Drying, Fourth Edition, pp. 283–302. doi: 10.1201/b17208.

Sigma-Aldrich. Product Information. Sodium dodecyl sulfate. [product information sheet]. [referred 3.11.2021]. Available: Sodium dodecyl sulfate (L3771) - Product Information Sheet (sigmaaldrich.com)

Sintef. 2021. Latest news. Developing the world's 'hottest' heat pump ever. [network publication]. [referred 14.10.2021]. Available: Developing the world's 'hottest' heat pump ever - SINTEF

Smith, M. K et al. 1974. Structure and Properties of Paper Formed By a Foaming Process. Tappi, pp. 107–111.

Smook, G. A. 1982. Handbook For Pulp and Paper Technologists. ISBN: 0-919893-00-7.

Souza, R. J. M. and König, A. 2012. Manufacturing of a Viscometer for Monitoring Oil Content In Polluted Water. HOLOS, Ano 28, vol 6, pp. 147-161. doi: 10.15628/holos.2012.1094

T 227 om-94: 1984. Freeness of pulp (Canadian standard method). [network publication]. [referred: 24.9.2021].

Timofeev, O. and Jetsu, P. 2021. Drying of foam formed materials. BeLight project. Research report. Confidential.

Touchette, R. V. and Jenness. L. C. 1960. Effect of Surface Active Agents on Drainage and Physical Strength Properties of Sulfite Pulp. Tappi vol. 43, No. 5, pp. 484-489.

Valmet. 2012. White papers. Drying and air systems. Impingement Drying. Valmet Technical Paper Series. [network publication]. [referred 1.11.2021]. Available: White paper: Air Systems, Impingement Drying (valmet.com)

Vargaftik, N. B. et al. 1983. International Tables of the Surface Tension of Water. J. Phys. Chem. Ref. Data, vol. 12, pp. 817-820.

Wołowicz, A. and Staszak, K. 2020. Study of surface properties of aqueous solutions of sodium dodecyl sulfate in the presence of hydrochloric acid and heavy metal ions. Journal of Molecular Liquids, 299. doi: 10.1016/j.molliq.2019.112170.

Wu, J. 2018. A Basic Guide to Thermocouple Measurements. Texas Instruments Incorporated, (September), pp. 1–37. Available at: www.ti.com.

Ylli, H. 2020. BeLight project develops biobased, lightweight and recyclable applications for packaking and construction industry. Tampere University of Applied Scienses. [network publication]. [referred 25.10.2021]. Available: BeLight project develops biobased, lightweight and recyclable applications for packaging and construction industry | Tampere universities (tuni.fi)

Annex 1: Trial points of the laboratory experiments

Sample number	Drying method	Fibers	Consistency [%]	Mold [mm]	Jet speed [m/s]	Jet temperature [°C]	Microwave power [%]	Drying time [min]	Mass change	Temperature
1	Impingement	ÄKI pine	4	60	30	150		70	x	
2	Impingement	ÄKI pine	4	60	50	150		86	x	
3	Impingement	ÄKI pine	4	60	50	150		115		x
4	Impingement	ÄKI pine	4	60	50	200		98		x
5	Impingement	ÄKI pine	4	60	50	200		66	x	
6	Impingement	ÄKI pine	4	30	50	150		47	x	
7	Impingement	ÄKI pine	4	60	50	150		115	x	
8	Impingement	ÄKI pine	4	60	50	200		98	x	
9	Microwave	ÄKI pine	4	39			40	12	x	x
10	Microwave	ÄKI pine	4	39			30	20	x	x
11	Microwave	ÄKI pine	4	39			20	37	x	x
12	Microwave	ÄKI pine	4	39			20	37	x	
13	Microwave	ÄKI pine	4	39			60	8	x	x
14	Microwave	ÄKI pine	4	39			50	8	x	x
15	Microwave	ÄKI pine	4	39			70	6	x	x
16	Microwave	ÄKI pine	4	39			80	5	x	x
17	Microwave	ÄKI pine	4	49			80	7	x	x
18	Microwave	ÄKI pine	2	39			80	3	x	x
19	Microwave	ÄKI pine	9	39			80	8	x	x
20	Microwave	ÄKI pine	9	39			100	6	x	x
21	Microwave	ÄKI pine	4	39			100	6	x	x
22	Microwave	ÄKI pine	4	39			90	6	x	x
23	Microwave	ÄKI pine	2	49			40	7	x	x
24	Microwave	ÄKI pine	4	79			80	8	x	x
25	Microwave	ÄKI pine	2	39			50	5	x	x
26	Microwave	ÄKI pine	4	79			100	8	x	x
27	Microwave	ÄKI pine	4	79			100	8	x	x
28	Microwave	CTMP	2,5	39			100	2	x	x
29	Microwave	CTMP	2,5	39			50	3	x	x
30	Microwave	CTMP	2,5	49			30	5	x	x
31	Microwave	CTMP	2,5	39			20	26	x	x
32	Microwave	CTMP	2,5	49			20	20		x
33	Microwave	CTMP	5	39			80	6	x	x
34	Microwave	CTMP	5	39			100	6	x	x
35	Microwave	CTMP	5	39			60	8	x	x
36	Microwave	CTMP	10	39			100	7	x	x
37	Microwave	CTMP	7,5	39			100	6	x	x
38	Microwave	CTMP	7,5	39			80	6	x	x
39	Microwave	ÄKI pine	6,5-7	79			100	8	x	x
40	Microwave	ÄKI pine	6,5-7	79			100	6		x
41	Microwave	ÄKI pine	6,5-7	79			80	7	x	x
42	Microwave	ÄKI pine	6,5-7	79			60	9	x	x
43	Microwave	ÄKI pine	3-3,5	39			20	28	x	x
44	Microwave	ÄKI pine	3-3,5	49			40	7	x	x
45	Microwave	ÄKI pine	3-3,5	39			60	2	x	x
46	Microwave	ÄKI pine	3-3,5	49			50	5	x	x
47	Microwave	ÄKI pine	3-3,5	39			40	6		x
48	Microwave	ÄKI pine	2,5-2,8	39			20	20	x	x
49	Microwave	ÄKI pine	2,5-2,8	49			40	6	x	x
50	Microwave	ÄKI pine	3	39			40	6		x
51	Microwave	ÄKI pine	3	79			50	6	x	x
52	Microwave	CTMP	3	39			40	6	x	x
53	Microwave	CTMP	3	49			20	9	x	x
54	Microwave	CTMP	3,5	39			20	10	x	x
55	Microwave	CTMP	4	39			20	30	x	x
56	Microwave	CTMP	4	49			20	30		x